Democratic and Popular Republic of Algeria

Ministry of Higher Education and Scientific Research

University Med Khider of Biskra

Faculty of Exact Sciences and Sciences of Nature and Life

Department Of Matter Sciences   Domain Of Matter   Physics

Section of Physics

Speciality Physics of Materials
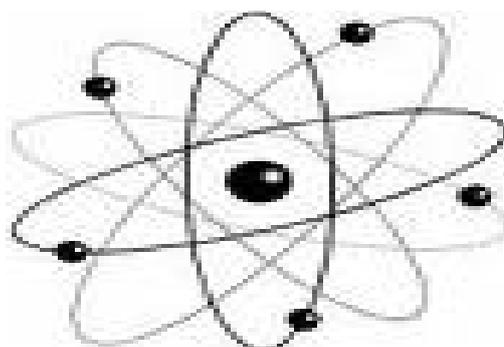
Final Dissertation in Master

Entitled

ROTATIONAL SPEED AND SOLVENT EFFECT ON THE STRUCTURAL AND OPTICAL PROPERTIES OF ZNO THIN FILMS PREPARED BY SOL-GEL (SPIN COATING) METHOD

Presented by:

SAADI ABDEL HAKIM

To the Jury composed by:

A.CHALA	*Professor*	*University Med Khider of Biskra*	*President*
A.ATTAF	*Professor*	*University Med Khider of Biskra*	*Reporter*
S.RAHMANE	*M.C. « A »*	*University Med Khider of Biskra*	*Examiner*

Academic Year

2013- 2014
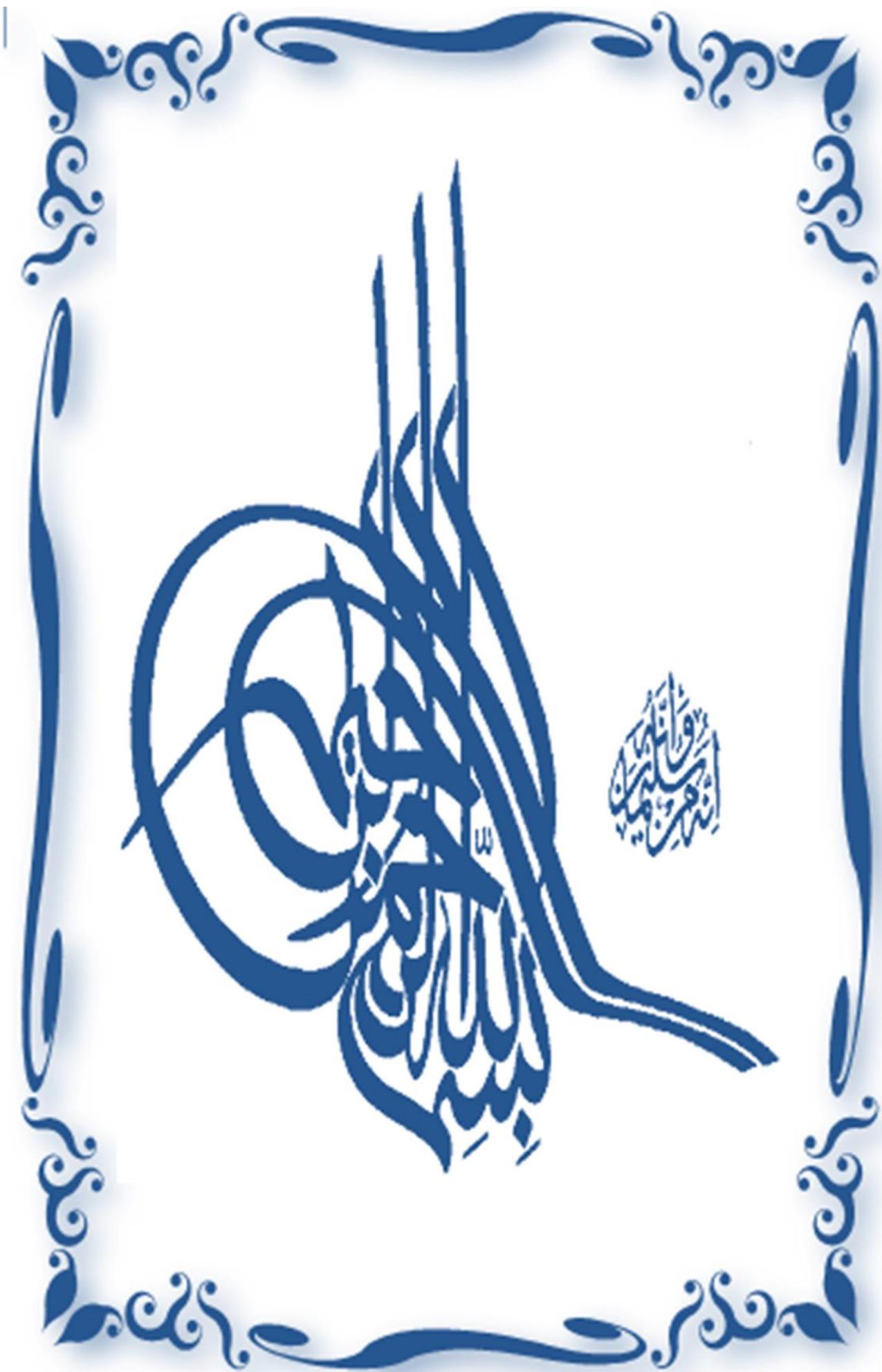
الحمد لله رب العالمين

و الصلاة و السلام على

أشرف المرسلين.

﴿ وقل بي زدني علما ﴾

Dedicate

I Dedicate this modest work to :

My parents treasured and I ask God to protect them

To my wife and my children

To my brothers and sisters and their children

To all my family

And all my friends

Acknowledgements

GENERALE INTRODUCTION

During the last thirty to forty years, the dominant TCOs have been tin oxide (SnO_2),

Indium oxide (In_2O_3), indium tin oxide (ITO). All of these materials have been mass-produced in very large volumes over a long period. The development of these materials is related to their interesting physical properties, which combine electrical conduction and optical transparency in the visible spectral field. [1]

The expanding use of these materials, especially for the production of transparent electrodes for optoelectronic device applications, is endangered by the scarcity, toxicity and high price of In. This situation drives the search for alternative TCO materials to replace ITO.

AZO , GZO and FTO (ZnO:Al , ZnO:Ga , SnO:F) are at present the only TCOs with electrical conductivity close to that of ITO, and with appropriate high optical transmission in the near-UV, VIS and NIR .In addition to the required electrical and optical characteristics, applied TCO materials should be stable in hostile environment containing acidic and alkali solutions, oxidizing and reducing atmospheres, and elevated temperature .These properties are strongly related to the methods of elaboration. Among these methods, one finds sol gel, which is the method, applied in our work. .

This work is focused on a study the effect of the rotational speed , and the solvent , on the properties of the ZnO thin films deposited on glass substrate by sol gel process spin coating for photovoltaic and optoelectronic applications (solar cells, gas sensors ...)but The main point in this work is the good understanding of this deposition method   .

Zinc acetate dehydrate, Ethanol (or Propanol) and monoethanolamine (MEA) was used as a starting material, solvent and stabilizer, respectively.

This report of work is organized in the following way:

The first chapter initially comprises the Fundamentals physics on TCOs and ZnO thin films and there applications.

The second chapter is devoted to the elaboration's methods and techniques of characterizations (structural, optical), and different methods of calculation of the deposits characteristics (the grains size, the thickness, index of refraction, the optical gap and disorder).

The third chapter, is devoted to expose the sol gel methods; know this way, its steps, the chemical reactions and all factors influential in this Method

The fourth chapter is devoted to the deposit thus the different experimental techniques to characterize our layers and the discussions relating to the results observed at the time of this study.

At last, we report general conclusion about the full results obtained in this work.

TABLE OF CONTENTS

Chapter-Iii: The Sol Gel Process

Chapter: I

Fundamentals on TCOs and ZnO thin films

In this chapter are summarized the fundamental physical properties of TCO materials, especially ZnO thin films. The physical theories on the electrical conduction mechanisms and on optical modelling are detailed.

I.1.INTRODUCTION:

Transparent conducting oxides (TCO) constitute a unique class of materials, which combine two physicals properties together - high optical transparency and high electrical conductivity. These properties are generally considered to be mutually exclusive of each other since high conductivity do metals possess a property while insulators are optically transparent. This peculiar combination of physical properties is achieved by generating free electron or hole carriers in a material having a sufficiently large energy band gap (i.e., >3.1 eV) so that it is non-absorbing or transparent to visible light [2].

The charge carriers are usually generated by doping the insulator with suitable dopants and by defects. It is no wonder that this unique material property makes TCOs technologically an important material and TCOs are widely used in commercial applications which will be mentioned later.

The TCOs used in technological applications should have following characteristics. First, they should be transparent for the visible part of light with transmittance > 80%. Second, they should be a good conductor of electricity with a high enough concentration of electrical carriers, i.e, an electron or hole concentration $>\approx 10^{19}$ cm $^{-3}$ and with a sufficiently large mobility $>\approx 1$ cm^2 V $^{-1}$s^{-1}. The three most common TCOs are tin doped indium oxide In $_2$O$_3$:Sn , fluorine doped tin oxide SnO$_2$:F, and aluminium doped zinc oxide ZnO:Al. All three of these materials have band gaps above that required for transparency across the full visible spectrum. Note that although these TCOs are considered to be good conductors from the perspective of a semi -conductor, they are actually very poor conductors compared to metals [2].

For example, the best conductivity of In$_2$O$_3$:Sn (for indium tin oxide or ITO)is about a factor of 10 to 60 lower than that of a typical integrated circuit contact metal. The low conductance of TCOs compared to metals has important consequences for both TCO and transparent electronics applications.

Therefore, an appropriate quantitative measure of the performance of TCOs is the ratio of the electrical conductivity (σ) to the visible absorption coefficient (α). Thus the figure of merit of TCO material, is used for quantitative description of TCO performance [2].

$$Figure\ of\ merit\ \ =\ \frac{\sigma}{\alpha} \qquad (\ I.1)$$

Figures of merit for some TCOs are given in Table 1.1.

Material	Sheet resistance ($\Omega/\ cm^2$)	Visible absorption coefficient (α)	Figure of merit (Ω^{-1})
ZnO:F	5	0.03	7
Cd_2SnO_4	7.2	0.02	7
ZnO:Al	3.8	0.05	5
In_2O_3:Sn	6	0.04	4
SnO_2:F	8	0.04	3
ZnO:Ga	3	0.12	3
ZnO:B	8	0.06	2
SnO_2:Sb	20	0.12	0.4
ZnO:In	20	0.20	0.2

Table I.1: Figures of merit σ/α of some TCOs

I.2. TCO MATERIALS:

A plethora of systems have been studied as candidate material for a TCO [3].Table 1.2 lists the commonly used TCO host materials and corresponding dopants. These include binary oxides, ternary oxides and also multicomponent oxides.

Table 1.2: TCO materials.

Material	Dopant or compound
In_2O_3	$Sn, Ge, Mo, F, Ti, Zr, Hf, Nb, Ta, W, Te$
SnO_2	Sb, F, As, Nb, Ta
ZnO	$Al, Ga, B, In, Y, Sc, F, V, Si, Ge, Ti, Zr, Hf$
CdO	In, Sn
$ZnO - SnO_2$	$Zn_2SnO_4, ZnSnO_3$
$ZnO - In_2O_3$	$Zn_2In_2O_5, Zn_3In_2O_3$
$In_2O_3 - SnO_2$	$In_4Sn_3O_{12}$
$CdO - SnO_2$	$Cd_2SnO_4, CdSnO_3$
$CdO - In_2O_3$	$CdIn_2O_4$
$GaInO_3, (Ga, In)_2O_3$	Sn, Ge
$CdSb_2O_6$	Y
$ZnO - In_2O_3 - SnO_2$	$Zn_2In_2O_5 - In_4Sn_3O_12$
$CdO - In_2O_3 - SnO_2$	$CdIn_2O_4 - Cd_2SnO_4$
$CuXO_2$	$X = Al, Ga, In$
$ZnXO_4$	$X = Al, Ga, Co, Rh, Ir$

I.3. ALTERNATIVE MATERIALS FOR TCO APPLICATIONS

Graphene, which is a single-layer of carbon, also exhibits high electrical conductivity and high optical transparency [4, 5]. The advantages of graphene over TCOs are its mechanical strength and exibility, in contrast to ITO, which is brittle. Moreover, since it is a carbon derivative it is cheap and available in abundance. Additionally, graphene films may be deposited from solution over large areas. Still it is unlikely to replace the TCOs in all the devices for practical reasons that there is an existing technology to synthesize and fabricate TCO devices, more over the graphene films are sensitive to surface roughness [6] while TCOs can be easily fabricated on rough surfaces. additionally a wide range of TCO material system also provides an access to a range of physical properties such as the work function.

I.4. BASIC PHYSICS OF TCOS:

I.4.1. ELECTRICAL CONDUCTIVITY:

TCOs are wide band gap (E_g) semiconducting oxides, with conductivity σ in the range 10^2 – 1.2×10^6 (S). The conductivity is due to doping either by oxygen vacancies or by extrinsic dopants. In the absence of doping, these oxides become very good insulators, with $\rho > 10^{10}$ Ω-cm. Most of the TCOs are n-type semiconductors. The electrical conductivity of n-type TCO thin films depends on the electron density in the conduction band and on their mobility:

$$\sigma = \mu n e \qquad (I.2)$$

, where **μ** is the electron mobility, **n** is its density, and *e* is the electron charge. The mobility is given by:

$$\mu = \frac{e\tau}{m^*} \qquad (I.3)$$

Where **τ** is the mean time between collisions, and m* is the effective electron mass. However, as *n* and **τ** are negatively correlated, the magnitude of **μ** is limited. Due to the large energy gap ($E_g >$ ~3 eV) separating the valence band from the conducting band, the conduction band cannot be thermally

populated at room temperature (kT~0.03 eV, where k is Boltzmann's constant), hence, stoichiometric crystalline TCOs are good insulators. [7]

To explain the TCO characteristics, various population mechanisms and several models describing the electron mobility were proposed. Some characteristics of the mobility and the processes by which the conduction band is populated with electrons were shown to be interconnected by electronic structure studies, [8] e.g., that the mobility is proportional to the magnitude of the band gap.

In the case of intrinsic materials, the density of conducting electrons has often been attributed to the presence of unintentionally introduced donor centers, usually identified as metallic interstitials or oxygen vacancies that produced shallow donor or impurity states located close to the conduction band. The excess or donor electrons are thermally ionized at room temperature, and move into the host conduction band. However, experiments have been inconclusive as to which of the possible dopants was the predominant donor. [9] Extrinsic dopants have an important role in populating the conduction band, and some of them have been unintentionally introduce. Thus, it has been conjectured in the case of ZnO that interstitial hydrogen, in the H^+ donor state, could be responsible for the presence of carrier electrons. [10]

The conductivity σ is intrinsically limited for two reasons. First, n and μ cannot be independently increased for practical TCOs with relatively high carrier concentrations. At high conducting electron density, carrier transport is limited primarily by ionized impurity scattering, i.e., the Coulomb interactions between electrons and the dopants. Higher doping concentration reduces carrier mobility to a degree that the conductivity is not increased, and it decreases the optical transmission at the near-infrared edge. With increasing dopant concentration, the resistivity reaches a lower limit, and does not decrease beyond it, whereas the optical window becomes narrower.

I.4.2. OPTICAL PROPERTIES:

When light proceeds from one medium into another, several phenomena occur. Some of the light radiation may be transmitted through the medium, some will be absorbed, and some will be reflected at the interface on the surface. Moreover, the intensity Io of the beam incident on the surface of the thin films must equal the sum of the intensities of the transmitted, absorbed, and reflected beams, which can be written as $I_O = I_T + I_A + I_R$. An alternate form of the above equation is T+A+R=1, where T, A, R, respectively, are the transmissivity (I_T/I_O), absorptivity (I_A / I_O), and reflectivity (I_R / I_O). Thus, materials that are capable of transmitting light with relatively little absorption and reflection are transparent.

The optical phenomena that occur within solid materials, such as ZnO thin films, involve inter-actions between the electromagnetic radiation and atoms, ions and electrons. Of these interactions, electronic polarization and electron energy transitions are the most important. Nevertheless, absorption by electronic polarization is only explained for the light frequencies in the vicinity of the relaxation frequency of the constituent atoms [11].

Thus, for non-metallic materials like ZnO films at short wavelength (<400nm), absorption phe-nomena can be explained by the fundamental energy gap [12], which depends on the electron energy band structure of the materials; band structures for semiconductors like ZnO thin films are an
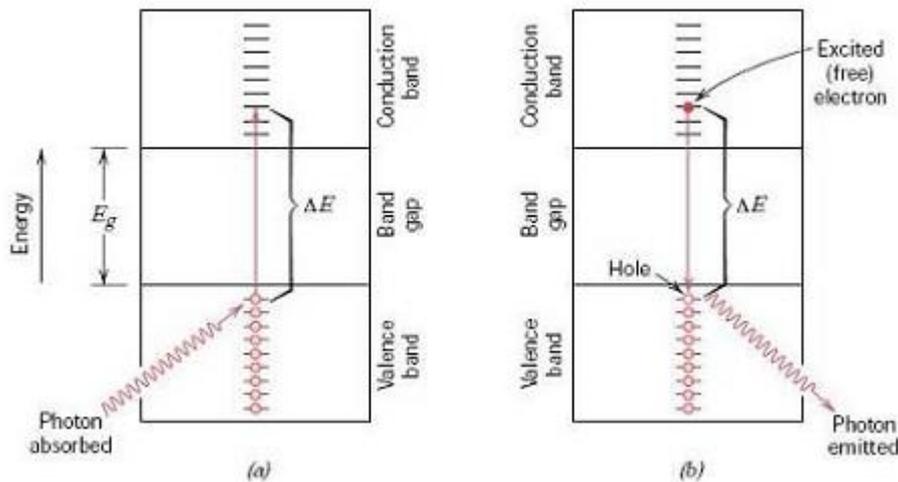
Figure I-1 (a) Mechanism of photon absorption for non-metallic materials in which an electron is excited across the band gap, leaving behind a hole in the valence band. The energy of the photon absorbed is ΔE , which is necessarily greater than the band gap energy Eg . (b) Emission of a photon of light by a direct electron transition across the band gap [12]

important property.

As demonstrated in Figure I-1, absorption of a photon of light probably occurs by the promotion or excitation of an electron from the nearly filled valence band, across the band gap, and into an empty state within the conduction band; a free electron in the conduction band and a hole in the valence band are created. Furthermore, the energy of excitation ΔE is related to the absorbed photon frequency based on the electron transitions equation: $\Delta E = h\upsilon$. Thus, absorption phenomena can take place only if the photon energy is greater than the band gap Eg, that is represented as: $h\upsilon > Eg$. Based on the above theory in which the absorption occurs by $h\upsilon > Eg$, we extend our discussion to metallic materials. As shown in Figure 1-3, since metallic materials lack a band gap, every photon has enough energy to excite the electron into a higher energy unoccupied state. In contrast, for semiconductors like ZnO thin films, the absorption phenomenon occurs when the energy of the photon in some

range of wavelength is greater than Eg while the transparency phenomenon occurs as that of photon under some range of wavelength is smaller than Eg. Hence, that is the reason why the ZnO thin films are only transparent in the visible range; visible light lies within a very narrow region of the spectrum with wavelengths raging between 400 nm to 700 nm [13] (shown in Figure 1-2).
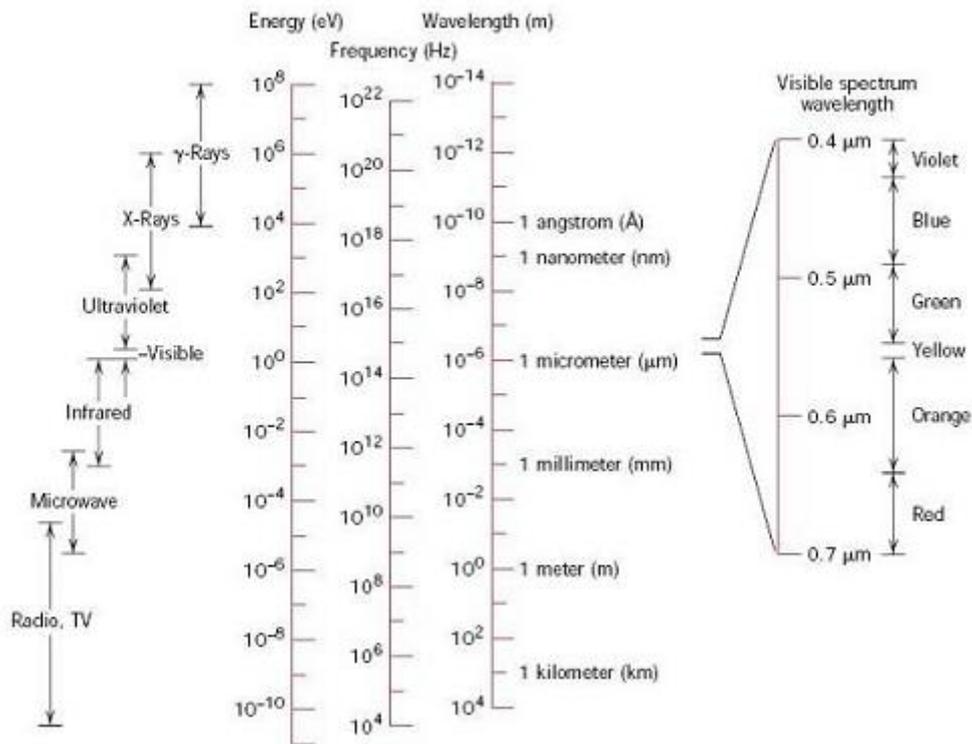
Figure I-2 The spectrum of electromagnetic radiation , including wavelength ranges for the various

colors in the visible [12]

a)

b)
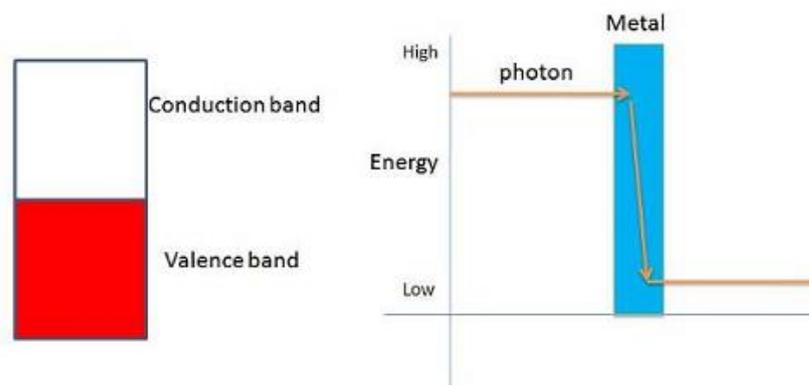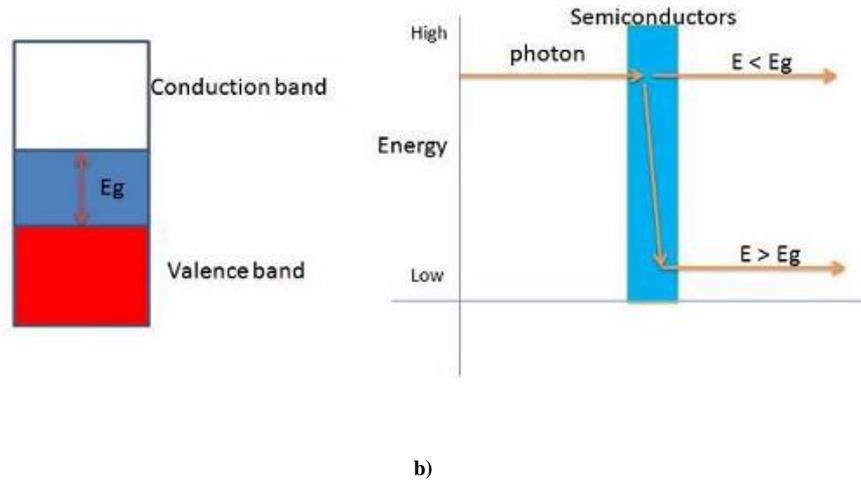
Figure I-3) a)The relation between absorption and the energy band :Metal

b) The relation between absorption and the energy band : semi-conductors [18]

The transmittance and reflectance data can be used to calculate absorption coefficients of the films at different wavelengths. The absorption coefficient, α , is given by the relation: [24]

$$\alpha = \frac{1}{t} \ln \frac{(1-R)^2}{T} \qquad\qquad (I.4)$$

where *t* is the film thickness, T is the transmittance and R is the reflectance. Additionally, the absorption coefficient data also can be transferred to another equation relative to the band gap (Eg), which can be represented as the following:

$$\alpha h\upsilon \approx B(h\upsilon - E_g)^m \qquad\qquad (I.5)$$

Where: *h v* is the photon energy, *Eg* is optical gap m and B are constants. *m* characterizes the optical type of transition and takes the values **½** for allowed direct transitions or 2 for allowed indirect transitions. [14].

The optical properties of TCOs transmission *T*, reflection *R*, and absorption *A*, are determined by its refraction index *n*, extinction coefficient *k*, band gap E_g, and geometry. Geometry includes film thickness, thickness uniformity, and film surface roughness. *T, R* and *, A* are intrinsic, depending on the chemical composition and solid structure of the material, whereas the geometry is extrinsic. There is a

negative correlation between the carrier density and the position of the IR absorption edge, but positive correlation between the carrier density and the UV absorption edge, as E_g increases at larger carrier density (Moss-Burstein effect). As a result, the TCO transmission boundaries and conductivity are interconnected.

As mentioned above, besides high conductivity ($\sim10^6$ S), effective TCO thin films should have a very low absorption coefficient in the near UV-VIS-NIR region. The transmission in the near UV is limited by E_g, as photons with energy larger than E_g are absorbed. A second transmission edge exists at the NIR region, mainly due to reflection at the plasma frequency. Ideally, a wide band gap TCO should not absorb photons in the transmission "window" in the UV-VIS-NIR region. However, there are no "ideal" TCOs thin films, and even if such films could be deposited, reflection and interference would also affect the transmission. Hence, 100% transparency over a wide region can not be obtained.

I.1.5 .ROLE OF DEFECTS:

It is observed that undoped as-grown TCO thin films and bulk crystals typically exhibit n-type conductivity. The origin of this unintentional conductivity is not clear and often it is attributed to native point defects. The unintentional conductivity is commonly attributed to the cation interstitials or oxygen vacancies based on its observed dependence on oxygen content in the growth environment. The defects and impurities in TCOs also play an important role in determining their electronic structure and physical properties as it is observed for semiconductors.

The formation energies are key quantities in the characterization of defects since we can derive equilibrium concentrations of defects, stability of different charge states and the electronic transition levels from them [15]. Thus, the electronic structure study of intrinsic defects is necessary to understand if defects are likely to contribute to the conductivity and can provide guidelines for experimental growth conditions facilitating a control over conductivity.

I.6. APPLICATIONS OF TCOS:

TCOs are widely used in a large number of optoelectronic devices and more applications are yet to be explored. The well-known applications are described briefly in the following.

Most of these devices use TCOs in the form of thin films coated over suitable substrates.

I.6.1 SOLAR CELLS :

The front surfaces of solar cells are covered by transparent electrodes. a typical architecture of (a) a thin film solar cell and (b) an organic solar cell is shown in Fig. 1.4. A TCO layer is generally used for the front contact of all-thin- film silicon solar cells, whereas are reflective contact material is needed at the back. In solar cell, TCOs are needed as a contact for collection of the photo-generated carriers while still allowing the light to reach the active solar absorber material. The optical qualities of these materials substantially affect the required thickness of the silicon absorber layer, in terms of facilitating the absorption of an optimal amount of irradiation. ITO is widely used in the organic solar cells due to its high transparency and low resistivity. However, limited supply of In makes it an expensive material and cheaper alternatives such as ZnO: Al have great demand by industries. [2].
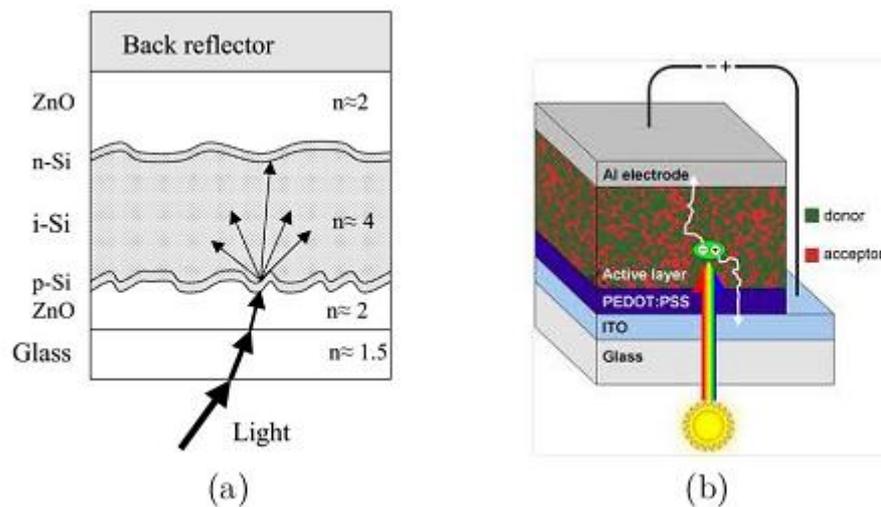
Figure I.4: A typical architecture of a) thin film solar cell and b) organic solar cell [29].

I.6.2 FLAT-PANEL DISPLAYS :

- The many different styles of at-panel displays use a transparent conductor as a front electrode. The role of TCOs is to pass the electrical signals to the pixels forming the display and simultaneously allow the light generated to pass on to viewer. Etch ability is a very important consideration in forming patterns in the transparent conducting electrode [2].

I.6.3 SMART WINDOWS :

- Smart windows use TCO coatings on glass. Typically, the function of a smart window is to electronically block some or all of the light incident onto a window. Since the plasma frequency can be tuned, the TCO coating can either block or allow the IR part of light thereby allowing control over room temperature. Thus in cold climates, TCO coated glass can be used to reject heat back into the residential space, while in hot climates the reverse approach is taken. In addition, the smart window eliminates the need for blinds or drapes, and, if UV is blocked, helps to protect carpeting and furniture from fading [2].

I.6.4 TOUCH SCREENS :

- Touch screens, commonly used in devices such as mobile phones or ATM machines are formed from etched TCOs on glass. They sense the presence of a finger by direct contact or capacitive through the glass. The resistive system consists of a normal glass panel that is covered with a conductive and a resistive metallic layer. These two layers are held apart by spacers, and a scratch-resistant layer is placed on top of the whole setup. An electrical current runs through the two layers while the device is operational. When a user touches the screen, the two layers make contact in that exact spot. The change in the electrical field is noted and the device further acts upon the coordinates of the point of contact. In the capacitive system, a layer that stores electrical charge is placed on the glass panel of the monitor. When a user touches the monitor with his or her finger, some of the charge is transferred to the user, so the charge on the capacitive layer decreases. This decrease is measured in circuits located at each corner of the device and further this signal is processed [2].

I.6.5 AUTOMOTIVE APPLICATIONS :

- An automobile affords numerous application venues for transparent electronics. Obvious candidate platforms include window glass, dashboards, and navigation systems.

I.6.6 TRANSPARENT ELECTRONICS :

- Most of TCOs show n-type conductivity, however, if p-type conducting TCO a is synthesized a transparent p-n junction can be formed. This may lead to an era of transparent electronics where the electronic circuits are transparent. Moreover, futuristic applications such as flexible electronic newspapers and wearable clothing displays may also be realized [2].

I.7 ZINC OXYDE :

Zinc oxide is an inorganic compound with the formula ZnO. ZnO is a white powder that is insoluble in water, and it is widely used as an additive in numerous materials and products including rubbers, plastics, ceramics, glass, cement, lubricants,[16] paints, ointments, adhesives, sealants, pigments, foods (source of Zn nutrient), batteries, ferrites, fire retardants, and first-aid tapes. It occurs naturally as the mineral zincite, but most zinc oxide is produced synthetically.[17]

The choice of zinc oxide comes from the reasons previously mentioned its several physical properties and variant applications in different domains. It has distinct advantages over other competitors, e.g., abundance in earth crust, non-toxicity, low material costs, chemical stability, high transparency in the visible and near infrared spectral region, etc.

I.7.1 ZINC OXIDE PROPERTIES:

In the Table (I.3) we summarize most of the properties of zinc oxide, which will discussed some of it later

Crystal structure	Hexagonal, wurtzite
Molecular weight	Zn:65.38, O:16 and ZnO:81.38
Lattice constant	a = 3.246 Å, c = 5.207 Å
Density	5.67 g/cm^3 or 4.21 x 10^{19} ZnO molecules/mm^3
Cohesive energy	E$_{coh}$ = 1.89 eV
Melting point	T$_m$ = 2250 °K under pressure
Heat of fusion	4, 470 cal/mole
Thermal conductivity	25 W/mK at 20 °C
Thermal expansion coefficient	4.3 x 10^{-6} / °K at 20 °C 7.7 x 10^{-6} / °K at 600 °C
Band gap at RT	3.37 eV
Refractive index	2.008
Electron and hole effective mass	m$_e$* = 0.28, m$_h$* = 0.59
Debye temperature	370 °K
Lattice energy	964 kcal/mole
Dielectric constant	ε_0 = 8.75, ε_∞ = 3.75
Exciton binding energy	E$_b$ = 60 meV
Pyroelectric constant	6.8 Amp./sec/cm^2/°K x 10^{10}
Piezoelectric coefficient	D$_{33}$ = 12 pC/N

Table I.3) Properties of Zinc Oxide

I.7.1.1. Structural Properties:

ZnO belongs to the group of II-VI binary compound semiconductors which crystallize in either a cubic zinc-blende or hexagonal wurtzite structure where each anion is surrounded by four cations at the corners of a tetrahedron, and vice versa. The bonding of this tetrahedral coordination is characteristic of sp3 covalent bonding, but these materials also have substantial ionic character. Therefore, as shown in Figure 1-5, the crystal structures of ZnO are wurtzite (B4), zinc blende (B3), and rock-salt (B1). Under ambient conditions, the thermodynamically stable phase is wurtzite, while the zinc-blende ZnO structure is only revealed by growth on cubic substrates; moreover, the rock-salt (NaCl) structure probably grows at relatively high pressure [18]

The wurtzite structure has a hexagonal unit cell with two lattice parameters, **a** and **c**, in the ratio of **c/a** =1.633. The schematic structure is shown in Figure 1-6 , and this structure has two interpenetrating hexagonal-close-packed (hcp) sub-lattices. Each sub-lattice consists of one type of atom represented with respect to each other along the threefold c-axis by the amount of **u**=3/8 =0.375 (in an ideal wurtzite structure) in fractional coordinates. [18]
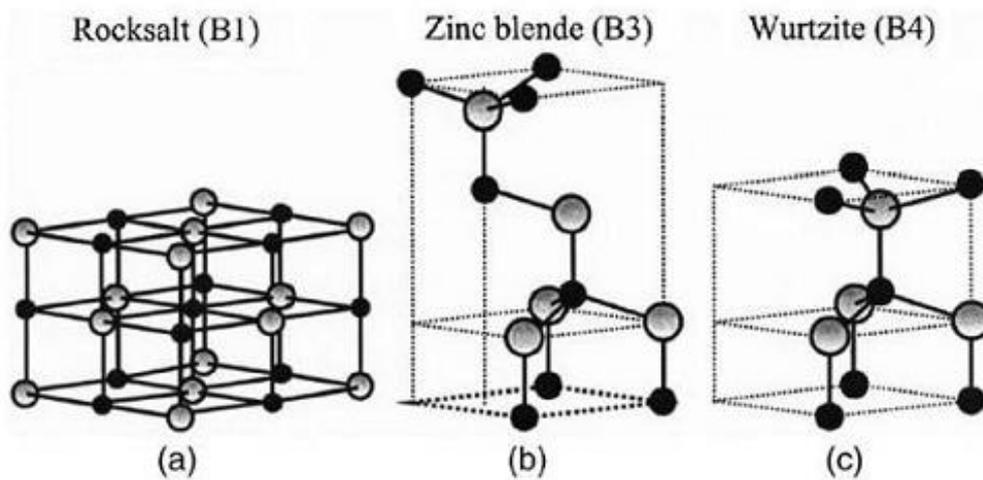
Figure I-5) Stick and ball representation of ZnO crystal structures: (a) cubic rock-salt(B1), (b) cubic zinc blend (B3), and (c) hexagonal wurztie (B4). The shaded gray and black spheres denote Zn and O atoms, respectively.[21]
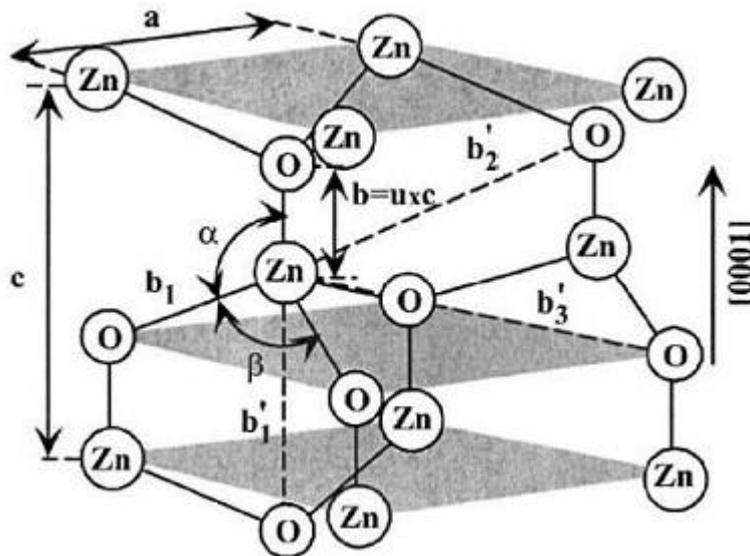
Figure I-6) Schematic representation of a wurtzitic ZnO structure having lattice constant a in the basel plane and c in the basel direction; u parameter is expressed as the bond length or the nearest-neighbor distant b divided by c (0.375 in ideal crystal), and α and β (109.47o in ideal crystal) are the bond angles.[21]

I.7.1.2 Electrical Properties of ZnO:

The electronic band structure of the zinc and oxygen are:

$$O: 1s^2 2s^2 2p^4$$

$$Zn: 1s^2 2s^2 2p^6 3s^2 3p^6 3d^{10} 4s^2$$
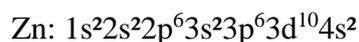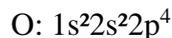
The electrical resistivity (ρ) of ZnO films is determined by the carrier concentration (n) and carrier mobility (μ), which is also presented as $\rho = 1/ (n\,e\,\mu)$ where e is the electron charge.

It is known that e is a constant, so, for obtaining low resistivity, the carrier concentration (n) and carrier mobility (μ) should be simultaneously maximized, and most research papers have suggested that the method of achieving maximum carrier concentration is by oxygen vacancies and doping.

The literature [11] indicates, "If an oxygen vacancy is created in a perfect crystal, two electrons are created in the crystal and contributed as ionized donors." But, if there is too much oxygen created in the thin films, sub-oxides will form, causing the resistivity to rise."

In addition to the oxygen vacancies, doping also can change the electrical conduction of TCOs.

As host cations are substituted by elements with a valence higher than that of the host, the extra electrons can become conduction electrons. To avoid the charge neutrality, substitution of a higher valence element creates extra electrons.

It is well known that pure zinc oxide films usually have a characteristic high resistivity due to their low carrier concentration. Therefore, in order to decrease resistivity, we can increase either the carrier concentration or the carrier mobility in zinc oxide thin films.

The former is probably obtained by oxygen and/or zinc non-stoichiometry, or doping with an impurity. However, Hu et al. [26] Pronounced that non-stoichiometric films have excellent electrical and optical properties, but they become very unstable as the ambient temperature becomes higher. On the other hand, for obtaining stable low resistivity ZnO thin films, doped ZnO thin film is probably a good approach.

In conclusion, the majority of research for achieving low resistivity ZnO thin films is focused on increasing the free carrier concentration in thin films through use of dopants and oxygen

vacancies. But, Johnson et al. [20] in 1947 stated that increasing the carrier density via doping or oxygen vacancies is self-limiting because the increase of the number of free carriers decreases the mobility of carriers due to carrier-carrier scattering.

Therefore, there is a trade-off relation between the carrier density and the carrier mobility for obtaining low resistivity.
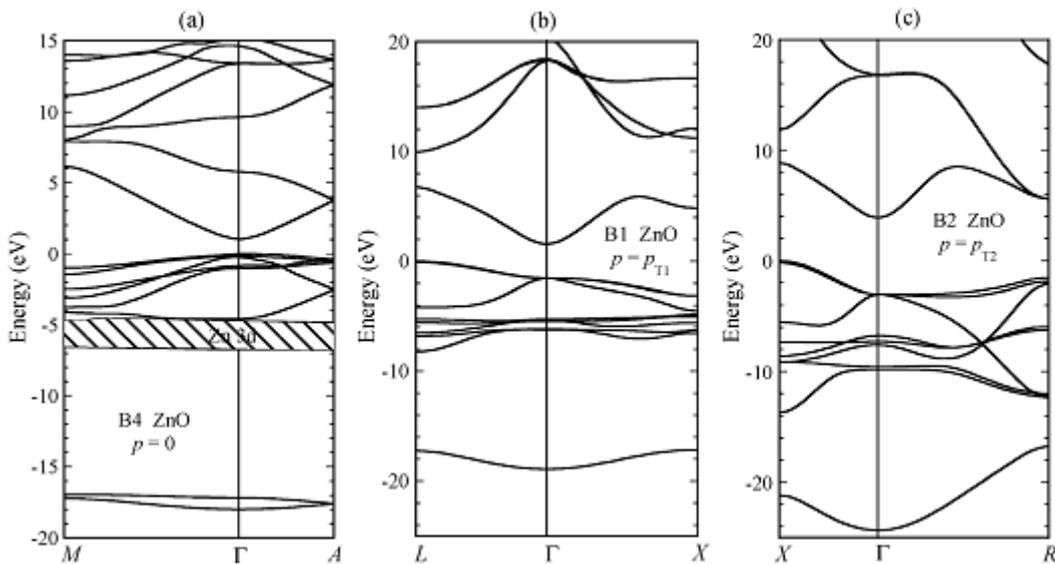
Figure I.7 *Band structure for ZnO : (a) B4 structure at p = 0, (b) B1 structure at p=p_{T1} , (c) B2 structure at p= p_{T2}. [24].*

I.7.1.3 Optical Properties of ZnO :

ZnO is a material transparent in the visible, it is of considerable interest that resides in its excellent properties such as the width of its forbidden band; which permits transmission of ultraviolet to visible. On the other hand, the direct gap induces very efficient radiative recombination [22].

In thin layers, we can distinguish three zones according to the spectrum of the reflection and transmission of ZnO:

-In the ultraviolet, there is a total absorption of the light by the electrons of the valence band that transit to the conduction band. Transmission decreases rapidly and vanishes.

-In the visible, the transmission is high; while the absorption is very low.

-In-infrared absorption by free carriers area is characterized by low transmission zero and high reflection . [23]

The figure 1.8 (curve) summarizes the different transmission zones:
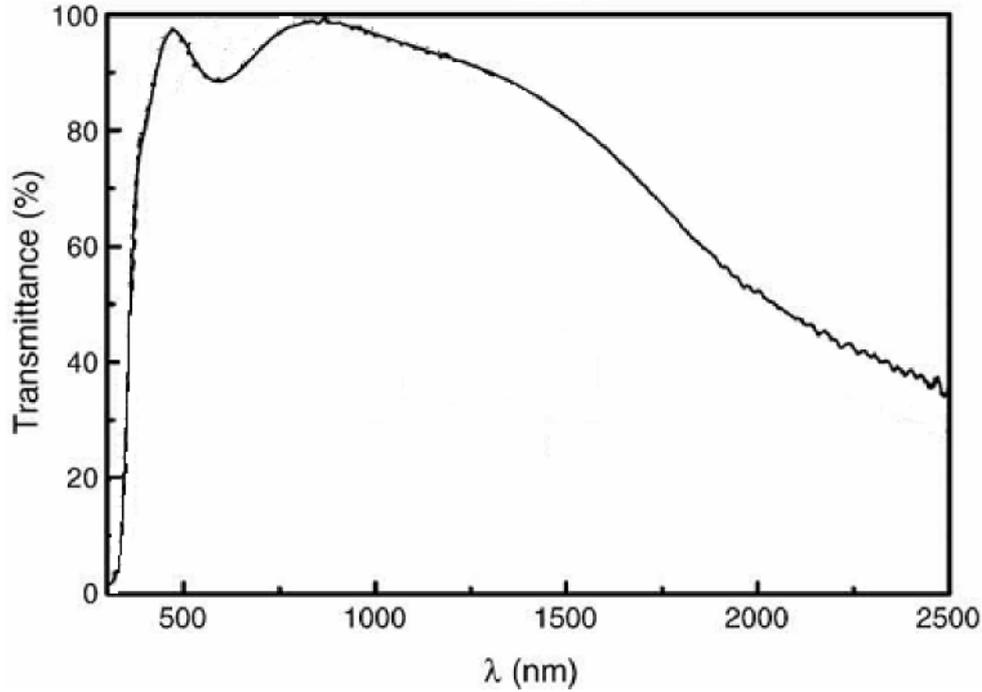
Fig.I.8) Transmission of optical thin film ZnO: Al annealed at 500 ° C [25].

The refractive index n of ZnO, which is defined as the ratio between the velocities of the electromagnetic waves (light) in a vacuum (c = 3.10 ^{8} m / s) and the solid ZnO (v) is equal to:

$$n = c \, / \, v = 2 \qquad \text{(I.6)} \quad [33].$$

Thin film has a value between 1.7 and 2.2. The value of the index n and the absorption coefficient is dependent on the conditions of elaboration of the thin layers. The optical absorption coefficient is defined by the ratio between the absorbance and the optical path length traversed by an electromagnetic wave in a given medium [14]. The refractive indices of the film are determined from the values of transmissions corresponding to the position of the first minimum of transmission [27].

$$n = \left[\sqrt{n_0 n_2} \left(\frac{1 + \sqrt{1 - T_{min}}}{\sqrt{T_{min}}} \right) \right]$$

$$\text{(I.7)}$$

n_0: Index of refraction of vacuum

n_2: refractive index of the substrate

The wavelengths corresponding to the minima of the first transmission wave is used to determine the thickness **d** of films; and this after calculating **n** [27].

$$nd = \left[\frac{1}{4}(2m + 1)\lambda\right]$$

(I.8)

Were .λ. is the wavelength.

m = (0, 1, 2,3) is the order of the minima.

I.7.2. APPLICATION OF ZNO THIN FILMS:

Nowadays , the use of ZnO as thin layers became frequent in technology : Whether in electronics, optics, chemistry , or mechanics. ZnO thin film now occupies a prominent place in what follows we include some of the main applications:

• ZnO thin films are used as electrical contact to the transparent thin film solar cells of amorphous silicon and / or microcrystalline and they may be used in photovoltaic solar cells [28] . Moreover they are used in varistors and in electronic devices such as rectifiers and filters. They are also used in telecommunications in the resonators (for Radio Communications) , and in the image processing as well as devices surface acoustic wave [28] .

• The optical properties of ZnO thin film sensors are operated in the integrated optical waveguides . It can also be used to manufacture ultraviolet photodetector . In this case the layers are often doped aluminum and upon illumination by an appropriate monochromatic light (350 nm) photocurrent is generated.

• Due to their piezoelectric properties , the ZnO thin films can be used as pressure sensor .

• Their chemical properties conferred by their characteristic gas detection [28] , we Example include methane gas which is highly volatile when mixed with air , it may explode due to its flammability . It is 20 times more harmful than CO_2. this is why recent research is underway to detect its presence in our environment and our atmosphere [28] .

Chapter-II

The Deposition Processes And The Characterizations Techniques

In this chapter, we take an interest in the depositions techniques used to develop TCO films. We also describe the various methods adopted for characterizations of their structural and optical properties

II.1. INTRODUCTION TO THIN FILMS:

Over the past two decades, the development of materials in the form of thin films has contributed to an explosion of performance of professional electronics, including reducing the cost of components for mass production. However, since the invention of the transistor in 1947, has seen the integration of several thousands of components (such as semiconductor components). Thereby, to trivialize devices like calculators and personal computers, which provide computing capacity and memory far superior to the first computers.

Thin films can be prepared from a nearly infinite range of compositions such as conductive materials, insulators, refractory (oxyds , nitrides, carbides) and polymers among others. The structure of the deposited films can be mono or multilayer may vary with thickness of an atomic plane (several Angstroms) to several hundreds of micrometers.

The development of a thin layer is a decisive step, because the physical properties of the material depend on it.

II.2. THIN FILM DEPOSITION PROCESSES.

All the processes of deposition of thin layers contain four (sometimes five) successive steps, as the Figure II.1 shows it :
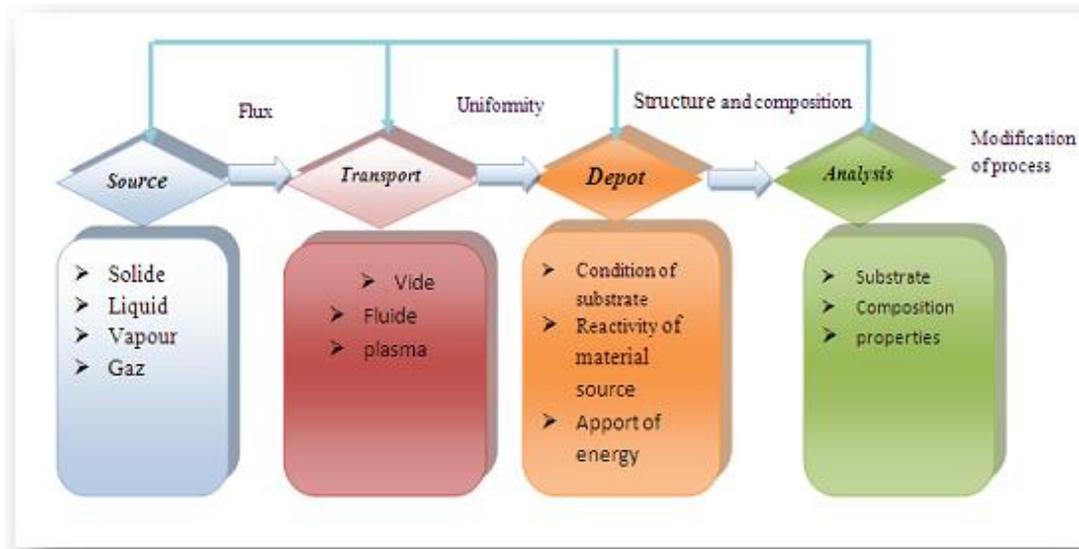
Figure II.1: Diagram presents steps of manufacturing process of thin film [30]

The elaborations methods can be classified in two ways [31,32]:

- Physical methods.

- Chemical methods.

The most commonly used deposition techniques of thin films arising out of these two categories are presented in the following table II.1:

Thin Film Deposition Techniques

PHYSICAL   CHEMICAL

Sputtering	Evaporation	Gas Phase	Liquid Phase
Glow discharge DC sputtering	Vacuum Evaporation	Chemical vapour Deposition	**Electro-deposition**
Triode sputtering	Resistive heating Evaporation	Laser Chemical vapour deposition	Chemical bath deposition (CBD) / **Arrested Precipitation Technique (APT)**
Getter sputtering	Flash Evaporation	Photo-chemical vapour deposition	Electro less deposition
Radio Frequency sputtering	Electron beam Evaporation	Plasma enhanced vapour deposition	Anodisation
			Liquid phase Epitaxy
Magnetron sputtering	Laser Evaporation	Metal-Organo Chemical Vapour Deposition (MO-CVD)	Sol- gel
Ion Beam sputtering			Spin Coating
			Spray-pyrolysis technique (SPT)
A.C. Sputtering	Arc		Ultrasonic (SPT)
	7) R. F. Heating		Polymer assisted deposition (PAD)

Table II.1: Presentation of the principal processes of deposit of thin layers .

Within the framework of this memory, we will present initially some techniques of deposition, while reserving a thorough development with the method by sol gel (spin coating), technique which was selected for this work.

II.2.1.PHYSICAL DEPOSITION:

Physical deposition uses mechanical, electromechanical or thermodynamic means to produce a thin film of solid. Since most engineering materials are held together by relatively high energies, and chemical reactions are not used to store these energies, commercial physical deposition systems tend

to require a low-pressure vapor environment to function properly; most can be classified as physical vapor deposition (PVD).

II.2.1.1 Physical Vapor Deposition :

Physical Vapor Deposition is the transfer of material to be deposited in form of vapor, which is obtained by heating this one by different means:

Joule effect, induction (coupling of a generator high frequency), electron gun, laser beam or electric arc. Evaporation is carried out under a high vacuum (pressure of the order of 10^{-3} with 10^{-4} Pa) with an aim of increasing its speed and to avoid contamination of the films .

As the vapor flow is localized and directional, it is often necessary to print with the substrate a translation or rotational movement compared to the source of evaporation, so as to carry out a homogeneous deposit and uniform thickness. Better results are obtained on surfaces practically perpendicular to the flow of vapor. When the pressure is not sufficiently low the deposits are not very adherent and often amorphous.
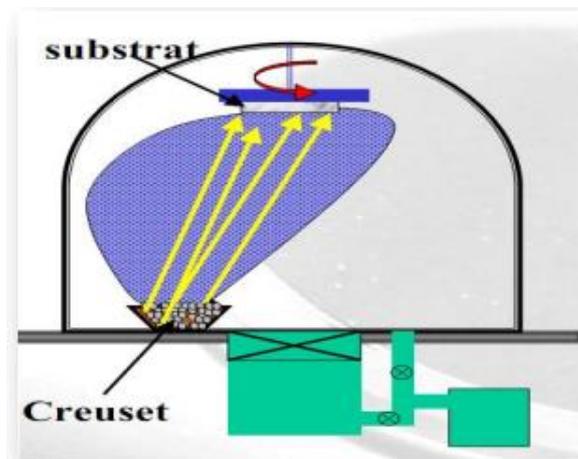
Figure II.2): Vacuum evaporation principle [33]

II.2.1.1.a) Thermal evaporator

The process comprises the uses of an electric resistance heater to melt the material and raise its vapor pressure to a useful range. This is done in a high vacuum, both to allow the vapor to reach the substrate without reacting with or scattering against other gas-phase atoms in the chamber, and reduce the incorporation of impurities from the residual gas in the vacuum chamber. therefor this technique cannot be app lied to high melting point materials and poor thermal conductors *[34]*

II 2.1.1.b) Electron Beam Evaporator

This technique is based in the heat produced by high energy electron beam bombardment on the material to be deposited. The electron beam is generated by an electron gun, which uses the thermoionic emission of electrons produced by an incandescent filament (cathode). Emitted electrons are accelerated towards an anode by a high difference of potential (kilovolts). The crucible itself or a near perforated disc can act as the anode. A magnetic field is often applied to bend the electron trajectory, allowing the electron gun to be positioned below the evaporation line (see diagram, Figure III -3)

As electrons can be focalized, it is possible to obtain a very localized heating on the material to evaporate, with a high density of evaporation power (several kW). This allows to control the evaporation rate, from low to very high values, and best of all, the chance of depositing materials with high melting point (W, Ta, C, etc.). Cooling the crucible avoids contamination problems from heating and degasification. The source of electrons as well as secondary electrons, trapping and electron beam arcing, are the problems associated with this technique .
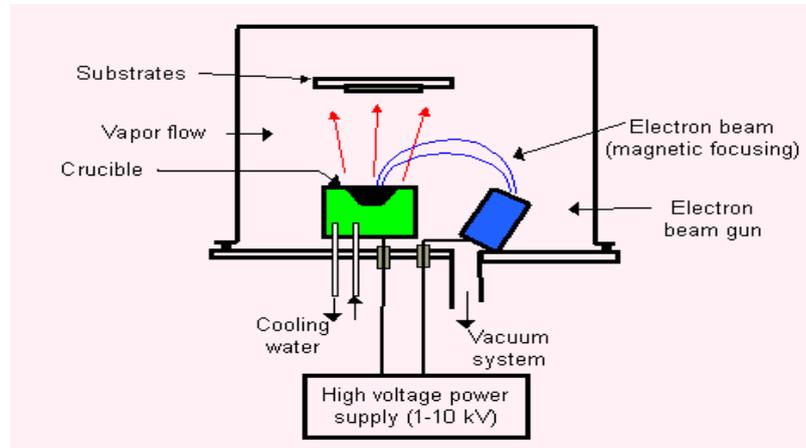
Figure II.3) General diagram of Electron Beam Evaporator [35]

II 2.1 1 .c) Molecular Beam Epitaxy (MBE)

Selected elements, e.g. Ga, As, Al, etc. are heated in vacuum furnaces called effusion cells. Evaporated atoms and molecules leave the cells in collimated beams and impinge on a heated surface of a monocrystalline wafer. Here they enter different processes (physical adsorption, chemisorption,

migration) , undergo transformation (dissociation, association, etc.) and at last form a monocrystal-line lattice. Molecular beams can be interrupted by shutters placed in front of the cell oriffices. By this way it is possible to change composition and properties of grown layers. Some cells usually contain dopant elements (Si and Be for n- or p- doping in GaAs) which control the type of electrical conductivity. Growth process is realized in ultra-high vacuum chamber with ultimate pressure in the order of 10-11 mbar. The chamber is equipped with a number of efussion cells, with manipulator for sample heating (0 – 1000 C$^{\circ}$) and azimuthal rotation, with an electron gun and screen for RHEED and other accessories. Inner chamber walls are surrounded by cryopannels, which are cooled by liquid nitrogen (-197 C°) during the growth.).
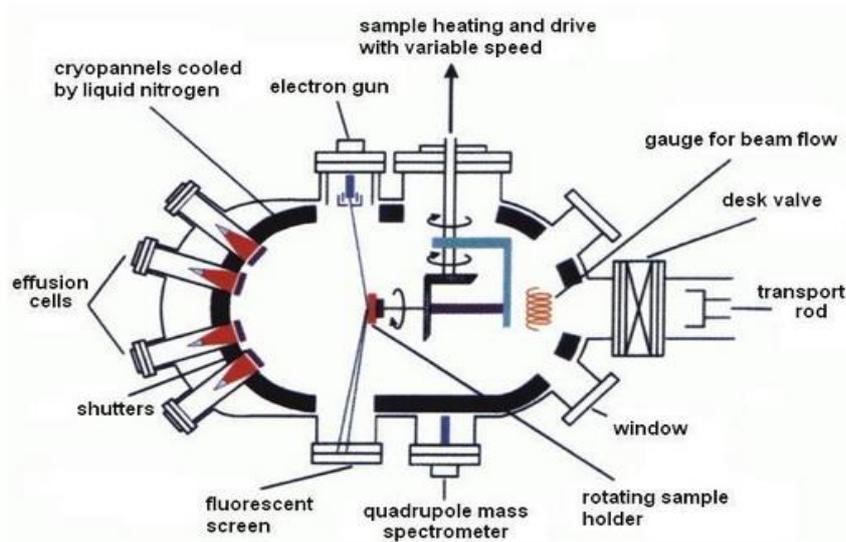
The MBE growth chamber design
The sample is fixed in the chamber center on a rotating holder

Figure II.4) The MBE growth chamber design The sample is fixed in the chamber center

on a rotating holder [36]

II. 2 1. 1.d) Sputtering

Sputtering involves the ejection of material from the impact of particles (ions or atoms) of the material to be deposited . In this technique, the material to be deposited , called the target, is in the form of circular or rectangular plate, fixed by adhesive bonding or soldering to the cathode. The latter is connected to a DC or AC power supply depending on the type of material to be deposited. A gate serving as anode substrate is arranged parallel to the target, at a distance of a few millimeters.

The main parameters influencing the quality of the deposit are: the pressure of the gas used in the chamber, the power of the power which acts on the deposition rate and the substrate temperature [36]
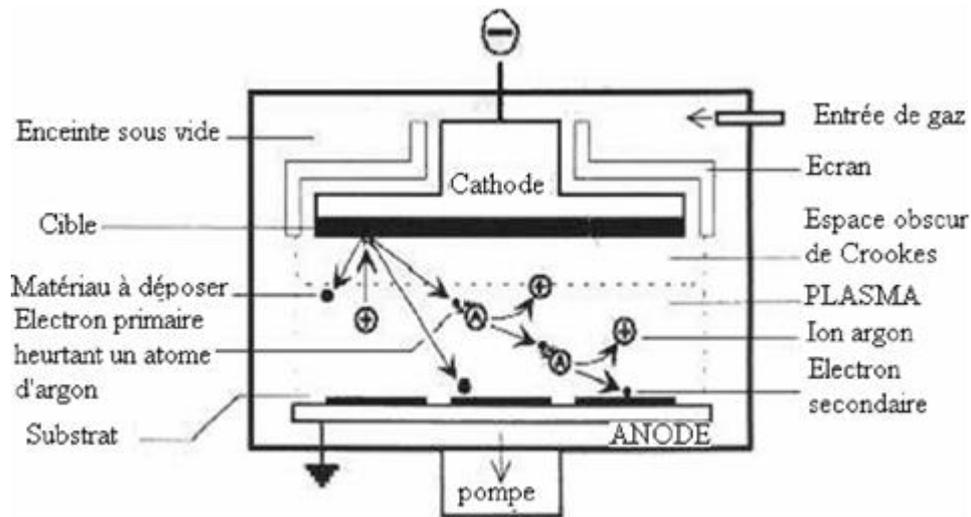
Figure II.5) Schematic of the principle of Sputtering [36]

II 2.1.1 e) Pulsed Laser Deposition:

Systems work by an ablation process. Pulses of focused laser light vaporize the surface of the target material and convert it to plasma; this plasma usually reverts to a gas before it reaches the substrate.
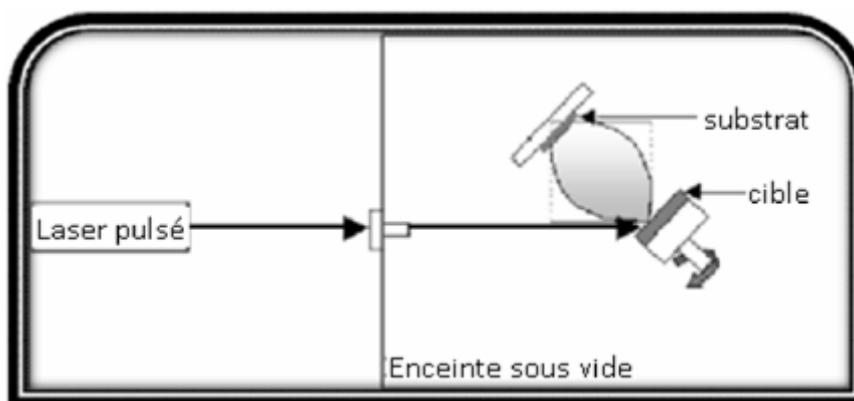
Figure II.6) Schematic of Pulsed Laser Deposition [37]

II 2.1.1.F) Cathodic Arc Deposition(Arc-Pvd)

Which is a kind of ion beam deposition where an electrical arc is created that literally blasts ions from the cathode. The arc has an extremely high power density resulting in a high level of ionization

(30–100%), multiply charged ions, neutral particles, clusters and macro-particles (droplets). If a reactive gas is introduced during the evaporation process, dissociation, ionization and excitation can occur during interaction with the ion flux and a compound film will be deposited.
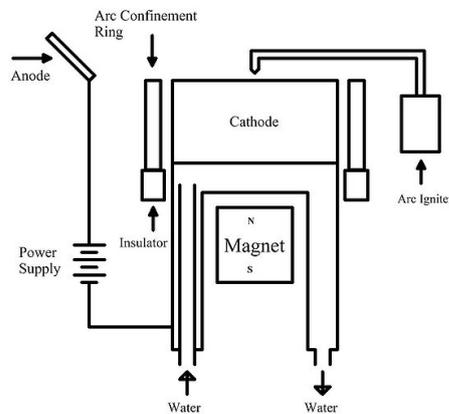
Figure II.7) Cathodic Arc Source (Sablev type) [38]

II.2.2 CHEMICAL DEPOSITION:

Here, a fluid precursor undergoes a chemical change at a solid surface, leaving a solid layer. An everyday example is the formation of soot on a cool object when it is placed inside a flame. Since the fluid surrounds the solid object, deposition happens on every surface, with little regard to direction; thin films from chemical deposition techniques tend to be *conformal*, rather than *directional*.

Chemical deposition is further categorized by the phase of the precursor:

II.2.2.1)Chemical Vapor Deposition (Cvd)

Generally uses a gas-phase precursor,The volatile compounds of material to be deposited are possibly diluted in a carrying gas (often a halide or hydride of the element to be deposited)   and introduced into an enclosure where the substrates are placed. The film is obtained by reaction chemical enters the phase vapor and the heated substrate. In certain cases, a rise in temperature is necessary to maintain the reaction chemical. The CVD is a field interdisciplinary, it includes/understands a whole of chemical reactions, a process thermodynamics and kinetics, phenomenon of transport. The chemical reaction is with center these disciplines: it determines nature, the type and the species present ,   For example In the case of MOCVD, an organometallic gas is used.

II.2.2.1. a) *Plasma enhanced CVD (PECVD)*

Plasma-enhanced chemical vapor deposition (PECVD) is a process used to deposit thin films from a gas state (vapor) to a solid state on a substrate. Chemical reactions are involved in the process, which occur after creation of a plasma of the reacting gases. The plasma is generally created by RF (AC) frequency or DC discharge between two electrodes, the space between which is filled with the reacting gases.
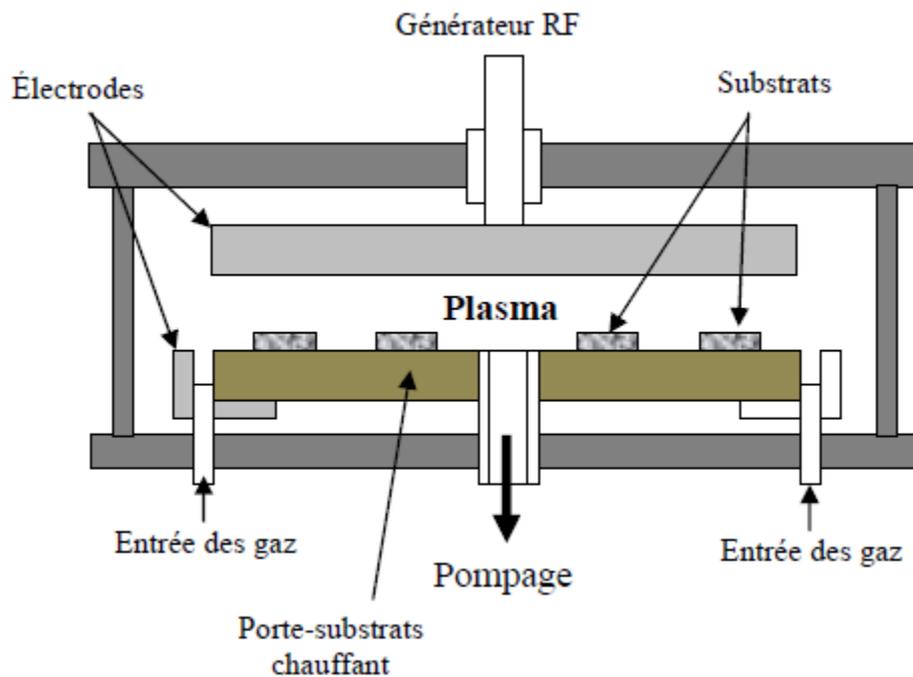
Figure II.9) Principe of the PECVD system [39]

II .2.2.2) *Pyrolysis spray technique*

A solution containing the various constituents of the material to be deposited is sprayed into fine droplets, either by a conventional pneumatic system or by an atomizer using an ultrasonic generator. These systems convert the solution into a spray of very fine droplets of a few tens of microns in diameter. The jet enters the substrate surface heated to a temperature sufficient for decomposition of the dissolved products in the solution and enable the reactions that produce the desired material. A these temperatures, some products of the reactions will be immediately removed (volatile components), it only remains that the compound to be deposited on the substrate *[45]*
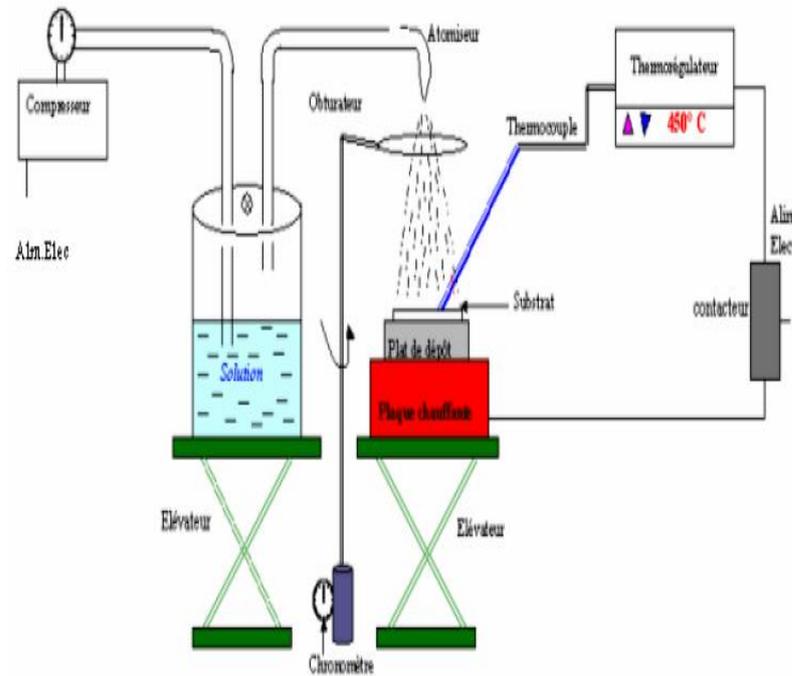
Fig II.10 : pyrolysis spray [40]

II.3 .CHARACTERIZATION TECHNIQUES OF THIN FILMS :

II.3.1)STRUCTURAL CHARACTERIZATION AND MEASURMENT:

For the structural characterization, crystallographic orientation and determination of the size average of the grains we made the recording diagrams of X-ray diffraction (XRD) of the samples, and compare it with the ASTM files .

II.3.1.1) X- Ray Diffraction (XRD) Technique :

X-ray powder diffraction (XRD) is a rapid analytical technique primarily used for phase identification of a crystalline material and can provide information on unit cell dimensions. The analyzed material is finely ground, homogenized, and average bulk composition is determined.

X-ray diffractometers consist of three basic elements: an X-ray tube, a sample holder it may be powder, single crystal or thin film., and an X-ray detector. *Figure (II.11 .a , b)*

a)   b)
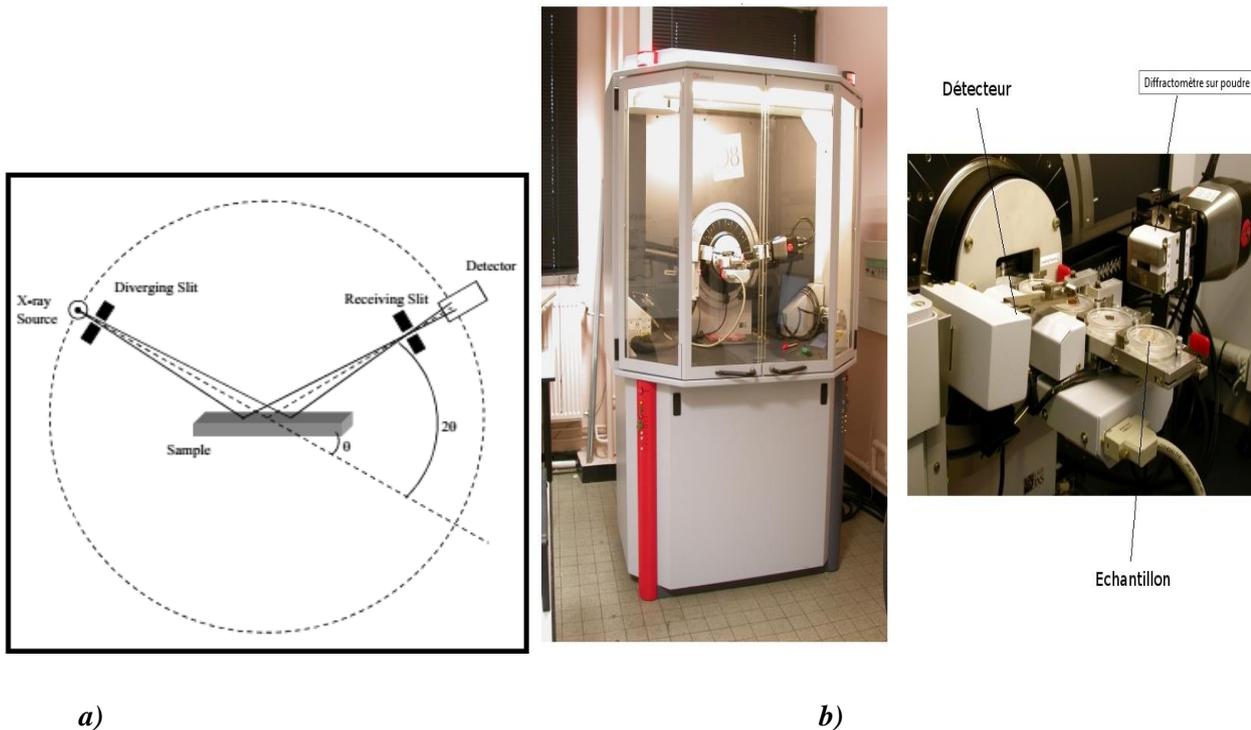
Figure II.11) a) Schematics of X-ray diffractometer. [41] b) Bruker's X-ray Diffraction D8-Discover instrument[36]

X-rays are generated in a cathode ray tube by heating a filament to produce electrons, accelerating the electrons toward a target by applying a voltage, and bombarding the target material with electrons. When electrons have sufficient energy to dislodge inner shell electrons of the target material, characteristic X-ray spectra are produced. These spectra consist of several components, the most common being K_α and K_β. K_α consists, in part, of $K_{\alpha 1}$ and $K_{\alpha 2}$. $K_{\alpha 1}$ has a slightly shorter wavelength and twice the intensity as $K_{\alpha 2}$. The specific wavelengths are characteristic of the target material (Cu, Fe, Mo, Cr). Filtering, by foils or crystal monochromers, is required to produce monochromatic X-rays needed for diffraction. $K_{\alpha 1}$ and $K_{\alpha 2}$ are sufficiently close in wavelength such that a weighted average of the two is used. Copper is the most common target material for single-crystal diffraction, with CuK_α radiation = 1.5418Å. These X-rays are collimated and directed onto the sample. As the sample and detector are rotated, the intensity of the reflected X-rays is recorded. When the geometry of the incident X-rays impinging the sample satisfies the Bragg Equation Eq (II.1) **,** constructive interference occurs and a peak in intensity occurs. A detector records and processes this X-ray signal and converts thesignal to a count rate which is then output to a device such as a printer or computer monitor. *[41]*
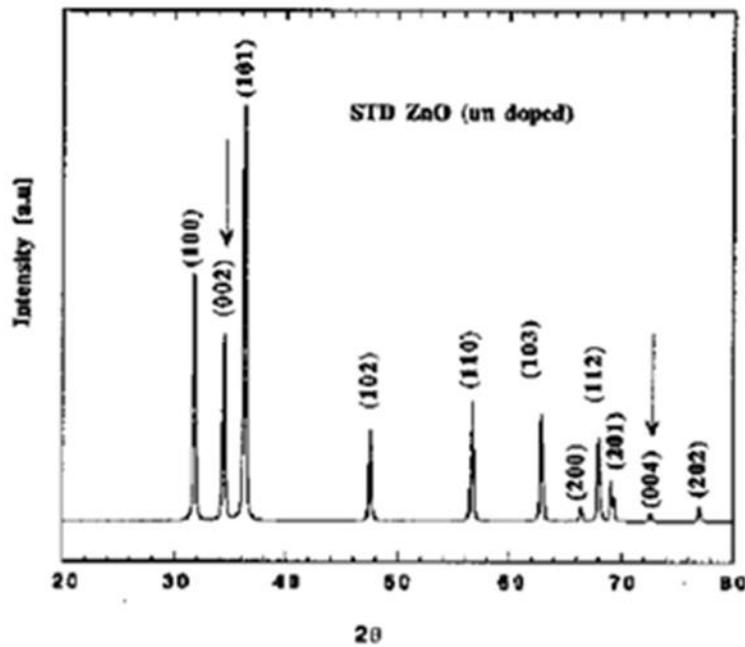
Figure II.12) Spectrum of X-ray diffraction (XRD) , by a ZnO stoichiometric powder. (ASTM 36-1451) [41]

The geometry of an X-ray diffractometer is such that the sample rotates in the path of the collimated X-ray beam at an angle θ while the X-ray detector is mounted on an arm to collect the diffracted X-rays and rotates at an angle of 2θ. The instrument used to maintain the angle and rotate the sample is termed a *goniometer*. For typical powder patterns, data is collected at 2θ from ~5° to 70°, angles that

are preset in the X-ray scan. *[41]*

the Bragg Equation

$$2d_{hkl} \sin\theta = n\lambda \qquad\qquad (II.1)$$

d_{hkl} = interplaner spacing

h,k,l= Miller's indices

θ= diffraction angle

λ= wavelength of x-ray

n = order of diffraction
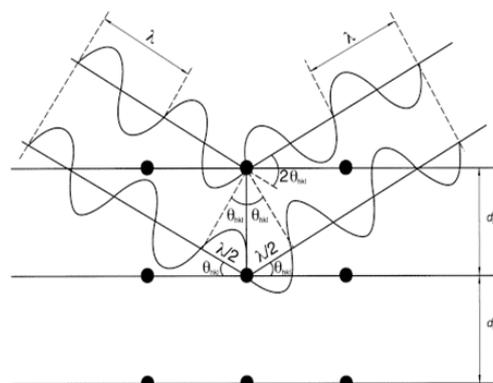
Figure 2.9.33.-1. – Diffraction of X-rays by a crystal according to Bragg's law

Figure II.13) Diffraction of X-rays by a crystal according to Bragg's law [42]

II.3.1.2) Structural Measurement:

II.3.1.2.a) Determination of the interreticular distances and the cell parameters :

The X- ray diffraction data can be used to determine the dimension of the unit cell. , were The relation connecting the interreticular distances of the plans (hkl) to the crystallographic parameters is as follows (for or hexagonal wurtzite structure):

$$d_{hkl} = \frac{a}{\sqrt{4/3(h^2+k^2+hk)+l^2\frac{a^2}{c^2}}}$$ (II.2)

and

$$\frac{c}{a} = \sqrt{\frac{8}{3}} = 1.63$$ (II.3)

d $_{hkl}$ = interplaner spacing (interreticular distance) used in Barrg's law

a,c = the cell parameters

h,k,l = Miller's indices

II.3. 2.1.b) Determination of the grains size:

The crystallite size of the deposits is estimated from the full width at half maximum (FWHM) of the most intense diffraction line by Scherrer's formula as follows [28]

$$D = \frac{0.9\lambda}{\beta cos\theta}$$ (II.4)

where, D is crystallite size, λ is wavelength of X-ray used, β is full width at half maxima of

the peak (FWHM) in radians, θ is Bragg's angle. [43]
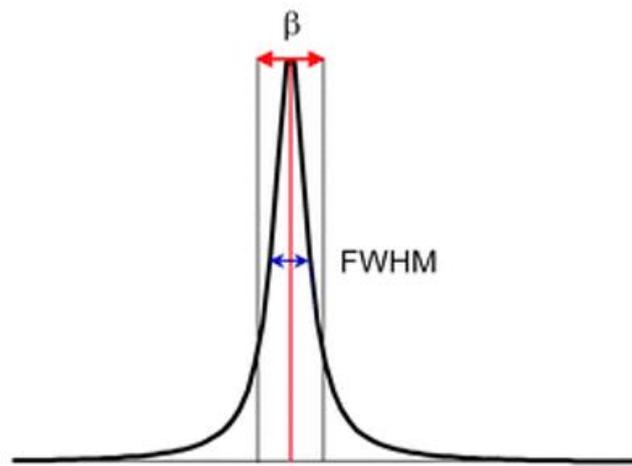
Figure II.14): Illustrate the peak widths FWHM (ΔΘ=β). [37]

II.3.2.1.d) Stress determination :

The measurement of the cell parameters will give an indication on the stresses state of the films . the internal stresses can be calculated starting from the following expression:

$$\sigma = \left[2.c_{13} - \frac{(c_{11} + c_{12}).C_{33}^{film}}{c_{13}} \right].e_{ZZ} \qquad (II.5)$$

With :
$$c_{33}^{film} = \frac{0.99\ c_{33}^{cristal}}{(1 - e_{ZZ})^4} \qquad (II.6)$$

$$e_{ZZ} = \frac{c_0 - c}{c} \qquad (II.7)$$

with e_{ZZ} is the strain , and C_{ij} are elastics constantes , for example for ZnO :

$C_{11,}C_{12,}C_{13}$ and C_{33}, the values are 209.7 GPa ,121.1GPa, 105.1 GPa then 210.9 GPa respectively

II.3.2) OPTICAL CHARACTERIZATION AND MEASURMENT:

The fields of spectroscopy are generally distinguished by the range of wavelength in the measuring process is made , in our case the fields are distinguished, ultraviolet, visible and infrared.

The measurement of transmittance of the sample was carried out with UV-VIS-NIR dual beam spectrophotometer type (UVI-3101 PC SHIMADZU). Which its working principle are shown **in**

figure (II.17).
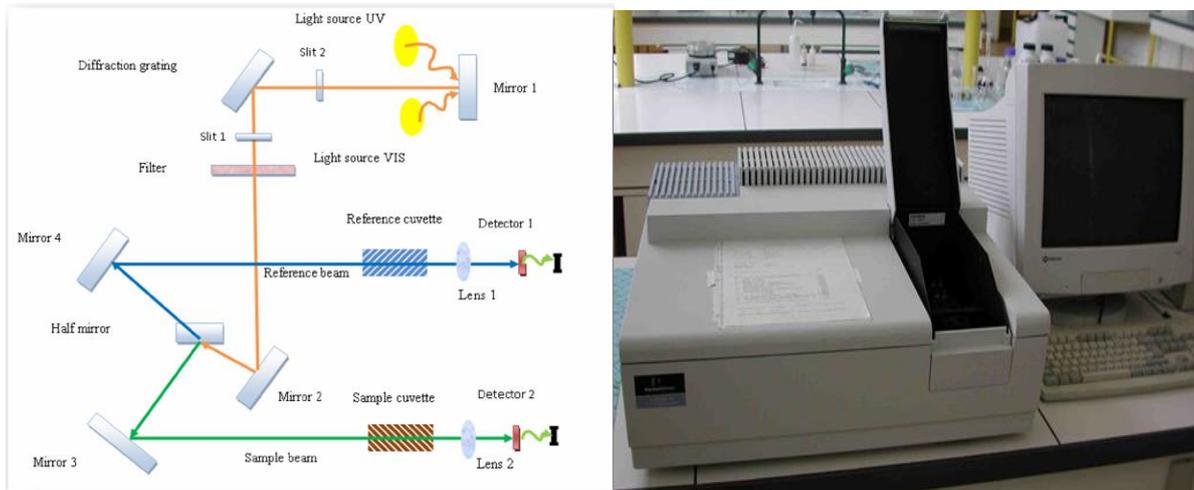
Figure II.15) The principle of operation of UV-visible spectrophotometer [30]

By exploiting the curves representing the variation of the transmittance (T%) in function of the wave-length(nm) , and by using some relation , it is possible to calculate, the thickness of the films , thresh-old of optical absorption hence optical gap , the absorption coefficient, the refractive index, the energy of Urbach (E_{00} , the disorder) .

II.3.2. 1). THE THICKNESS OF THE FILM:

There are several ways to measure the thickness of thin layers, including:

II.3.2.1.A) The Approximate Gravimetric Method

The thickness of the thin films can be calculated with :

Using the approximate gravimetric method, where the weight measurement of the substrate before and after deposition using a very sensible balance , and with the knowledge of the density of the material (thin film) and the surface of substrate, using the following relationship:

$$t=\frac{\Delta m}{Pt \times A_0} \tag{II.8}$$

t*: the thickness of the thin film ,* ***P_t*** *: the density of the film ,* ***A_0*** *: the surface of the substrate*

II.3.2.1.B) The Interference Fringes Method

We can determine the film thickness as follows:

$$d = \lambda 1 \lambda 2 / 2 (2n1 - \lambda 1 n2) \qquad \text{(II-9)}$$

$n1$ and $n2$ are the refraction index of the film for the wavelength $\lambda 1$ and $\lambda 2$

We can calculate $n1$ and $n2$ from the following relation:

$$n_{1(2)} = [N_{1(2)} + (N^2_{1(2)} - S^2)^{1/2}]^{1/2} \qquad \text{(II.10)}$$

And

$N1(2)$ can be obtained using this relation:

$$N_{1(2)} = 2S(T_M - T_m) / T_M T_m + (S^2 + 1) / 2 \qquad \text{(II.11)}$$
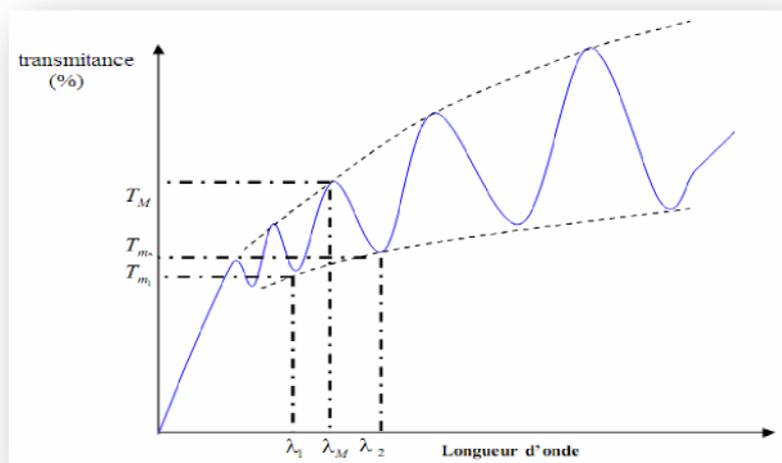
Fig.II.16): Method of interference fringes of s to determinate the thickness [36]

II.3.2.1.C) Spectroscopic Ellipsometry

The ellipsometry (Figure II.5) is a technique based on optical analysis the interaction of a laser with the surface of the sample beam. The apparatus comprises a laser source (He-Ne; $\lambda = 6328$Å), a polarizer, an analyzer, a compensator, a filter and a detector. One can set the angle of incidence of the laser beam to 30,50, or 70 °. Once the unit is turned on, we fix the arms of the polarizer and the analyzer

angle 70 ° and then moves the sample so that the reflected beam is centered on the orifice of the analyzer , the drum is operated and the polarizer of the analyzer to have a maximum extinction of the reflected beam at the detector, and identifies the azimuths of the apparatus, a software (ELIPSO AU-TOST-) is used to calculate the thickness of layer and its refractive index [30]..

II.3.2.3) The Optical Gap :

From the transmittance spectrum in the UV-visible, one can quickly determine the optical gap .

In high energy, absorption results from electronic transitions between wide states of band to band. It is usually described by Tauc law:

$$(\alpha h\upsilon) = A \, (h\upsilon - E_{00})^m \qquad\qquad (\text{I-4})$$

Where: $h\,\upsilon$ is the photon energy, E_g is optical gap m and A are constants. m characterizes the optical type of transition and takes the values ½ for allowed direct transitions or 2 for allowed indirect transitions.

In order to determine the nature of the transition from films produced in this study, we will plot the curves $(\alpha \, h\upsilon)^2 = f(h\upsilon)$, and by extrapolation to $(\alpha \, h\upsilon)^2 = 0$ we can obtain Eg value (as showing in figure (II.21):
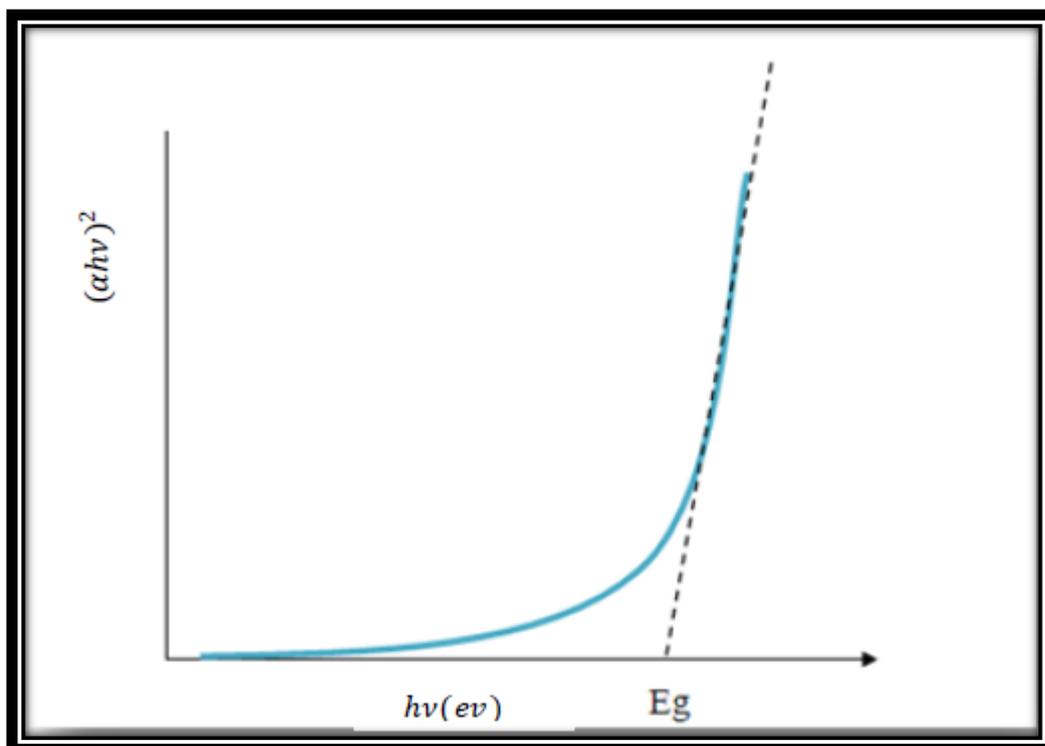
Figure II-17): determination of Eg [30].

II.3.2.2.) The Absorption Coefficient

In the spectral field where the light is absorbed, and by knowing the film's thickness, we can determine the absorption coefficient for each value of transmittance T in (%) which corresponds to energy by the law of Beer-Lambert:

$$T = \frac{I}{I_0} \times 100$$

(II.12)

Where

$$\frac{I}{I_0} = \exp{-\alpha d} = \frac{T}{100}$$

(II.13)

I0 is the incidental light intensity, *I* the transmitted light intensity, α coefficient of absorption and d the thickness of the film. This relation can be written:

$$\alpha = \frac{1}{d} \ln\left(\frac{I_0}{I}\right)$$

(II.14)

If we express *T(λ)* in (%), this expression becomes:

$$\alpha = \frac{1}{d} \ln\left(\frac{100}{T}\right)$$

(II.15)

This approximate relation is established, by neglecting the reflexions with all interfaces; air/film, air/substrate. [30].

II.3.2.4) Disorder calculating

An other important parameter, which characterizes the material disorder, is Urbach energy. According to the Urbach law of the expression of the absorption coefficient is as follow:

$$\alpha = \alpha_0 \exp[h\upsilon/E_{00}]$$

(II-17)

By drawing the **ln(α)** on function of *hν* , one can determinate **E_{00}** value[44] :

$$\ln\alpha = \ln\alpha_0 + h\upsilon E_{00} \qquad\qquad (\text{II-18})$$

The following figure presents how we can estimate E_{00}
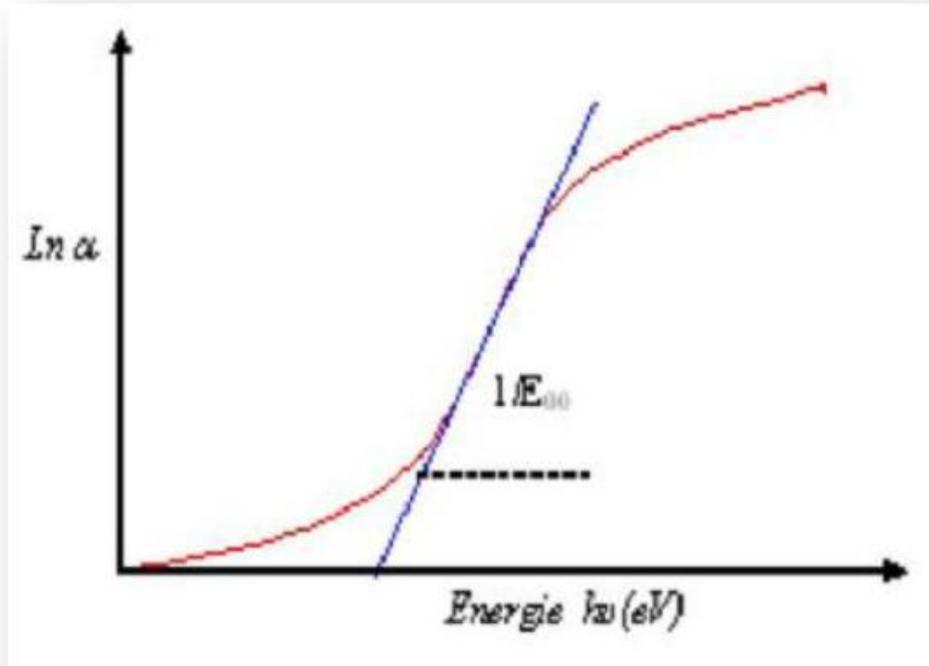
Figure II.18): Determination of the disorder by extrapolation starting from the variation of

ln(α) has in function of hv [45].

Chapter-III:
The Sol Gel Process

In this chapter, we focus on the deposition technique used in this work ; know this way, its steps, the chemical reactions and all factors influential in this Method

III.1)SOL GEL PROCESS :

Sol–gel processes are particularly adapted to produce ZnO colloids [47,48] and films [46,49,50] in a simple, low-cost and highly controlled way. The sol–gel process, called also soft chemistry, allows elaborating a solid material from a solution by using a sol or a gel as an intermediate step (Scheme 1), and at much lower temperatures than is possible by traditional methods of preparation. It enables the powderless processing of glasses and ceramics, and thin films or fibres directly from solution. The synthesis of solid materials via 'soft chemistry' often involves wet chemistry reactions and sol–gel chemistry based on the transformation of molecular precursors into an oxide network by hydrolysis and condensation reactions [51,52].

Scheme IV. 1) shows the main steps of preparation of thin films and powder by the sol–gel process. We can summarize, for example, the film preparation in three parts: (i) preparation of the precursor solution; (ii) deposit of the prepared sol on the substrate by the chosen technique; and (iii) heat treatment of the xerogel film. The xerogel is the dried gel at ambient pressure (the dried gel in supercritical conditions is called aerogel).
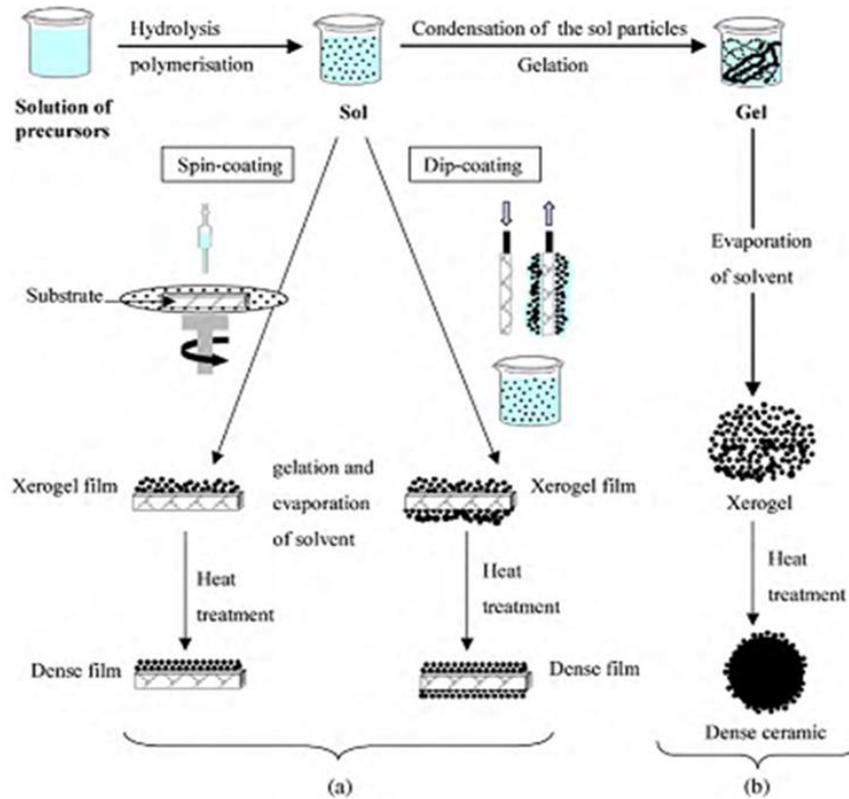
Fig IV. 1. *Overview showing two synthesis examples by the sol–gel method; (a) films from a colloidal sol; (b) powder from a colloidal sol transformed into a gel [59]*

In the sol–gel process, a molecular precursor in a homogeneous solution undergoes a succession of trans-formations: (a) hydrolysis of the molecular precursor; (b) polymerization via successive bimolecular additions of ions, forming oxo-, hydroxyl, or aqua-bridges; (c) condensation by dehydration; (d) nucleation; and (e) growth [53,54]. Depending on the nature of the molecular precursors, two sol–gel routes are currently used: metal alkoxides in organic solvents or metal salts in aqueous solutions [51]. The main methods of ZnO film elaboration, as reported in the literature, involve several steps and are in fact intermediate between the two sol–gel methods since they use metal salts in alcoholic solutions. Indeed, ZnO films are obtained starting from inorganic salts –nitrates, chlorides, perchlorates – or organic salts like acetates and acetyl acetonates, dissolved in alcoholic media. It is believed that in such media the process involves two steps. The first one consists of insitu formation of alkoxide or lkoxy-complexes. In the second step, these complexes undergo transformation through hydrolysis and polymerization to lead to the oxide.

➢ Table (IV. 1) summarizes the sol–gel undoped ZnO thin film elaboration methods including chemical systems used and results concerning crystallographic orientation.

References	Precursor (mol L^{-1})	Alcohol	Additive (r)	H$_2$O (h)	Aging time	Substrate	Pre-heat treatment (°C)	Post-heat treatment (°C)	Thickness (nm)	Crystallographic orientation
Natsume and Sakata [61]	ZAD (0.02)	MeOH	-	-	-	Pyrex	80	500–575	160–230	(0 0 2)
González et al. [62]	ZAD (0.59)	MeOH	-	-	24 h	Corning glass	50	300, 450 150	35–204	(1 0 0)(0 0 2)(1 0 1) (**1 0 0**)(0 0 2)(1 0 1)
Santos et al. [63,64]	ZAD[a]	MeOH	-	-	-	Glass	120	350	(18L)[a]	(0 0 2)
Sagar et al. [65,66]	ZAD (0.6)	MeOH	MEA (0–1)	-	48 h	Corning glass	300	400–600	180–190	(0 0 2)
Liu et al. [67,68]	ZAD (0.6)	EtOH, PEG (14 g/L)	DEA (1)	(2)	-	Glass	100	500	220 (6L)	(1 0 0)(0 0 2)(**1 0 1**)
Wang et al. [69]	ZAD (0.5)	EtOH	DEA (1)	-	-	Quartz	400	400–800	300 (6L)	(1 0 0)(0 0 2)(**1 0 1**)
Kumar et al. [70]	ZAD (0.2)	EtOH	DEA (1)	-	48 h	p-Si(1 0 0)	250	350–450	~250	(1 0 0)(**0 0 2**)(1 0 1)
Shaoqiang et al. [4]	ZAD (0.46)	EtOH	-	-	-	n- and p-type Silicon	40	500 (directly) 500 (Gradually)	200	(0 0 2) (1 0 0)(**0 0 2**)(1 0 1)
Znaidi et al. [47,48]	ZAD (0.05)	EtOH	MEA (2)	-	72 h	Glass	100–135	450	-	(1 0 0)
Wang et al. [71]	ZAD (1.8)	EtOH	MEA (1.5)	-	72 h	Glass	300	350–600	(5L)[a]	(1 0 0)(0 0 2)(1 0 1)
Wang et al. [72]	ZAD (0.19)	EtOH	Ac. Ac. (0.35)	(11.1)	24 h 2 h	Glass	100	450	-	(1 0 0) Amorphous film
Bao et al. [46]	ZAD (0.4)	EtOH	Lactic Ac.	-	-	Quartz	300	500, 550 450, 600	300 (6L)	(0 0 2) (1 0 0)(0 0 2)(1 0 1)
Bole and Patil [73]	ZAD[a]	EtOH	Lactic Ac.	-	-	Glass	300	300–425	375–275	(**1 0 0**)(0 0 2)(1 0 1)
Kavanagh and Cameron [74]	ZAD[a]	EtOH	Lactic Ac.	(2)	-	Silicon	240	700	-	(1 0 0)(0 0 2)(1 0 1)
Bahadur and Rao [75]	ZAD[a]	EtOH	LiOH·H$_2$O	-	-	F:SnO$_2$	80	400	800 (5L)	(1 0 0)(0 0 2)(**1 0 1**)
Brenier and Ortéga [76]	ZAD (0.15)	1-PrOH	TMAH	-	4 weeks	Silicon	80	250 (O$_2$)	20–60	(1 0 0)(0 0 2)(**1 0 1**)
Peterson et al. [77]	ZAD (0.3)	1-PrOH	Glycerol	-	-	Si(1 0 0), quartz	300	700	180 (4L)	(1 0 0)(**0 0 2**)(1 0 1)
Raoufi et al. [78]	ZAD (0.3)	1-PrOH	MEA (1)	-	-	Glass	250	300–500	500 (8L)	(1 0 0)(**0 0 2**)(1 0 1)
O'Brien et al. [79] and Rao et al. [80]	ZAD (0.3–0.7) (1.3)	2-PrOH	MEA (1)	-	24 h	UV fused silica	60	450–650	84–437	(1 0 0)(0 0 2)(1 0 1) (1 0 0)(0 0 2)(**1 0 1**)
Kim et al. [3]	ZAD (0.3–0.5) (0.7) (1–1.3)	2-PrOH	MEA (1)	-	24 h	Corning glass	250	650	-	Amorphous film (1 0 0)(0 0 2)(1 0 1) (1 0 0)(0 0 2) (1 0 1)[b]
Lin and Kim [81]	ZAD (0.5)	2-PrOH	DEA (1)	-	24 h	Si(1 0 0), Glass Si(1 0 0)	300	450–550 700, 800	280 (7L)	(1 0 0)(0 0 2) (1 0 1)[b] (1 0 0)(**0 0 2**)(1 0 1)
Aslan et al. [82]	ZAD (0.4)	2-PrOH	DEA (1)	(0.5)	-	Glass	250	450–550	1000–1600 (10–15L)	(1 0 0)(0 0 2)(1 0 1)
Chakrabarti et al. [83]	ZAD (0.24)	2-PrOH	DEA (0.006)	-	-	Glass p-Si(1 0 0), Soda-lime, quartz, alumina	100	550 700	-	(0 0 2) (1 0 0)(0 0 2)(1 0 1)
Jiwei et al. [84]	ZAD (0.4)	2-PrOH	DEA (1)	(2)	-	SiO$_2$/Si(1 1 1), fused-quartz	200 (O$_2$)	300–650 (O$_2$)	230–350	(1 0 0)(0 0 2)(1 0 1)
Wang et al. [85]	ZAD (0.32)	2-PrOH	DEA (1)	-	-	Si/SiO$_2$/Ti/Pt	300–450	550–800	500 (6L)	(1 0 0)(0 0 2)(1 0 1)
Bae and Choi [86]	ZAD (0.25)	2-PrOH	DEA (1.5)	-	-	Alumina	300	400–900	125–240 (3–6L)	(1 0 0)(0 0 2) (1 0 1)[b]
Ohya et al. [44,87] and Takahashi et al. [88]	ZAD (0.25/0.5)	2-PrOH	DEA (1)	(2)	-	Glass	110	350–600	13–33/L	(1 0 0)(0 0 2)(1 0 1)
Mridha and Basak [89]	ZAD (0.1)	2-PrOH	DEA	-	-	Glass	120	550	260	(1 0 0)(0 0 2)(1 0 1)
Dutta et al. [90]	ZAD (0.03–0.1)	2-PrOH	DEA	-	-	Glass	350	550	36–247	(1 0 0)(0 0 2)(**1 0 1**)
Basak et al. [91]	ZAD (0.6)	2-PrOH	DMA	-	-	Sapphire	120	550	300 (10L)	(1 0 0)(0 0 2)(1 0 1)
Ghosh et al. [6,92,93]	ZAD (0.6)	2-PrOH	DMA	-	-	Quartz Glass, Si/SiO$_2$ GaN	120	550	400 (10L)	(1 0 0)(0 0 2)(**1 0 1**) (1 0 0)(0 0 2)(1 0 1) (0 0 2)
Zhang et al. [94]	ZAD (0.3)	PVA	-	-	-	Si(1 0 0)	120	600	434	(1 0 0)(**0 0 2**)(1 0 1)
Pal and Sharon [95]	ZA (<0.03)	2-PrOH	NaOH (1)	-	-	Glass	-	400	(5–6L)[a]	(1 0 0)(0 0 2)(**1 0 1**)
Abdel Aal et al. [96]	ZAD[a]	2-PrOH	NaOH	-	-	Glass	-	550	(6L)[a]	(0 0 2)
Caglar et al. [97]	ZAD (1)	2-ME	MEA (1)	-	-	p-type single crystal Si	300, 450	550–750	(10L)[a]	(1 0 0)(0 0 2)(1 0 1)
Ohyama et al. [98]	ZAD (0.75)	2-ME	MEA (1)	-	-	Silica	300	600	100–260	(0 0 2)
Li et al. [99,100]	ZAD (0.75)	2-ME	MEA (1)	-	-	Silica	300	600	300 (7L)	(0 0 2)
Zhu et al. [101]	ZAD (0.75)	2-ME	MEA (1)	-	-	Glass	60	400–550	(4L)[a]	(1 0 0)(0 0 2)(1 0 1)
Fujihara et al. [102]	ZAD (0.75)	2-ME	MEA (1.1)	-	-	Glass	400–500	400–500	200 (5L)	(0 0 2)
Znaidi et al. [47,48]	ZAD (0.75)	2-ME	MEA (2)	-	-	Glass	300	500–550	76 (3L)	(0 0 2)
Ohyama et al. [45]	ZAD (0.6)	2-ME	MEA (1) DEA (1)	-	-	Silica	500	500	-	(0 0 2) (1 0 0)(0 0 2) (1 0 1)[b]
Nagase et al. [103]	ZAD (0.6)	2-ME	MEA (1)	-	-	Quartz	200	Laser irradiation	35–190	(0 0 2)
Hsieh et al. [104,105]	ZAD (0.6)	2-ME	MEA (1)	-	-	SiO$_2$/Si	270	600–900	-	(1 0 0)(0 0 2)(1 0 1)
Yoon et al. [106]	ZAD (0.5)	2-ME	MEA (1)	-	72 h	SiN$_x$/Si, Pt(1 1 1)/Si	300	700	140 (5L)	(0 0 2)

Table 1 (*Continued*)

References	Precursor (mol L^{-1})	Alcohol	Additive (r)	H$_2$O (h)	Aging time	Substrate	Pre-heat treatment (°C)	Post-heat treatment (°C)	Thickness (nm)	Crystallographic orientation
			DEA(1)			SiN$_x$/Si,				(100)(002) (101)^b
			DEA(1)			Pt(1 1 1)/Si				(002)
Choi et al. [107]	ZAD (0.5)	2-ME	MEA(1)	-	-	Pt/TiO$_2$/SiO$_2$/Si	300	400–700	180	(002)
Srinivasan et al. [108–110]	ZAD (0.5)	2-ME	MEA(1)	-	-	Glass, quartz (001) sapphire	350 100, 400	500 450–600	(8L)^a 530(10L)	(100)(002)(101) (100)(002)(101)
Kokubun et al. [111]	ZAD (0,45)	2-ME	MEA(1)	-	-	Silica	90/300	500/600	150	(100)(002)(101)
Lee et al. [112]	ZAD (0.35)	2-ME	MEA(1)	-	48 h	Corning glass	350	600	200	(002)
Xue et al. [113]	ZAD (0.35)	2-ME	MEA(1)	-	24 h	Fused silica	300	500	800 (12L)	(100)(002)(101)
Castanedo-Pérez et al. [114]	ZAD (1.14)	EG, 1-PrOH	Glycerol, TEA	(0.31)	30 h	Soda-lime glass, silicon	100	450	160	(100)(002)(101)
Delgado et al. [115]	ZAD^a	EG, 1-PrOH	Glycerol, TEA	-	24 h	Glass	100	200–600	450 (5L)	(100)(002)(101)
Kamalasanan and Chandra [116]	ZAD (<1.98)	EG, 1-PrOH	Glycerol, TEA	-	-	Soda glass, silicon	-	450	200/L	(100)(002)(101)
Chatterjee et al. [117]	ZNH^a	PVA	-	-	-	Silicon	-	700–850	~1000	(100)(002)(101)
Toyoda et al. [118]	ZNH^a	2-ME	-	-	-	Platinized Si	25	250–450 600	^{a}	(002) (100)(002)(101)
Okamura et al. [43,119]	Zn(OEt)$_2$^{a}	1-BuOH	Acac	-	-	p-Si(111)	-	700 (O$_2$)	20/L	(100)(002) (101)^b
Ohya et al. [44,87]	Zn(OPr^a)$_2$ (0.2/0.5)	2-PrOH	DEA(1)	(2)	-	Glass	110	600	11–33/L	(100)(002)(101)

Abbreviations (Abbrev.):

Abbrev.	Product name	Chemical formula	Abbrev.	Product name	Chemical formula
ZAD	Zinc acetate dihydrate	[Zn(CH$_3$COO)$_2$·2H$_2$O]	MeOH	Methanol	CH$_3$OH
ZA	Zinc acetate anhydrous	[Zn(CH$_3$COO)$_2$]	EtOH	Ethanol	C$_2$H$_5$OH
ZNH	Zinc nitrate hexahydrate	[Zn(NO$_3$)$_2$·6H$_2$O]	1-PrOH	1-Propanol	C$_3$H$_7$OH
MEA	Monoethanolamine	(HOCH$_2$CH$_2$)NH$_2$	2-PrOH	2-Propanol	(CH$_3$)$_2$CHOH
DEA	Diethanolamine	(HOCH$_2$CH$_2$)$_2$NH	1-BuOH	1-Buthanol	C$_4$H$_9$OH
TEA	Triethanolamine	(HOCH$_2$CH$_2$)$_3$N	2-ME	2-Methoxyethanol	CH$_3$O(CH$_2$)$_2$OH
DMA	Dimethylamine	(CH$_3$)$_2$NH	EG	Ethylene glycol	HO(CH$_2$)$_2$OH
PVA	Polyvinyl alcohol	[-CH$_2$CH(OH)-]$_n$	PEG	Polyethylene glycol	H(OCH$_2$CH$_2$)$_n$OH
TMAH	Tetramethylammonium hydroxide	(CH$_3$)$_4$N(OH)	Ac. Ac.	Acetic Acid	CH$_3$COOH
Acac	Acetylacetone	CH$_3$COCH$_2$COCH$_3$	Lactic Ac.	Lactic Acid	CH$_3$CHOHCOOH

In the thickness column: L: layer. The numbers between brackets for additive and water columns correspond to r and h values, respectively where:
r = [additive]/[Zn^{2+}], h = [H$_2$O]/[Zn^{2+}].
In the crystallographic orientation column: diffraction peak indicated in bold corresponds to highly oriented films according to one of three main orientations.
^{a} The precursor concentration in the chemical system and thickness are indicated only when they are mentioned in the corresponding reference.
^{b} The peaks intensities are very close.

Table III.1:Main chemical systems used for undoped ZnO thin films elaboration by sol–gel process in alcoholic medium and resulting film crystallographic orientation [59].

III.2) PARAMETERS INFLUENCING ON THE PROCESS :

The sol–gel synthesis of undoped ZnO thin films and to highlight the chemical and physical parameters influencing their structural properties. ZnO thin film synthesis involves several parameters:

(1) the nature of the precursor and its concentration

(2) the type of solvent and the acidity of the medium (The pH)

(3) the type of additive species and their concentrations,

(4) the aging time of the early mixture,

(5) the method of coating of substrates and its speed,

(6) the nature of the substrate

(7) the pre- and post-heat treatment of the materials.

A survey of the literature shows that all these parameters play a key role on the evolution of texture in zinc oxide films [59].

III.2.1). PRECURSORS:

Several zinc precursors have been used: nitrate, chloride, per-chlorate, acetylacetonate and alkoxides such as ethoxide and propoxide, but the most often used is the acetate dehydrate .

III.2.2) SOLVENTS:

The solvent must present a relatively high dielectric constant in order to dissolve the inorganic salts [53,55,56]. Most alcohols are dipolar, amphiprotic solvents with a dielectric constant that is dependent on the chain length [49]. Table 2 shows the dielectric constants and boiling points of most alcohols used [53,].We recall that alcohols with low carbon number, up to 4, are the most used solvents: methanol, ethanol, 1-propanol, 2-propanol, 1-butanol and 2-methoxyethanol (Table 1).

Alcohol	Formula	Dielectric constant at 20 °C	Boiling point (°C)
Methanol	CH_3OH	32.35	64.7
Ethanol	CH_3CH_2OH	25.00	78.3
1-Propanol	$CH_3CH_2CH_2OH$	20.81, 20.10 (at 25 °C)	97.2
2-Propanol	$CH_3CH(OH)CH_3$	18.62	82.2
1-Butanol	$CH_3CH_2CH_2CH_2OH$	17.80	117.7
2-Butanol	$CH_3CH_2CH(OH)CH_3$	15.80 (at 25 °C)	99.5
2-Methoxyethanol	$CH_3OCH_2CH_2OH$	16.90	124.6

Table III.2: Dielectric constants and boiling points for some alcohols, [54,58,59].

III.2.3) ADDITIVES:

Additives are chemical species presenting at least one functional group ,which enables these species to play several roles. They act as basic or acid and/or chelating agent. Alkali metal hydroxides, carboxylic acids, alkanolamines, alkylamines, acetylacetone and polyalcohols are used for this purpose (Table 1). They may facilitate the zinc salt dissolution in some alcoholic media.

III.3)PREDOMINANT CHEMICAL REACTIONS :

This method makes use of molecular precursors in solution, which gradually transformed into a network of oxides by reactions polymerization. The starting solution is constituted by a generally metal precursor alkoxy of formula: M (OR) n or M: is an n-valent metal and R an alkyl string (C_nH_{2n-1}) to which a solvent is added, a catalyst and sometimes water. Namely, the chemical nature of the solvent and precursor dictates the appropriate catalyst. [60-61] The predominant reactions can be divided into two categories [62-63]:

III.3.1) HYDROLYSIS REACTIONS :

The process takes place by dissolving the alkoxide in alcohol and hydrolyzing the solution by adding water under acidic, basic, or neutral conditions as shown in the hypothetical reaction equation below:

$$M \ (OR)_n \ + H_2O \longrightarrow \ M \ (OR)_{n-1}(OH) + ROH$$

The solution thus obtained is called sol.
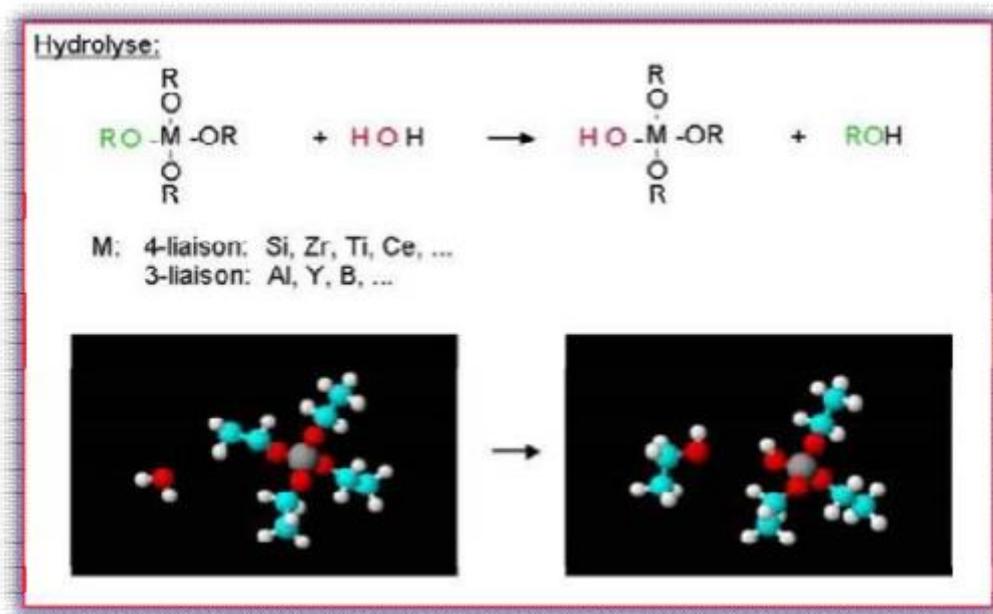
Figure III-2): schematization the hydrolysis process [64]

III.3.2) CONDENSATION REACTION :

The groups **(HO-M (-OR) n-1)** generated during the hydrolysis react either with each other to give a molecule of water (reaction 2) or with a molecule M of the alkoxy (-OR) to give an alcohol molecule (reaction 1) and leading to the creation of the or each flight MOM oxygen atom becomes a bridge connecting two atoms of the metal M. This leads to the formation of a gel whose it viscosity increases during time, this gel contains solvents and precursors which have not yet reacted. This process is governed by the following reactions at room temperature:

$$(OR)_{n-1}\text{-}M\text{-}OH + RO\text{-}M\text{-}(OR)_{n-1} \rightarrow (OR)_{n-1}\text{-} M\text{-}O\text{-}M\text{-}(OR)_{n-1} + R\text{-}OH.......(1)$$

$$(OR)_{n-1}\text{-}M\text{-}OH + HO\text{-}M\text{-}(OR)_{n-1} \rightarrow (OR)_{n-1}\text{-} M\text{-}O\text{-}M\text{-}(OR)_{n-1} + H_2O.........(2)$$

The second reaction can be schematically as follows:
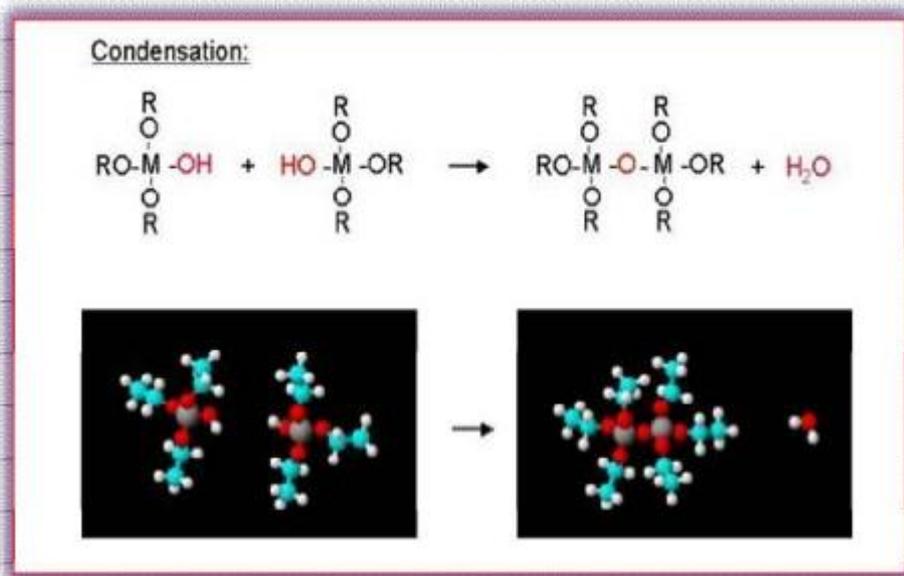
Figure III-3): condensation process [64]

III.4) SOL GEL TRANSITION:

The scheme generally adopted for gelation is the polymer chains growing by condensation which agglomerate and form clusters . During the progress of the hydrolysis and condensation reactions , clusters polymer whose size increases with time, are created. When one of these clusters reaches infinite dimension (ie in practical container size), the viscosity becomes also infinite : the

point of sol-gel transition . From this moment, the infinite cluster called " gel fraction " continues to grow by incorporating polymeric groups more small . When all connections have been used, the gel is formed . From a point of view macroscopically , the transition may be monitored by the mechanical behavior of the solution .

It is then reflected by the divergence of the viscosity of the solution and the growth of elastic constant G gel phase (or module coulomb) [66] . The change in viscosity a soil and of its Coulomb module are thus shown schematically in Figure III.4. according to the time : to complete the formation of the gel , the viscosity becomes infinite , while the spring constant approaches its maximum value . The solid mass formed from the basic solution may then be viewed as a nesting of the polymer chains forming a disordered solid structure. This structure still contains liquid masses imprisoned . [65] Their elimination is via evaporation chelating
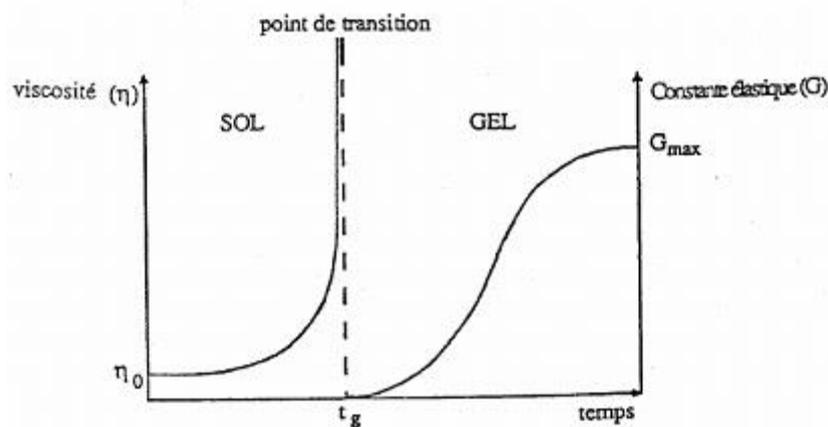
Figure III.4)Evolution of the viscosity of the solution and of the elastic constant of the gel. the
Point tg is the time after which the sol-gel transition is reached [65].

Like all chemical reactions , the sol- gel transition sensitive to its environment , such the temperature or humidity , which can thus according to its nature , alter the kinetics of reactions carried games [65].

III.5) ADVANTAGES AND DISADVANTAGES OF SOL GEL METHOD :

III.5.1) THE ADVANTAGES:

The advantages of this method are manifold making it a coveted method ,we quote here their main advantages :

- ✓ - Simplicity of the process and speed of execution .
- ✓ Simultaneously coating both sides of the substrate in a single operation (dip coating) and the ability to form multilayers.
- ✓ - Feasibility of multicomponent coatings by simply mixing the corresponding alkoxy in the starting solution.
- ✓ - Ability to optimize the morphology of the films based on re- searched applications.
- ✓ - Ability to produce thin layers of inorganic oxides at low temperature on heat sensitive substrates.
- ✓ - Possibility of making organo hybrid materials as thin or monolithic layers with specific properties.
- ✓ - Doping facilitated in large quantities.

III.5.2) THE DISADVANTAGES:

The main disadvantages are :

- ✓ Cost of high - alkoxide precursors.
- ✓ - Manipulation of a large amount of solvents.
- ✓ - the major drawback is the low thickness of the layers , so one must perform several steps of depositing and drying to obtain a thickness of several hundred nanometers , which increases the risk of cracking as the first deposited layers undergo all successive drying which increases the risk of short circuit when the electrical tests. [36]

III.6) THE DIFFERENT SOL GEL METHODS:

Several techniques can be used for the deposition of thin films on a given substrate: the "spin-coating", the "drain-coating" and "dip-coating". Each having their own characteristics, the choice of method of deposition depends on the characteristics of the substrate such that its geometry or size. The two methods presented below are the most commonly used [65].

III.6.1)DIP CAOTING :

The technique of dipping or "dip-coating" is particularly well suited to the production of thin films because it allows the deposition of very homogeneous films on large substrates. It allows more adjust the microstructure (porosity, crystallinity) deposits and to control the thickness. This method involves immersing the substrate in the solution, and remove under highly controlled conditions and stable for a regular film thickness (Figure 2.13). During ascent, the liquid will flow onto the substrate. At the end of flow, the substrate is covered with a very uniform porous film [65].
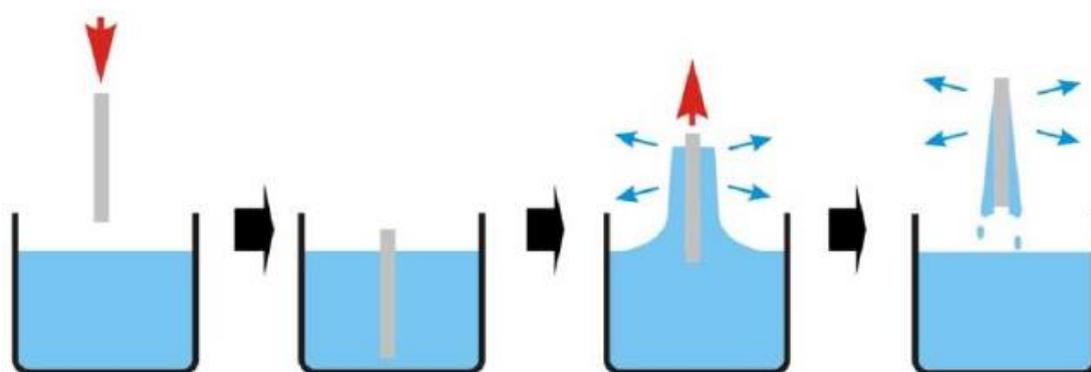
Figure III-5) Deposition of thin films by dipping-drawing [69].

Figure III-6) Dip coater [67].

III.6.2) SPIN CAOTING :

This method involves depositing a small puddle of a fluid resin onto the center of a substrate and then spinning the substrate at high speed. This technique has the advantage of being easily implemented, for moderate investments. It gives excellent results on planar substrates with dimensions of the order of cm².

This deposition method, can be divided into four phases, shown schematically in figure (III.7):
1) The deposition of the solution;
2) The start of rotation: the acceleration step causes the flow of liquid outwardly of the substrate;
3) Rotating at a constant speed allows the ejection of excess liquid in the form of droplets and the reduction of the thickness of the film uniformly;
4) Evaporation of the more volatile solvent which increases the reduction of the thickness of the deposited film [72].

Final film thickness and other properties depend on the rotational speed as well as the the previously mentioned factors and the parameters chosen for the spin process.
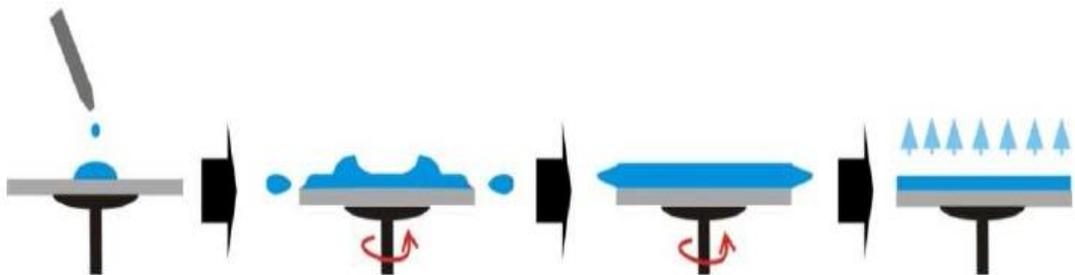
Figure III-7)The four steps of spin coating [69]

In this process, more to what we have said in paragraph (II .3.2.1), We can measure the film thickness by the   Eq.(III.1) , which shows how there is some parameters affect thickness:

$$h = \left(1 - \rho_A / \rho_{A0}\right) \cdot \left(\frac{3\eta.m}{2\rho_{A0}\omega^2}\right)^{\frac{1}{3}}$$

(III.1)

In which:

h: thickness

ρ_A: density of volatile liquid

η: viscosity of solution

m: rate of evaporation

ω:angular speed

Because we have to calculate evaporation rate experimentally, a simpler equation is suggested as below:

$$\text{Eq2:} \qquad h = A\omega^{-B} \qquad (III.2)$$

A ,B are constant parameters that should be calculated experimentally, but in most cases, it has been proved that B is some where between 0.4 and 0.7.
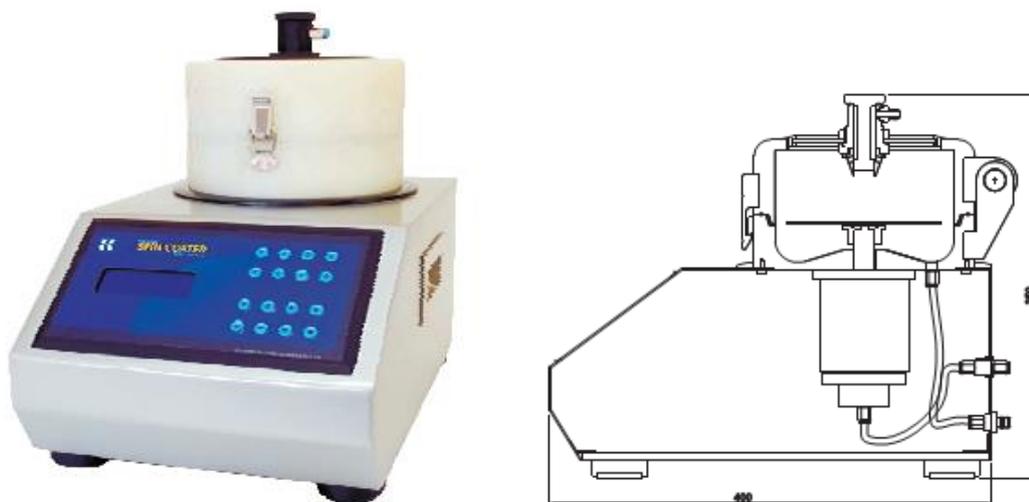
Figure III-8) Spin coater: [68]

Specifications:

Actuator	Brushless DC motor
Spinning speed	10 - 8000 rpm
Maximum substrate size	100 mm diameter
Power input	230V, 50Hz
Read out	20 X 4 line LCD
Acceleration	0 - 2000 rpm/sec
Spinning speed Accuracy	< 5%.
Programmable parameter	Speed, acceleration, dwell time and number of steps
Maximum number of steps	5
System memory	5 programs (non - volatile)

Chapter-IV:

The Deposition Process, Results and discussion

This chapter will be devoted on the deposition, and the results relating to the realisation and the characterization of Zinc Oxide thin films (ZnO). The influence of the Rotation speed and the Solvent, on the structural and the optical properties, will be studied.

IV.1)THE DEPOSITION PROCESS:

IV.1.1) PREPARATION   OF SUBSTRATES :
IV.1.*1.1*) *Choice of the substrate :*

The studied films are deposited on substrates of solid glass, the choice of glass for three reasons:

- ✓ The good agreement of thermal dilation which it presents with ZnO (α glass = 8, 5. 10^{-6}K, αZnO = 4.77 x 10^{-5} K^{-1} at 298 K) [70]
- ✓ To minimize the stress with the interface film/substrate, for their transparency which adapts well for the optical characterization of films in the visible one
- ✓ For economic reasons.

IV.1.1.2) Cleaning of the substrates:

The process of cleaning of the surface of the substrates is as follows:

- ✓   The substrates are cut using a pen with diamond point.
- ✓   Rinsing with the water distilled and then with acetone during 10 min.
- ✓   Rinsing with distilled water.
- ✓   Washing in methanol at ambient temperature.
- ✓ Cleaning in a water bath distilled
- ✓   Drying using a drier.

    All that in order eliminate the traces from greases and impurities stuck to surface of substrate then

IV.1.2) PREPARATION   OF THE SOLUTION:

Two types of solutions were prepared:

IV.1.2.1) Ethanol Solvent (Solution 1):

As a starting material, 3.2925 g zinc acetate dehydrate ($Zn(CH_3COO)_2.2H_2O$) was dissolved in a mixture of ethanol(20ml) and monoethanolamine (MEA)(1.8ml) solution , with a concentration of 0.75 mol L $^{-1}$

MEA it was put into the solution drop by drop, it acts at the same time as a base and a complexing agent and the MEA to zinc acetate molar ratio was fixed at 2 .

IV.1.2.2) Propanol Solvent (Solution 2):

As a starting material , 3.2925 g zinc acetate dehydrate ($Zn(CH_3COO)_2.2H_2O$) was dissolved in a mixture of propanol (20ml) and monoethanolamine (MEA)(1.8ml) solution with a concentration of 0.75 mol L^{-1}. MEA it was put into the solution drop by drop, it acts at the same time as a base and a complexing agent, the MEA to zinc acetate molar ratio was fixed at 2.

IV.1.3) PROPERTIES OF THE ELEMENTS USED IN THE PROCESS:

IV.1.3.1) Zinc Acetate Dihydrate:

Properties	
Molecular formula	$ZnC_4H_6O_4$ (dihydrate)
Molar mass	219.50 g/mol (dihydrate) 183.48 g/mol (anhydrous)
Appearance	White solid (all forms)
Density	1.735 g/cm^3 (dihydrate)
Melting point	Decomposes 237 °C (dihydrate loses water at 100 °C)
Boiling point	decomp.
Solubility in water	43 g/100 mL (20 °C, dihydrate)
Solubility	soluble in alcohol

Figure IV-1) http://upload.wikimedia.org/wikipedia/commons/d/da/Chromium%28II%29-acetate-dimer-3D-balls.png
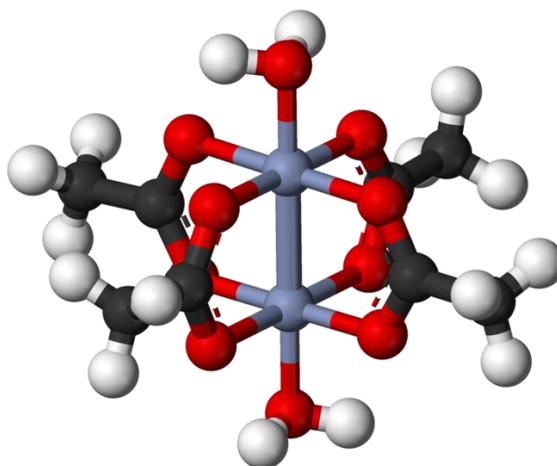
IV.1.3.2) Ethanol :

Properties	
Molecular formula	C_2H_6O
Molar mass	46.07 g mol^{-1}
Density	0.789 g/cm^3 (at 20°C)
Melting point	−114 °C (−173 °F; 159 K)
Boiling point	78.37 °C (173.07 °F; 351.52 K)
Acidity (pK_a)	15.9 (H_2O), 29.8 (DMSO)
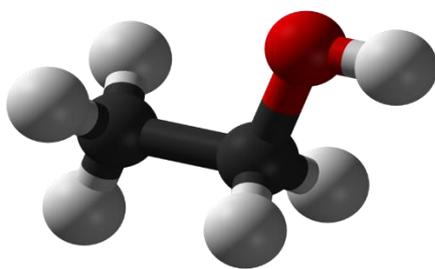
Figure IV.2) .wikimedia.org/wiki/File:Ethanol-alternative-3D-balls.png

IV.1.3.3) Propanol :

Properties	
Molecular formula	C_3H_8O
Molar mass	60.10 g mol^{-1}
Appearance	Colorless liquid
Density	0.786 g/cm^3 (20 °C)
Melting point	−89 °C (−128 °F; 184 K)
Boiling point	82.6 °C (180.7 °F; 355.8 K)
Solubility in water	miscible
Solubility	miscible in benzene, chloroform, ethanol, ether, glycerin soluble in acetone insoluble in salt solutions
Acidity (pK_a)	16.5
Refractive index (n_D)	1.3776
Viscosity	2.86 cP at 15 °C 1.96 cP at 25 °C 1.77 cP at 30 °C
Dipole moment	1.66 D (gas)
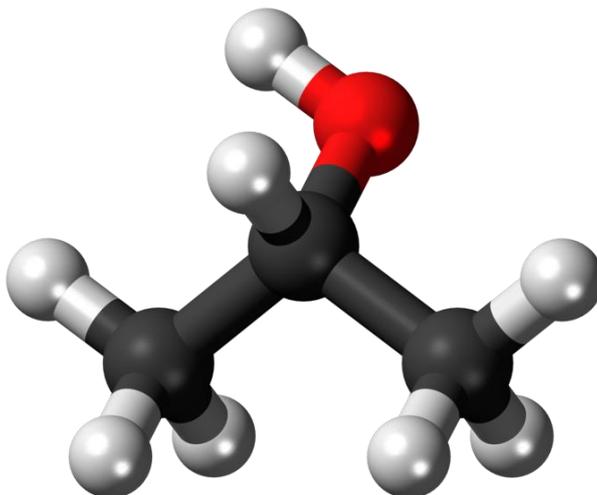
Figure IV.3) wikimedia.org/wiki/File:Propan-1-ol-3D-balls.png

IV.1.3.4)Glass :

	Properties
Density	*2.76 g/cm3*
Softening point	*8440°C*
Refractive index*:*	*1.5440, 1.5354 et 1.5311*
Dielectric constant	*5.84 MHz/ 200 C*
Résistivity	*13.1 ohm-cm à 2500 C*
Transmittance	*~70%(λ=320nm) ; ~90%(λ=360nm)*
	; >90%(λ=380 – 2200nm)

IV.2) DEPOSITING OF THIN FILMS :

ZnO thin films were synthesized by the Spin Coating process using the two solutions mentioned previously

The solutions were stirred for 2 h at room temperature until obtained a clear and homoge-nous solutions , then allowed to age for 3 day (72h) , then they were dropped (3 droppers in

each time)   onto glass substrates (2.5cm x 2.5cm). The   substrates were rotated by using spin coater at   different speeds:

(We have not been able to fixed the rotational speeds for both solutions, so we have based on the publications)

For solution 1: (2000, 2500,3000,3500,4000) rpm during 30s,

For solution 2 (propanol solvent): (350 ,500 ,650 ,800 ,950) rpm , during 30s .

The procedure was repeated five (5) time, to yield a smooth and uniform surface of thin films. After each deposition, the films were preheated (dried) at 100 C° for 10 min on a resistance to remove the solvent and organic residual , annealed , crystallized by post heating at 500c° for 2h, in a furnace , then left to cool down to ambient temperature .

The flow chart of the preparation of ZnO thin films is shown in Fig. IV .4:

Ethanol, (2-Propanol) 20ml	MEA 1.8ml	Zinc Acetate 075mol/l 3.2925 g

Stirring at room temperature for 2h

Clear solution

Solution1 with Ethanol solvent: 2000, 2500, 3000, 3500 and 4000 rpm

Solution 2 with Propanol solvent : 350, 500, 650,800 and 950 rpm

Aging for 72h

Spin caoting

Repeated for 5 times

Preheating for 10min at 100c°

Post- heating for 2h at 500c°
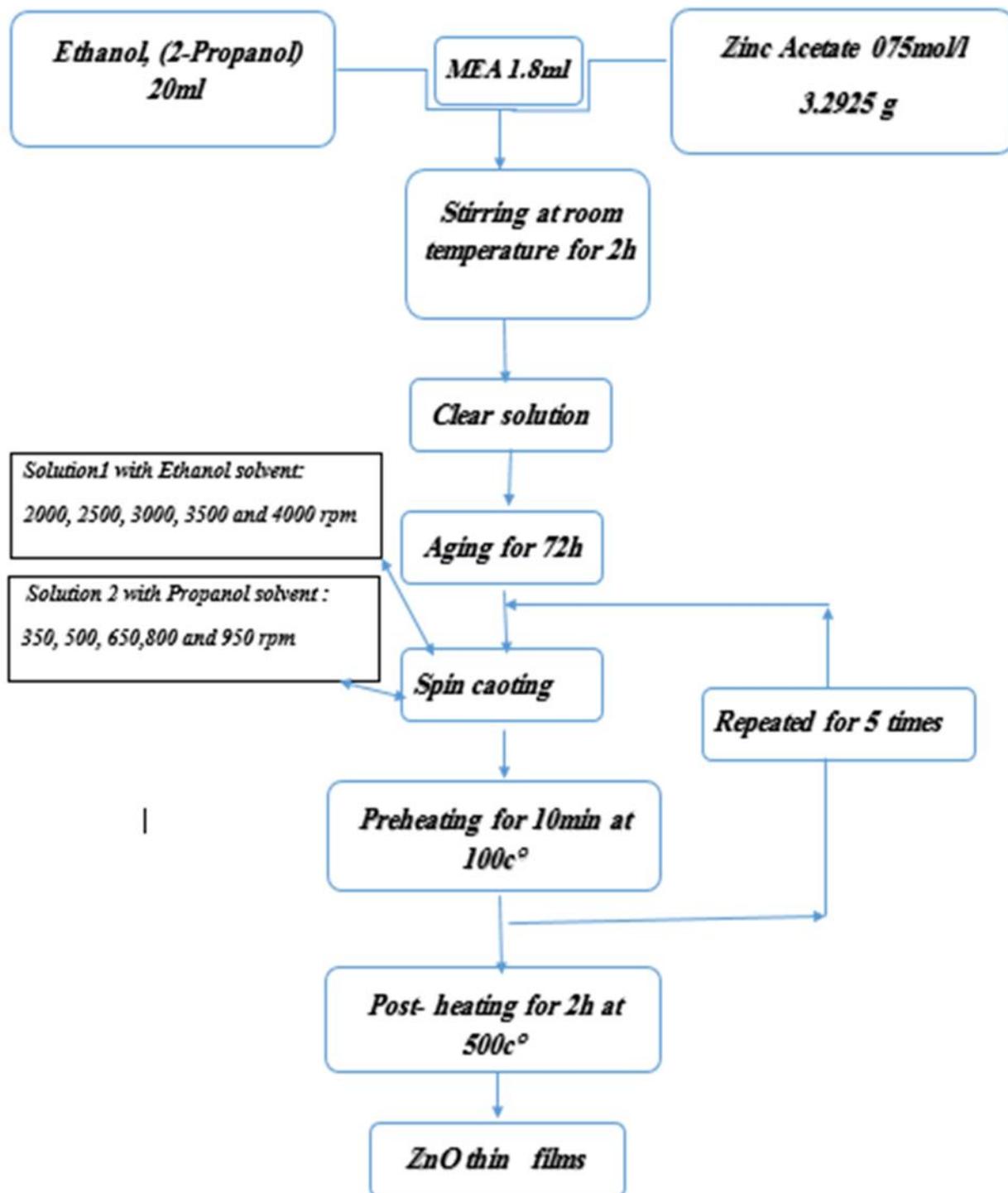
ZnO thin films

Figure IV.4).Flow chart of sol–gel method for preparation of ZnO thin films.

IV.3) RESULTS AND DISCUSSION:

In our calculations, we have followed the methods mentioned in the second chapter.

However, we consider that all thin-films thickness is one micron, this is due to the inability to measure it, and this is due to the lack of interference fringes on the transmittance curve.

IV.3.1) ETHANOL SOLVENT (SOLUTION 1) :
IV.3.1.1) Rotation Speed Effect On The Structural Properties Of ZnO Thin Layers:

We have reported in figure (IV.5) the spectra of x-rays diffraction of ZnO thin films for different rotation speeds for the first solution (ethanol solvent) :
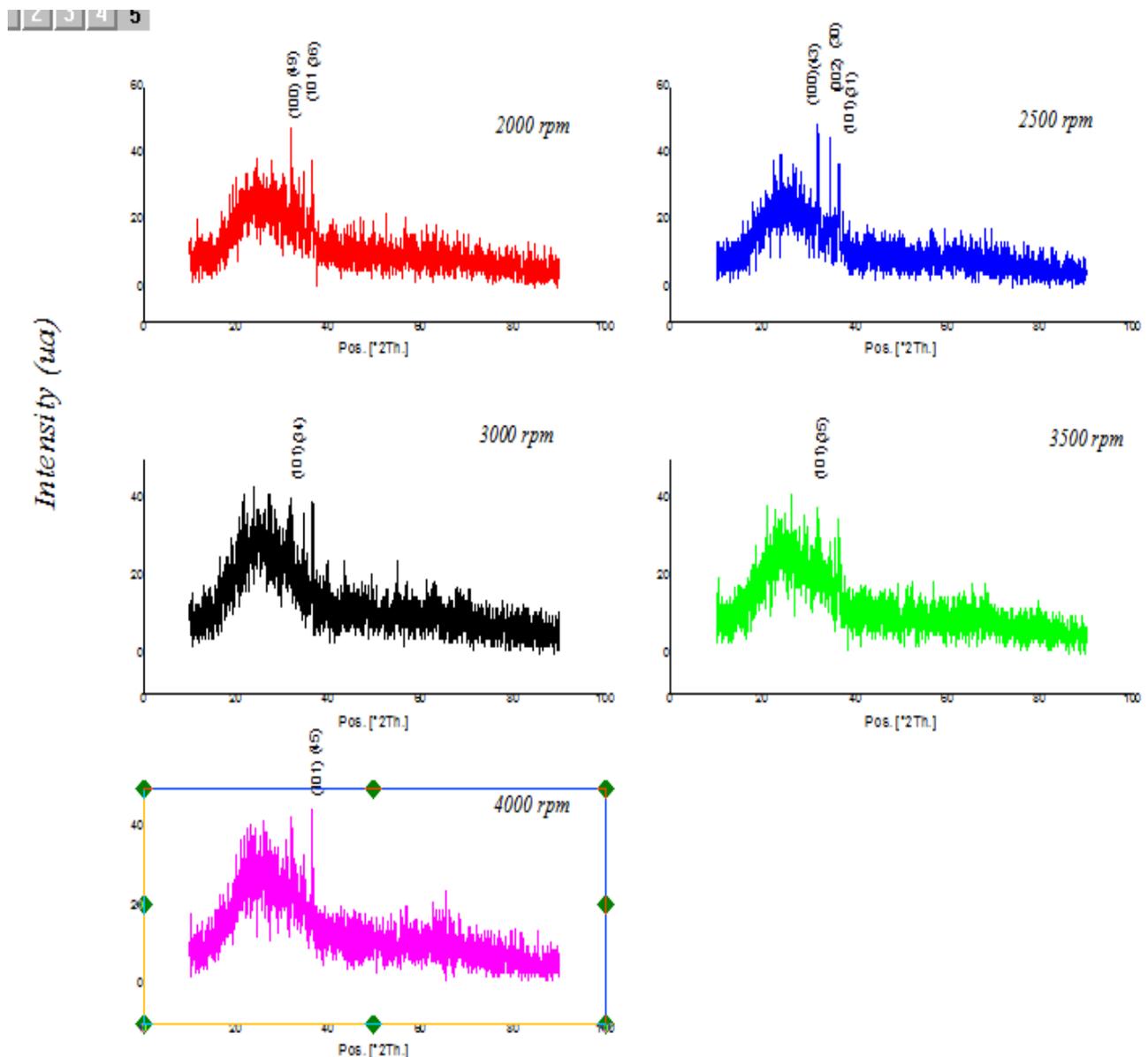
Figure IV.5) *Evolution of the spectra of X-rays diffraction of ZnO thin films for differences*

Rotation speeds solution 1 (Ethanol)

In the table (IV.1) we cite the different peaks observed (the intensity) and the corresponding angles and orientations.

hkl	*(100)*		*(002)*		*(101)*	
Chuck Rotation (rpm)	*2θ(°)*	*Intensity(ua)*	*2θ(°)*	*Intensity(ua)*	*2θ(°)*	*Intensity(ua)*
2000	*31.9892*	*49*	*-*	*-*	*36.4567*	*36*
2500	*31.9428*	*43*	*34.6058*	*30*	*36.4981*	*31*
3000	*-*	*-*	*-*	*-*	*36.5975*	*34*
3500	*-*	*-*	*-*	*-*	*36.4405*	*35*
4000	*-*	*-*	*-*	*-*	*36.5732*	*45*

Table (IV.1) Orientations for all Speeds.

XRD pattern of ZnO thin films obtained by adopting optimum levels of parameter combinations is shown in Fig IV.5). XRD scan was done over a 2-theta of 10°-90°, Three strongest diffraction peaks were detected at Bragg angles , indicating that the films are polycrystalline with a hexagonal wurtzite structure and preferred orientations along (100), (002) and (101) planes , where (100) for the 2000 rpm and 2500 rpm rotation speeds , and (101) for the three other rotation speeds 3000 ,3500 and 4000 rpm , which exactly matches with the Joint Committee of Powder Diffraction Standards (JCPDS) card file data for ZnO Powder [71] and matching to results of the Author [72]
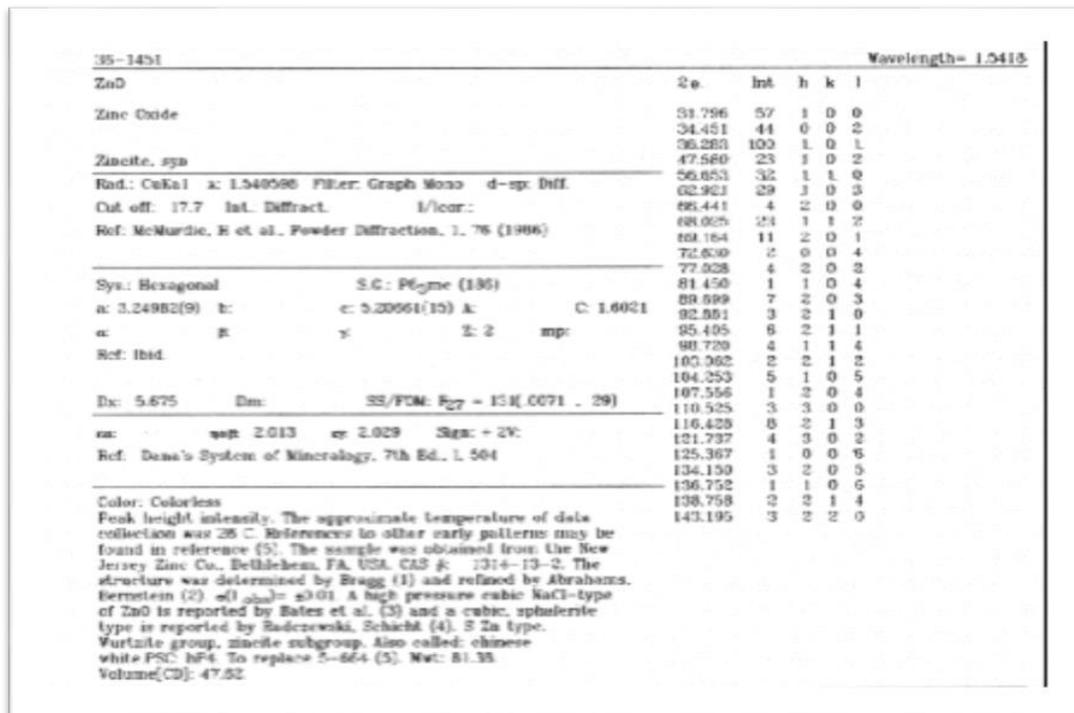
Figure IV.6): ASTM file of ZnO film [71]

IV.3.1.1.a) the grains (crystallite) size:

The grains size of the various ZnO thin films was calculated starting from the width with semi height of the most intense peak , using Sherrer formula (relation II.4 in the second chapter), and the results are illustrated in Table (IV.2)

Rotational Speed (rpm)	2000	2500	3000	3500	4000
D (nm)	28.7286	32.6449	31.1661	10.1103	20.2284

Table IV 2: Crystallites size

Using these results, we draw the variation of the crystallites size as function of Rotational Speeds, which is represented in the figure IV.6:
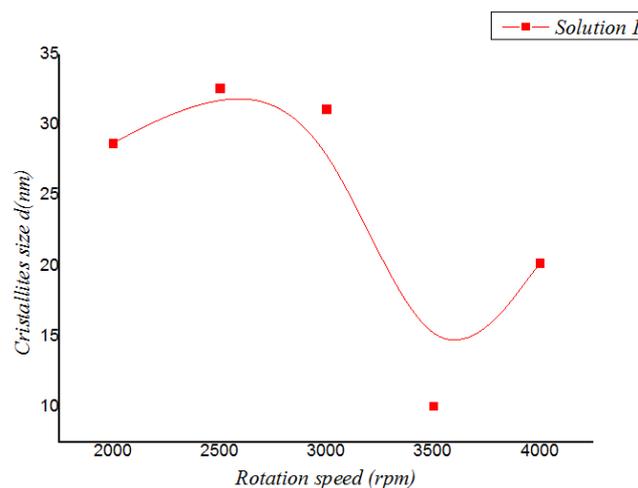
Fig. IV.6: Average crystallite sizes of the ZnO thin film as a function of The Rotation Speeds

We observe:

The crystallites size increases from ~ 28.7 nm to ~33.5 nm, then, it have a decrement until

~ 10 nm then a new increasing to 20 nm , *and the average size was estimated 28 nm* which is *good agreement with the literature reports [73]*.The larger D and smaller FWHM values , indicate better crystallization of the film , hence the 2500 rpm is the best rotational speed.

IV.3.1.1.b) C Axis parameter value, variation as function of Rotational speeds:

The C axis parameters of the various ZnO thin films was calculated using the relations II.2 and II.3 in the second chapter, and the results are illustrated in Table (IV.3)

Rotational speeds (rpm)	*2000*	*2500*	*3000*	*3500*	*4000*
C axis (A•)	*5.2607*	*5.2333*	*5.2335*	*5.2553*	*5.2369*

Table IV.3:C Axis parameter as function of Rotational speeds:

Using these results, we draw the curve of the C axis   as function of Rotational Speeds, which is represented in the figure IV.7:
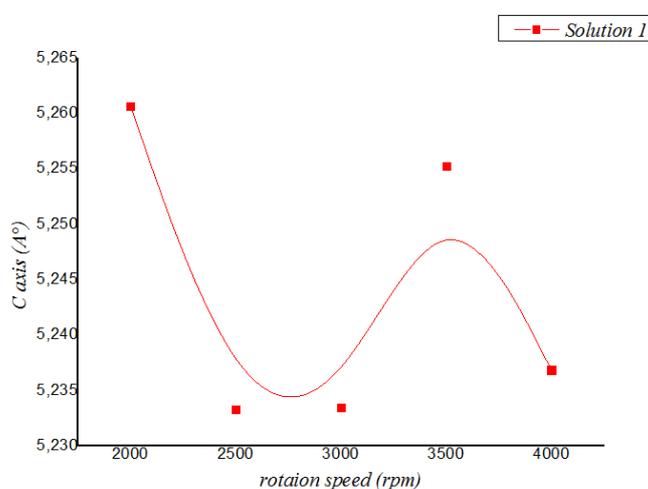
Fig. IV.7 : Average C axis as a function of rotation speeds

As can be seen from Table III.4 and (fig III.16), this films have an hexagonal unit cell which are close to the parameters of C_0 =5.207A˚ (JCPDS 36-1451, fig III.14) , and the most closer   value is in the 2500 rpm rotational speed .

IV.3.1.1.c) The Stress σ variation as function of Rotational speeds

The Stress values of differences thin layers were calculated using the relation II.5 in the second chapter, and the results are illustrated in Table (III.5)

Speeds Rotation (rpm)	2000	2500	3000	3500	4000
Stress σ (GPa)	4.4132	2.2749	2.2905	4.0025	2.5602

*Table (IV.4.) the Stress **σ** as function of Rotational speeds:*

Using these results we can plot the curve of stresses as a function of Rotational speeds.
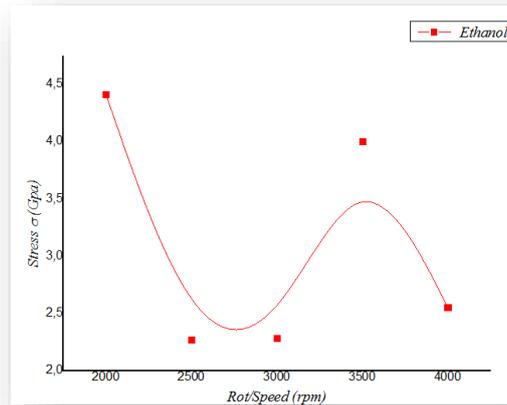
Fig. IV.8 : The *Stress of the ZnO thin film as a function of rotation speeds*

As can be seen from Table IV.4 and curve IV 8, the weakest stress is in the 2500-rpm rotation speed

IV.3.1.1.d) The dislocation density (δ) variation as function of Rotational speeds

The dislocation density (δ), defined as the length of dislocation lines per unit volume of the crystal ,can be estimated from the following relation using the simple approach of Williamson and Smallman [74]:

$$\delta = \frac{1}{D^2}$$

the results are illustrated in Table (IV.5)

Rotation Speed (rpm)	2000	2500	3000	3500	4000
$\rho \ (cm^{-2}*10^{14})$	1.2116	0.9384	1.0295	9.7830	2.4439

Using these results, we draw the curve of the C axis   as function of Rotational Speeds which is represented in the figure IV.9 :
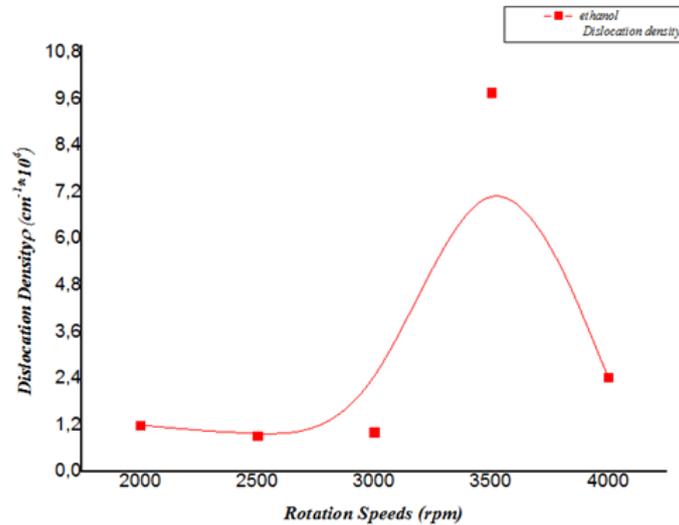
Fig. IV.9 : *The dislocation densities of the ZnO thin film as a function of rotation speeds*

From the Table III.6 , the values of the dislocation densities are stable from 2000 to 3000 rpm rotation speed and there is a augmentation until 3500 rpm , then it starts in decrement to 4000 rpm . And this explains the increase in the stress field of 3500 rpm speed.

Also it is observed the weakest value which means the better quality of the crystallized thin film, is in the 2500rpm rotational speed.

IV.3.1.2) The Rotational Speeds effect on the optical properties of zno thin layers:

The optical characterizations have been done using Constantine university's UV-Vis- Nir spectrophotometer.

IIV.3.1.2 .a) The Transmittance:

As can be seen from Fig. IV.10 , all Rotated ZnO thin films at different speeds , were highly transparent in the visible range (400 –800) nm with a transmittance of more than 80% , especially the 3500 rpm speed which have 95% , and sharp absorption edges are observed in the ultraviolet region
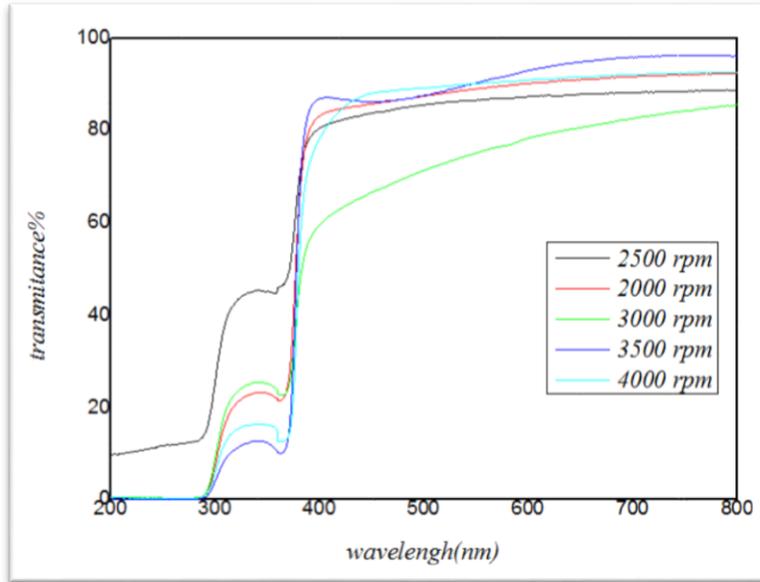
Fig.IV.10 : Optical transmittance spectra of ZnO thin films.

Also it can be seen another edge near 300 nm, in some works [78] The glass substrate was measured in order to determine the absorption edge of glass, this was found to be near 300 nm, and thus the observed edge in the films at 300 nm corresponds to the absorption of the glass substrate used in the experiments.

IV.3.1.2 .b) Optical Gap:

Using the method indicated in the (II.3.4.1.b) paragraph, we have obtained these curves for each speed fig IV.11:
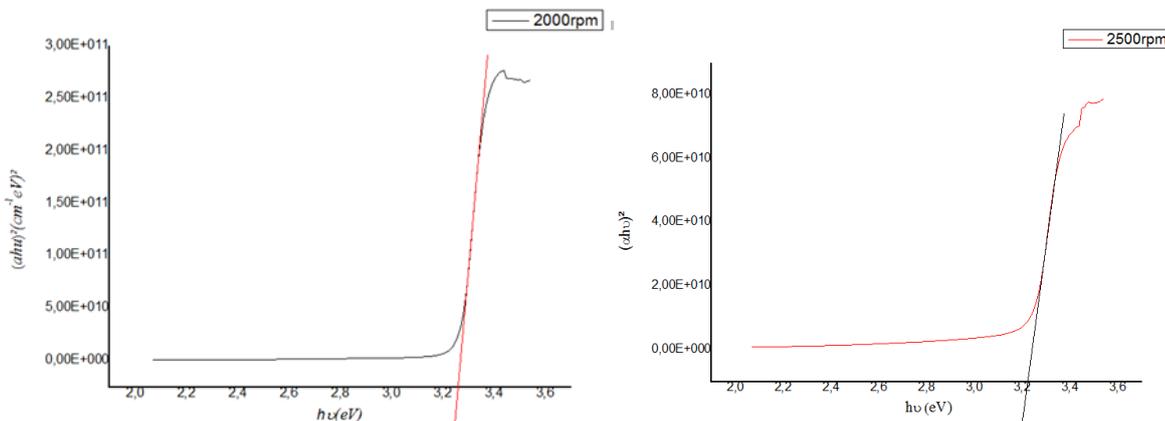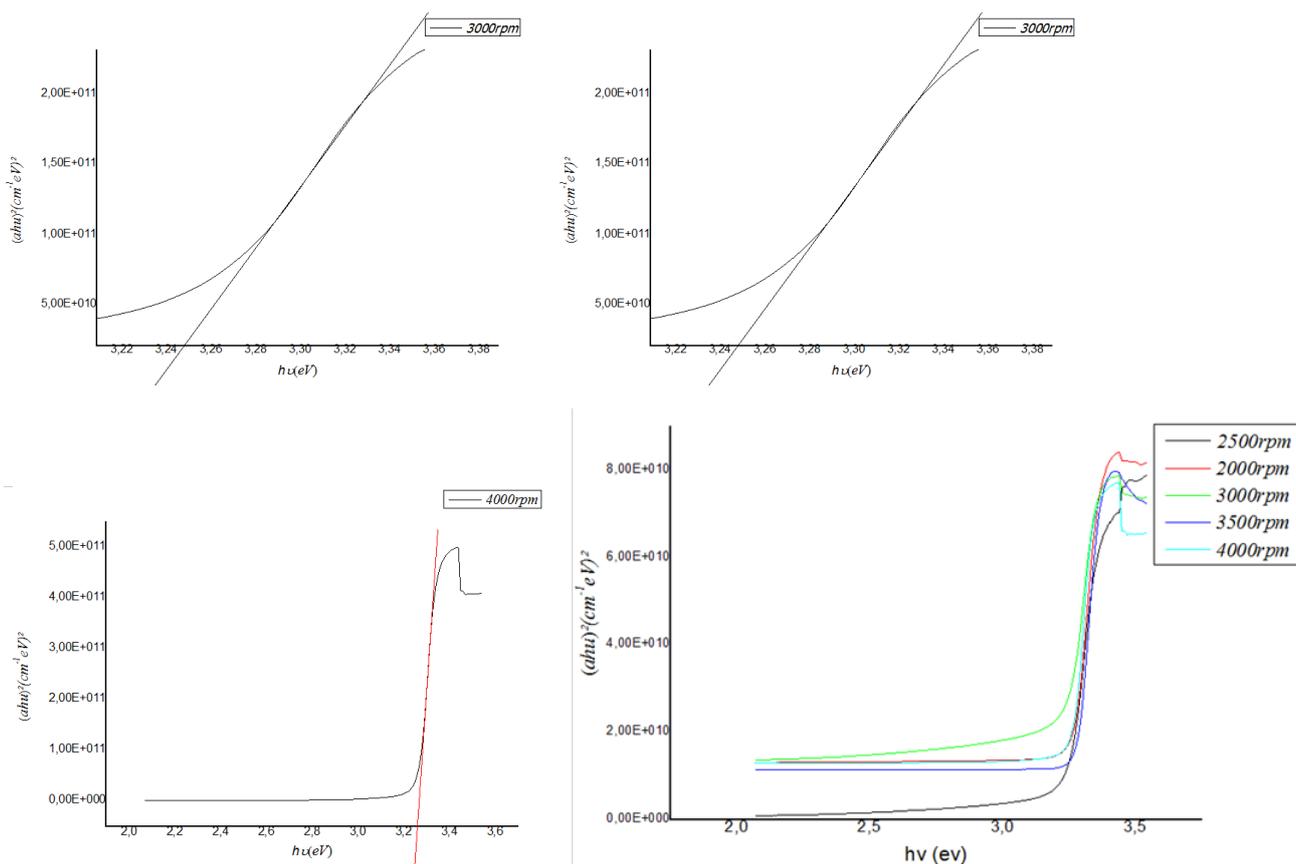
Fig.IV.11 : Optical gap of ZnO thin films for each rotational speed.

From these curves , we have obtained the various gap values which are represented in table III.6 and plotted as a function of the rotations speeds in the fig IV.12 :

Rotation Speed (rpm)	2000	2500	3000	3500	4000
Eg (eV)	3.202	3.273	3.248	3.262	3.265

Table IV.5: Optical Gap as Function of Rotational Speeds.
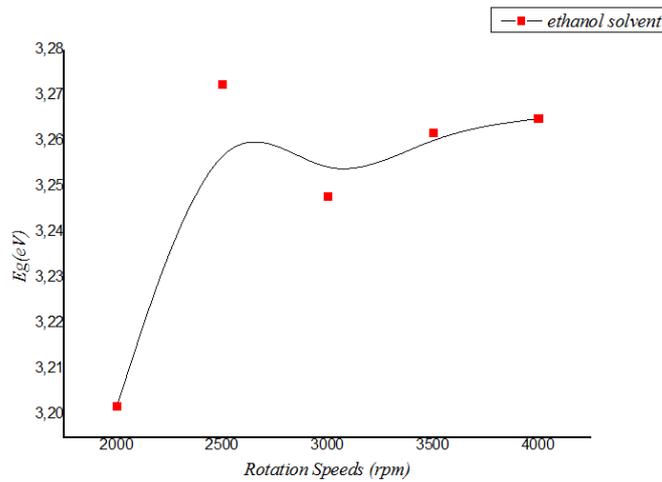
Fig. IV.12 :*The Gap value of the ZnO thin film as a function of rotational speed*

It is found that the Optical gap increased with increasing Rotation Speeds. The measured optical band gap values were in the range of 3.20–3.27 eV, which is very close to the band gap of intrinsic ZnO powder and are in good agreement with the literature reports [73].

IV.3.1.2 .c) The Disorder (Urbach energy) :

The same thing as the optical gap ,using the method indicated in the paragraph (II.3.4.3) we have obtained these curves for each speed fig IV.13:
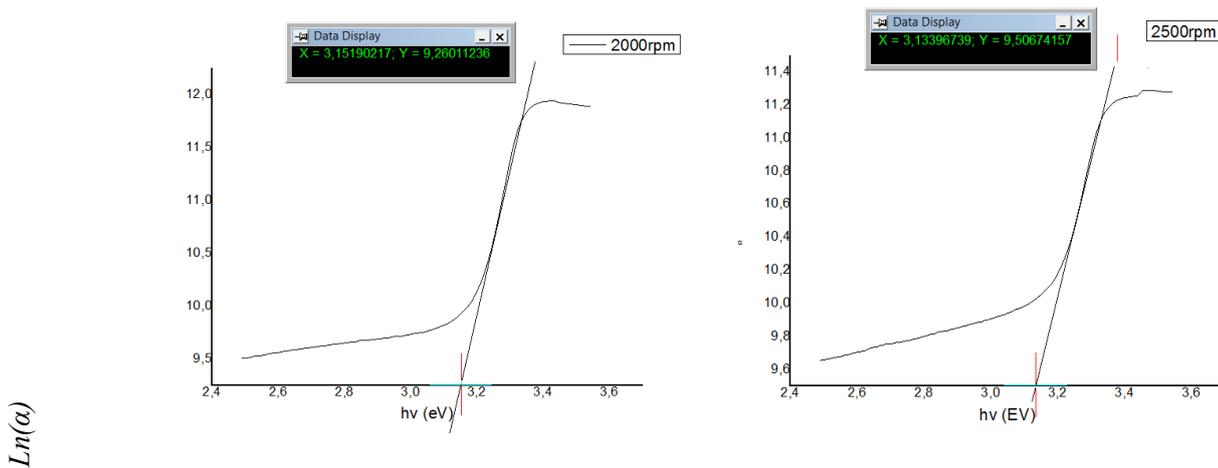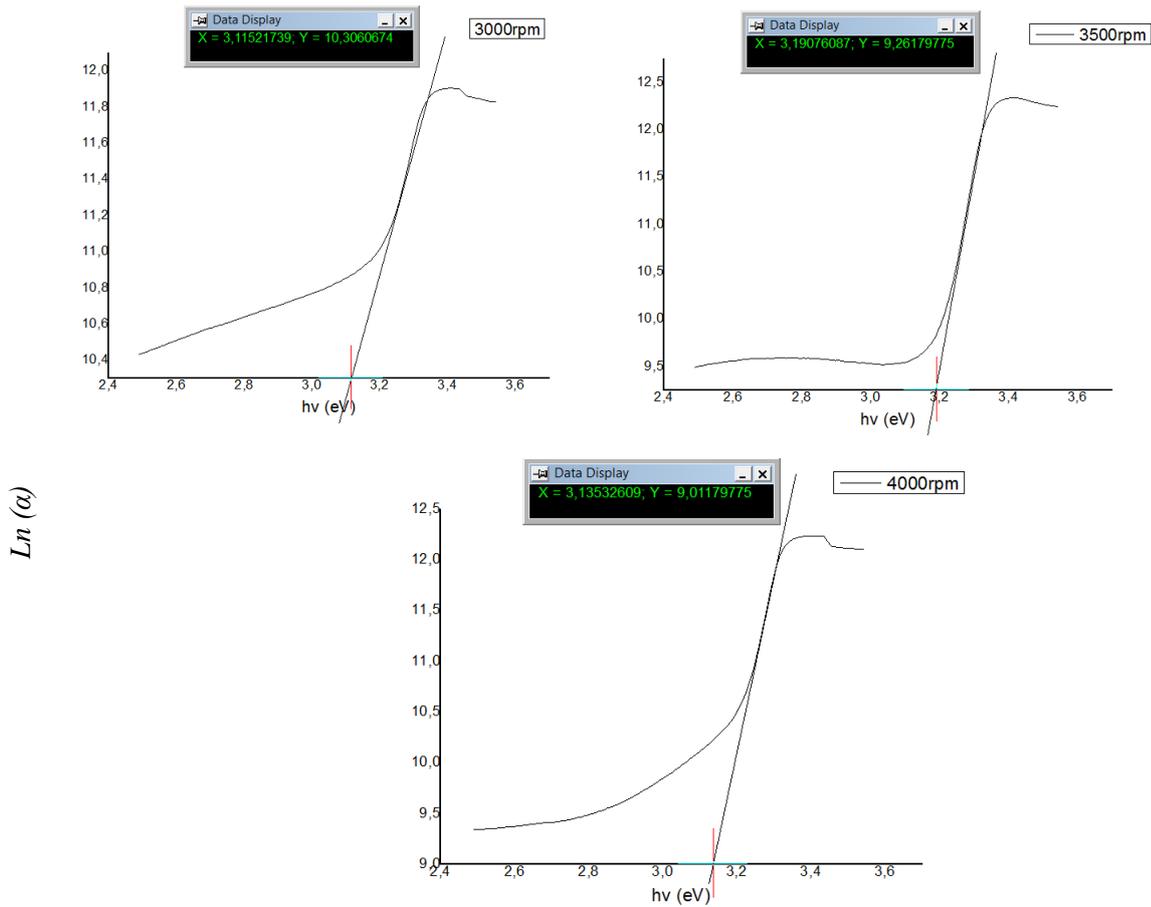
Fig. IV.13 : *The E_{00} value of the ZnO thin film as a function of rotational speeds*

From these curves, we have obtained the various disorder E00 values, which are represented in table IV.6 and plotted as a function of the rotations speeds in the fig IV.14 :

Rotation Speeds (rpm)	*2000*	*2500*	*3000*	*3500*	*4000*
1/E$_{00}$ (eV)$^{-1}$	*3.1519*	*3.1339*	*3.1152*	*3.1907*	*3.1353*
E00(eV)	*0,31727*	*0,31909*	*0,32101*	*0,3134*	*0,3189*

Table .IV. 6 : *The E_{00} value of the ZnO thin film as a function of rotation speed*

We observe that the disorder is in the range of 320 meV for all samples .
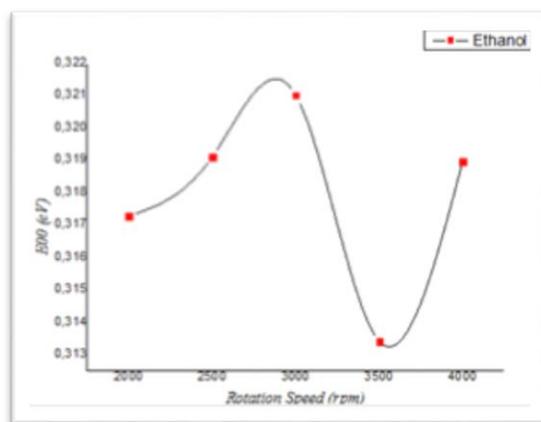
Fig. IV.14 : *The E_{00} value of the ZnO thin film as a function of rotation speed*

IV.3.2) PROPANOL SOLVENT (SOLUTION 2) :

IV.3.2.1) Rotation Speed Effect On The Structural Properties Of ZnO Thin Layers:

In the table (IV.7) we cite the different peaks observed (the intensities) and the corresponding angles and orientations.

hkl	(100)		(002)		(101)		(103)	
Chuck Rotation (rpm)	$2\theta(°)$	Intensity(ua)	$2\theta(°)$	Intensity(ua)	$2\theta(°)$	Intensity(ua)	$2\theta(°)$	Intensity(ua)
350	32.0440	60	34.7478	79	36.5365	63	63.0681	21
500	32.0218	47	34.6501	43	36.5094	52	-	-
650	32.1955	38	34.6721	60	36.5230	47	-	-
800	32.0474	56	34.6874	81	36.5165	60	63.1729	21
950	31.9859	39	34.6387	44	36.5131	45	-	-

Table (IV.7) Orientations for all Speeds.
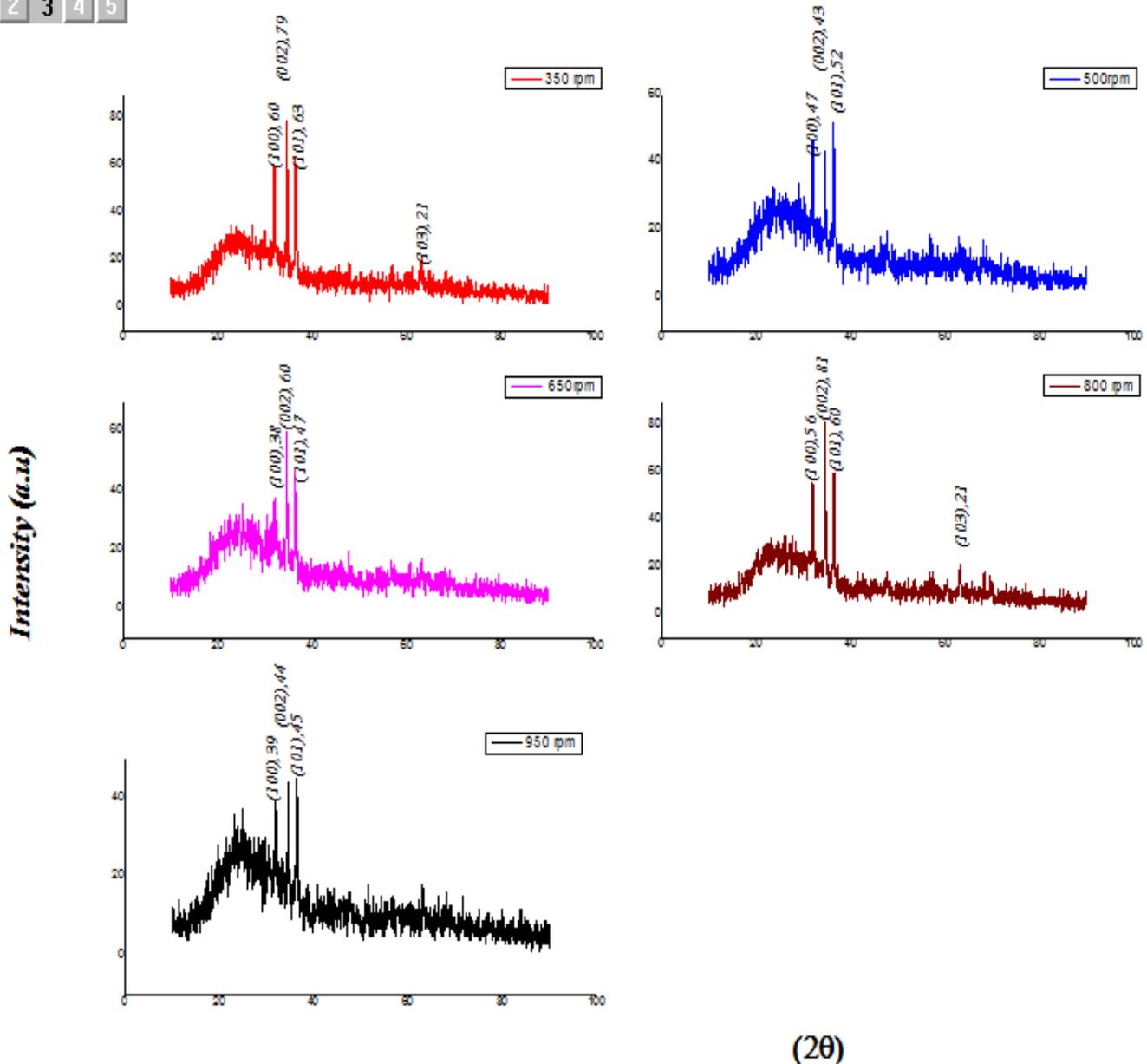
Figure IV.15: *Evolution of the spectra of X-rays diffraction of ZnO thin films for differences*

Rotational speeds solution 2 (Propanol)

So, it was found in the second solution ,all films were polycrystalline ,the XRD peaks (1 0 0), (0 0 2) , (1 0 1) and (1 0 3) were observed. The Films were preferentially oriented in the c-axis, or (0 0 2) plane, for the 350 rpm ,650 rpm and 800rpm rotation speeds, and oriented in the (1 0 1) plane for the other rotation speeds. It is believed that the preferential orientation is due to the minimization of surface energy and internal stress [75] (which will seen later). Also, the c-orientation might be resulted from the facilitated growth of the film along the c-axis as a result of the highest atomic density found along the (0 0 2) plane [76].

IV.3.2.1.a) the grains (crystallite) size:

The grains size of the various ZnO films were calculated using the Sherrer formula (relation II.3) in the second chapter , the results are illustrated in Table (IV.8).

Rotation Speed (rpm)	350	500	650	800	950
D (nm)	49.129	37.019	36.829	58.939	49.115

Table IV.8: Crystallites size

Using these results we draw the variation of the crystallites size in function of Speeds Rotation which is represented in the figure IV.16.
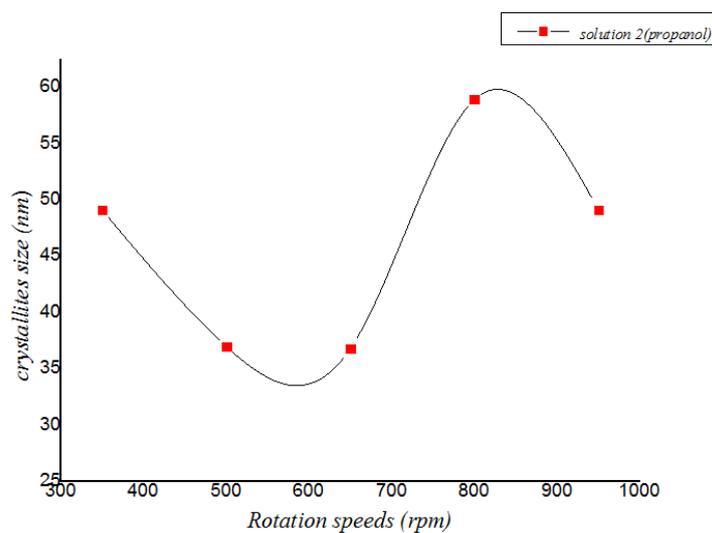
Fig. IV.16 : *Average crystallite sizes of the ZnO thin film as a function of The Rotational Speeds*

We have observed an instable variation in the values of the grains size , it decreases from ~49 nm to ~36 nm, then it have an augmentation until ~ 59 nm then a new increasing to 49 nm .

IV.3.2.1.b) C Axis parameter, variation in function in speeds Rotation

Using the same method used for the solution 1 we have obtained these values:

Speeds Rotation (rpm)	350	500	650	800	950
C axe (A°)	5.1564	5.2457	5.1673	5.1651	5.1721

Table IV.9:C Axis parameter as function of Rotational speeds:

Plotting these values , we obtain this curve fig IV.17:
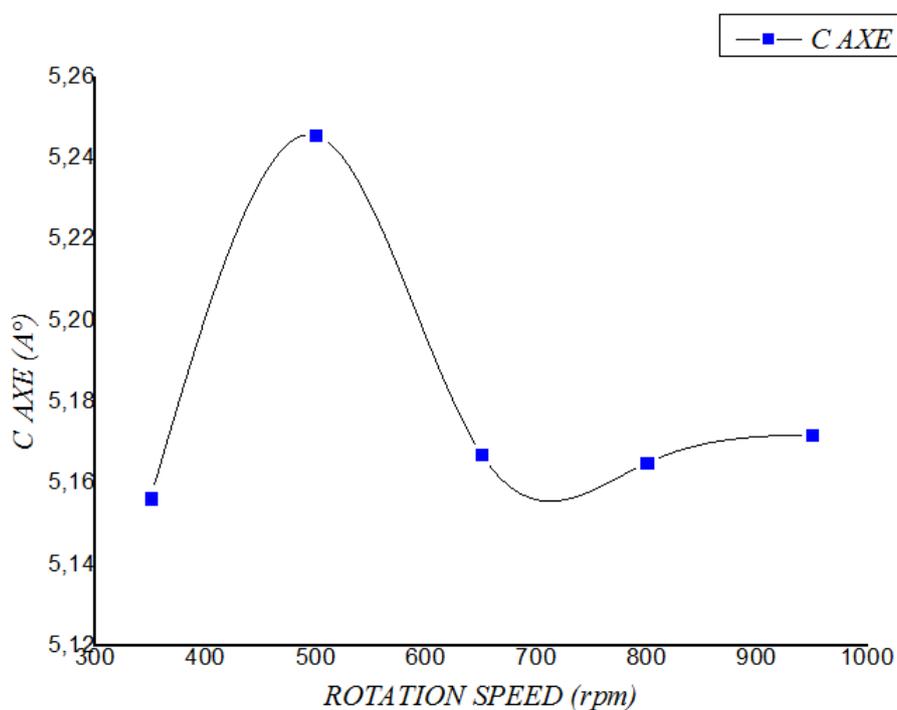
Fig.IV.17 :: C axis value as a function of rotational speeds

As can be seen , an augmentation of the C Axis values from 5.15 A° (350rpm) , to 5.25 A° (500rpm) , then a stable value of the 5.17 A° for the 650rpm , 800rpm and 950 rpm rotation speeds also these values are close to the parameter of c0 = 5.207A° (JCPDS 36-1451)

IV.3.2.1.c) The Stress σ variation as function of Rotation speeds

Using the relation II.5 in the second chapter, we have obtained the results illustrated in Table (IV.9)

Speeds Rotation (rpm)	350	500	650	800	950
Stress σ (GPa)	-4.5034	3.2600	-3.4701	-3.6774	-3.0206

Table (IV.9) the Stress σ as function of Rotation speeds:

Using these results, we have plotted the curve of stresses as a function of Rotation speeds Fig IV.18 :
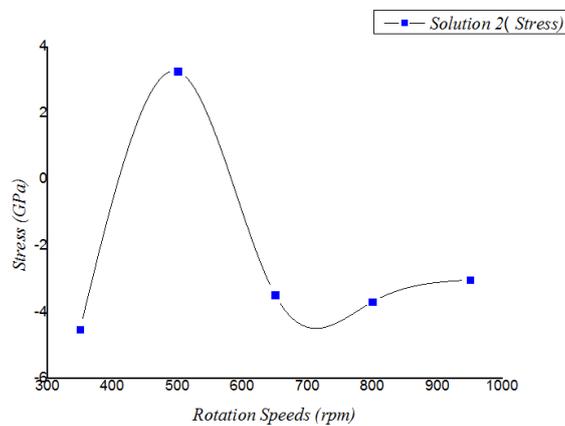
Fig. IV.18: The *Stress of the ZnO thin film as a function of rotation speeds*

As can be seen that the stress values are stable for the rotational speed 650 rpm ,800 rpm and 950 rpm , they are in the range of - 3.4 Gpa , The minus sign indicates that the residual stress is compressive.

IV.3.2.1.d) The dislocation density (δ) variation in function in speeds Rotation

The dislocation density (δ), defined as the length of dislocation lines per unit volume of the crystal ,can be estimated from the following relation using the simple approach of Williamson and Smallman :

$$\delta = \frac{1}{D^2}$$

the results are illustrated in Table (IV.10)

Rotation Speed (rpm)	350	500	650	800	950
D (nm)	49.129	37.019	36.829	58.939	49.115
ρ ($cm^{-2}*10^{14}$)	4.143	7.297	7.373	2.879	4.145

Using these results, we draw the curve of the C axis   as function of Rotational Speeds which is represented in the figure IV.19
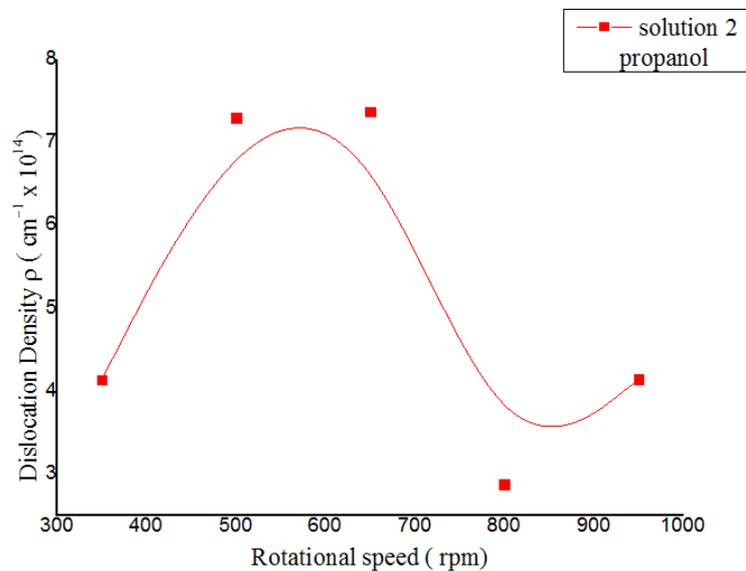
Fig. IV.19 : *The dislocation densities of the ZnO thin film as a function of rotation speeds*

The lower dislocation density means, the better quality of the crystallized thin film.

IV.3.2.2) The Rotation Speeds effect on the optical properties of zno thin layers:

IV.3.2.2 .a) Transmittance:

As can be seen , the transmittance increase with the Rotation speeds where   the highest one is in the 950 rpm,   speed which have 93% .And a sharp absorption edges are observed in the ultraviolet region.

In addition, it can be seen another edge near 300 nm.
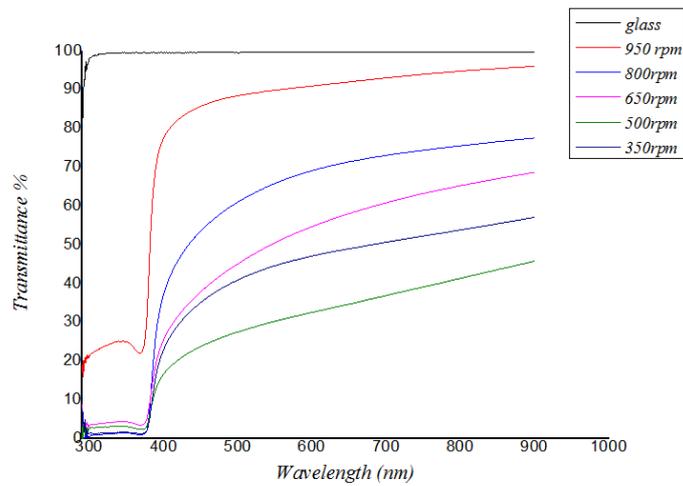
Fig.IV.19: Optical transmittance spectra of ZnO thin films.

IV.3.2.2 .b) Optical Gap

The curves obtained by using the method indicated   in the chapter II to calculate the Optical gap are illustrated in the fig IV.20 :
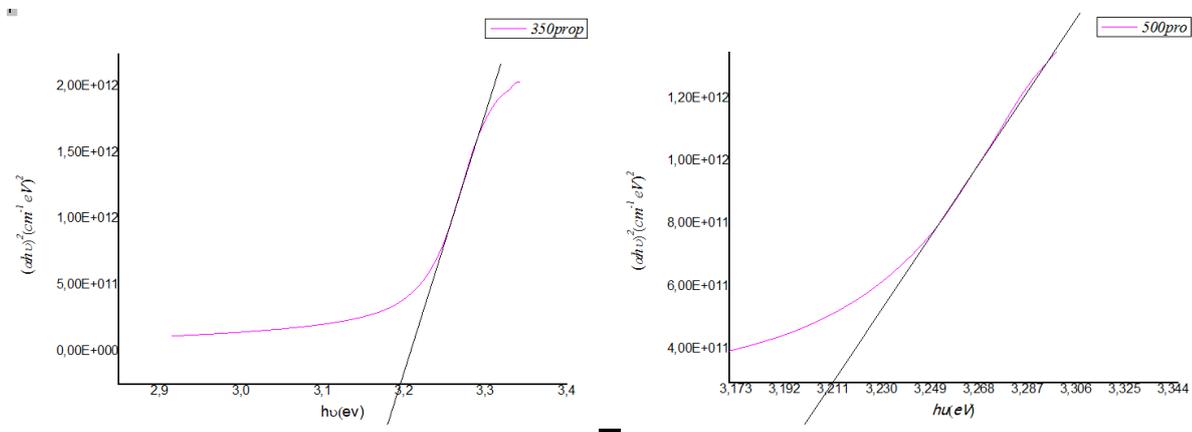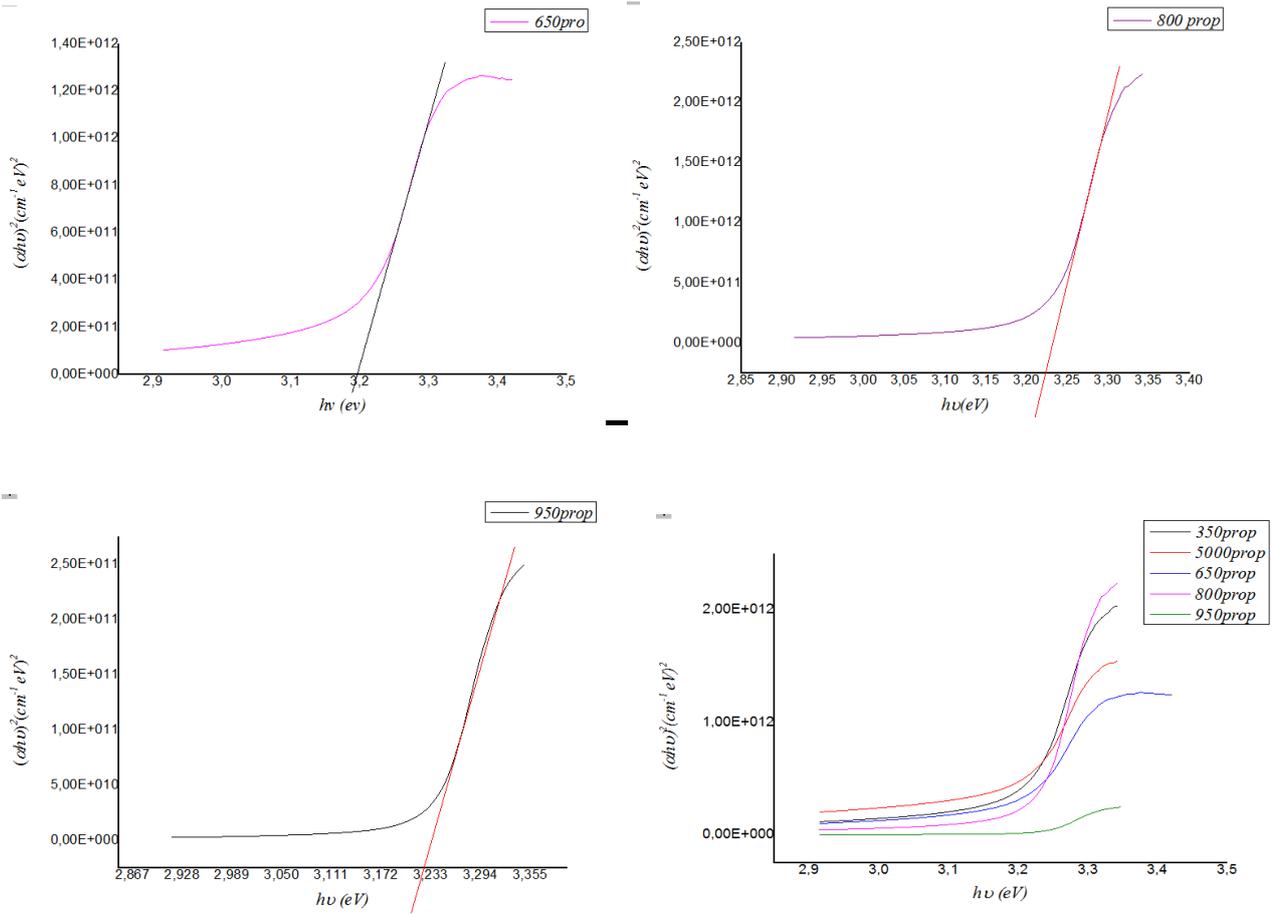
Fig.IV.20 : Optical gap of ZnO thin films for each rotation speed.

From these curves , we have obtained the various gap values which are represented in table III.11 and plotted as a function of the rotations speeds in the fig IV.21 :

Rotation Speed (rpm)	350	500	650	800	950
Eg (eV)	3.195	3.178	3.197	3.229	3.225

Table IV.11: Optical Gap as Function of Rotation Speeds.
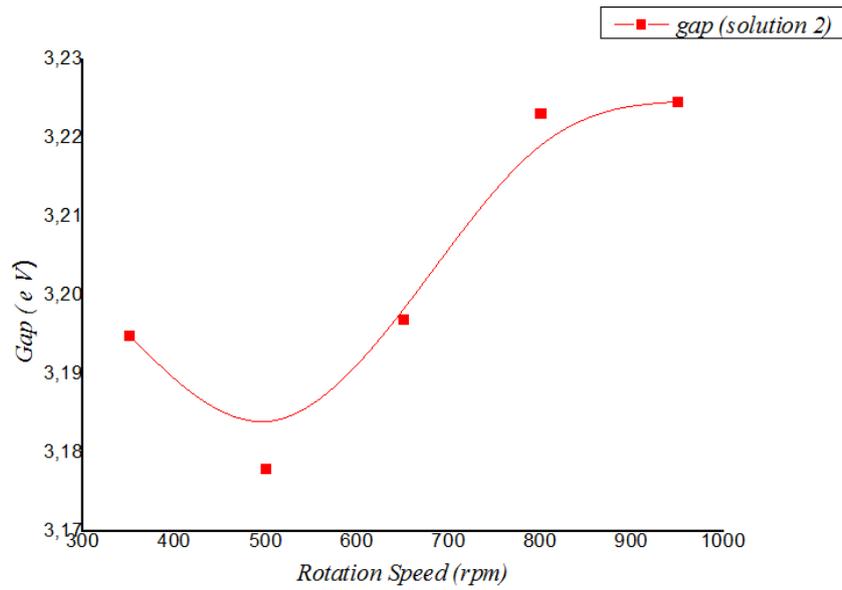
Fig.IV. 21 : *The Gap value of the ZnO thin film as a function of rotation speed*

    We remark that Eg values depend on the Rotational Speed, It increase with its augmentation , with a minima for the 500rpm rotational speed

IV.3.2.2 .c) The Disorder (Urbach energy) :

By drawing *ln (α)* on function of *(hv)* we can estimate the disorder's values Fig IV.22.
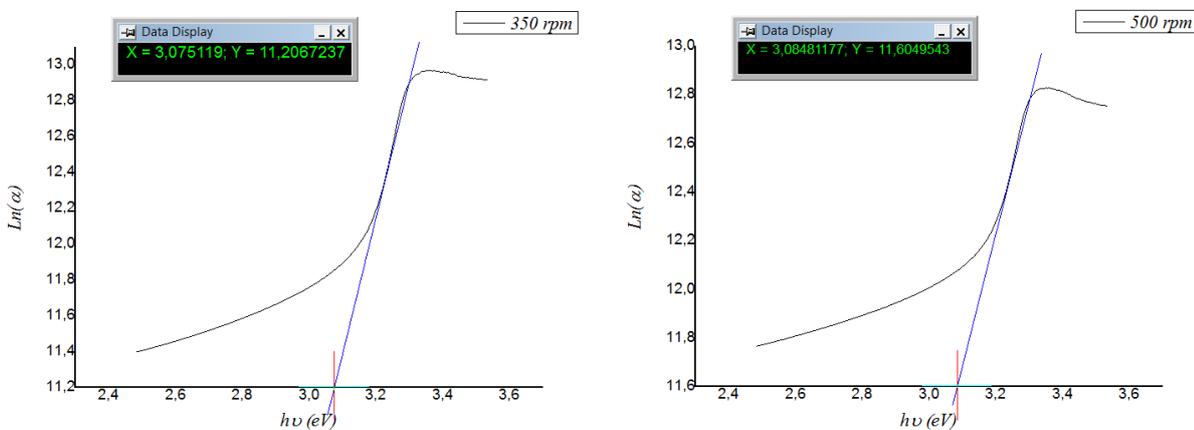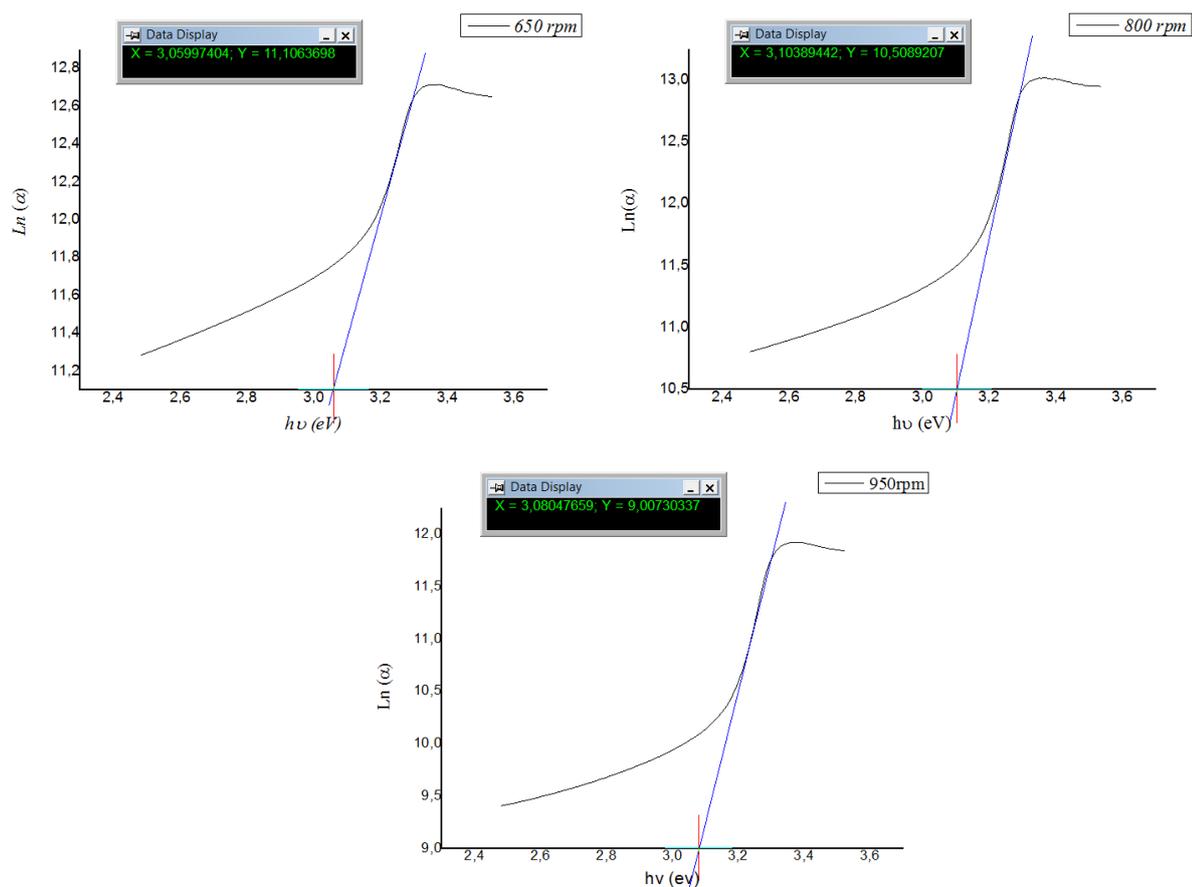
Figure IV.22: Variations of Ln (α) a function of hv

The following table gives the disorder's values :

Chuck Rotation (rpm)	*350*	*500*	*650*	*800*	*950*
$1/E_{00}$ $(eV)^{-1}$	*3.0805*	*3.1039*	*3.0600*	*3.0848*	*3.0751*
E_{00} (eV)	*0,3246*	*0.3222*	*0.3268*	*0,3134*	*0,3252*

Table (IV.12) Variations of Ln (α) a function of hv

These values are plotted as a function of the rotational speeds in the fig IV.23
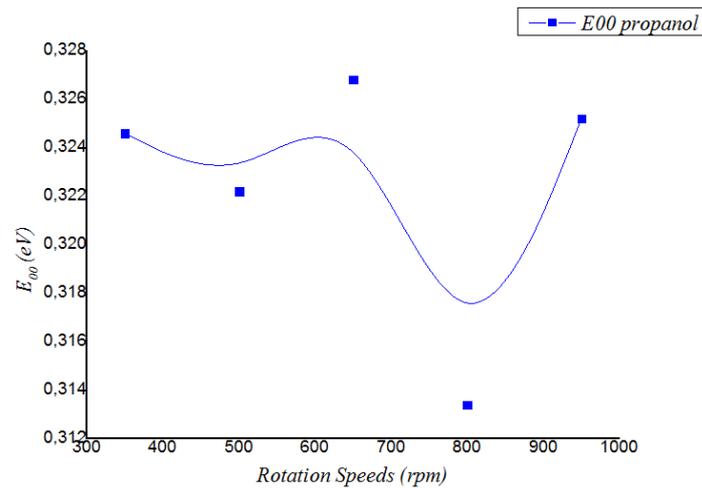
Fig. IV.23: *The E_{00} value of the ZnO thin film as a function of rotation speeds*

We observe that the disorder has very close values, in the order of 0.322 eV.

This table below (VI.13) summarize the best Search results that we have acquired for each solution, and compared them, in order to study the impact of the solution on the structural and optical properties of these thin films:

Solution / Properties	Solution 1 (ethanol solvent)	Solution 2 (propanol solvent)
Rotational speed (rpm)	2500	800
Orientation/ Intensity	(101)	(002)
Grains Size (nm)	32.645	58.930
C Axis(A°)	5.2333	5.16
Stress (Gpa)	2.2479	3.0206
Dislocation density ρ $(cm^{-2}*10^{14})$	0.9384	2.879
Average Transmittance(T%)	95%	85%
Optical band gap (eV)	3.273	3.229
E_{00} (eV)	0.3191	0.3134

Table (IV.13) The Best Values Of Each Solution

4. CONCLUSIONS

Two different solutions were used to obtain ZnO thin films for photovoltaic applications, by spin coating (Sol Gel) method. The influence of the solvent and the rotational speeds on the physical properties of the thin films were studied.

As a starting material, 3.2925 g zinc acetate dehydrate Zn(CH 3COO)2 .2H2O was dissolved in a mixture of :

20 ml of ethanol (solution 1) or 20ml of propanol (solution2), and 1.8 ml of monoethanolamine (MEA), where the concentration of the solutions become 0.75mole L -1.

The MEA was put into the solutions drop by drop, it acts at the same time as a base and a complexing agent , and the MEA to zinc acetate molar ratio was fixed at two (2).

Both solvents give good qualities of ZnO thin films, but with different rotational speed for each solvent.

From the XRD patterns, the ZnO thin films synthesized using solution1 exhibits its highest intensities of crystal growth orientation on the (101) plane in the range of 40 ua. However, those obtained by solvent 2 exhibits the highest intensities of crystal growth orientation on the (002) plane, with 81 ua.

The results show that the ZnO thin films prepared using solution 1 (Ethanol) produce the smallest crystallite size (10.1103 nm). However, the ZnO thin films prepared using solution 2 (propanol) produce the largest crystallite size (58.93 nm).

The ZnO thin films synthesized using ethanol solvents exhibit good transparency in the visible region, with optical transmittance higher than 95 %. By contrast, the propanol derived films exhibit a transmittance of 93%.Also an absorption edge is observed between 300 and 400 nm for most films.

At the end of this study we can say, that the solvent and the rotational speed have a big impact on the properties of the ZnO thin films. Also it can be said that Sol gel (spin coating) is well method adapted to the development of the thin layers of ZnO with good quality in photovoltaic applications, remaining the electrical characterizations later.

تم بحمد الله

REFERENCES

[1] T.J. Coutts, J.D. Perkins, and D.S. Ginley National Renewable Energy Laboratory T.O. Mason Northwestern University; Evanston, Illinois Conference Paper Mai 1999. 2

[2] H. Dixit First-Principles Electronic Structure Calculations Of Transparent Conducting Oxide Materials Doctorate Thesis University Antwerpen, Belgium July 2012

[3] T. Minami, Semicond. Sci. Technol. 20 (2005) S35

[4] S. Bae, H. Kim, Y. Lee, X. Xu, J.-S. Park, Yi Zheng, J. Balakrishnan, T. Lei, H. R. Kim, Y. I. Song, Y.-J. Kim, K. S. Kim, B. • Ozyilmaz, J.-H. Ahn, B. H. Hong And S. Iijima Nature Nanotechnology 5, (2010) 574-578

[5] K. S. Kim, Y. Zhao, H. Jang, S. Y. Lee, J. M. Kim, K. S. Kim, J.-H. Ahn, P. Kim, J.-Y. Choi And B. H. Hong, Nature 457, (2009) 706-710.

[6] C. M. Weber, D. M. Eisele, J. P. Rabe,Y. Liang, X. Feng, L. Zhi, K. M•Ullen, J. L. Lyon, R. Williams, D. A. Vanden Bout, And K. J. Stevenson ,Small 6, (2010) 184-189 .

[7] P. P. Edwards, A. Porch, M. O. Jones, D. V. Morgan, And R. M. Perks, Dalton Transactions. 19, (2004) 2995.

[8] H. Mizoguchi And P.M. Woodward, Chem. Mater, 16, (2004) 5233-5248.

[9] D.C. Look, B. Claflin, In: G.J. Brown, M.O. Manasreh, C. Gmachl, R.M. Biefeld, K. Unterrainer (Eds.), Progress In Compound Semiconductor Materials Iv-Electronic And Optoelectronic Applications, Boston , U.S.A., 2004, Materials Research Society Symposium Proceedings, Vol. 829, (2005), P. B8.6.1.

[10] C.G. Van De Walle, Phys. Rev. Lett., 85, (2000) 1012.

[11]. Eason, R., Pulsed Laser Deposition Of Thin Films. 2007: Wiley-Interscience, New York.

[12]. William D. Callister, J., Fundamentals Of Materials Science And Engineering. Fifth Edition Ed. 2000: John Wiley & Sons, Inc, New York.

[13] Srikant, V. And D.R. Clarke, Journal Of Applied Physics, 83 (10),(1998) . 5447-5451.

[14]. Tauc, J., R. Grigorovici, And A. Vancu, Physica Status Solidi (B), 1966. 15(2) (1966). 627-637.

[15] C. G. Van De Walle And J. Neugebauer, J. Appl. Phys, 95 (2004) 3851

[16] H. Ezbattez, A. Gonzalez, R. Viesca, J.L. Fernandez, J.E. Diazfernandez, J.M Machado, A. Chou, R, J.Riba., Wear **265** (3–4).(2008). 422-428

[17] Marcel De Liedekerke, "2.3. Zinc Oxide (Zinc White): Pigments, Inorganic, 1" In Ullmann's Encyclopedia Of Industrial Chemistry, 2006, Wiley-Vch, Weinheim, Doi: 10.1002/14356007 .A 20_243.Pub2

[18] Yu-Hsiu, Lin ,'' Structure And Properties Of Transparent Conductive Zno Films Grown By Pulsed Laser Deposition (Pld)'' , Master Thesis, University Of Birmingham Septembre 2009

[19] Hu, J. And R.G. Gordon, Journal Of Applied Physics, **71**(2) (1992) 880-890.

[20] . Johnson, V.A. And K. Lark-Horovitz, Physical Review, **92**(2) (1953) 226.

[21] . Jin, B.J., S. Im, And S.Y. Lee, Thin Solid Films, **366**(1-2) (2000) 107-110.

[22] J.T. Chen, J. Wang, R.F. Zhuo, D. Yan, J.J. Feng, F. Zhang, P.X. Yan, Applied Surface Science 255 (2009) 3959–3964.

[23] J. El Ghoul, "Elaboration Et Caractérisation Des Nanoparticules Zno Dopées Vanadium", Mémoire De Master, Universite De Tunis El Manar (2007).

[24] Jaffe, J.E., Snyder, J.A., Lin, Z. And Hess,.C. (2000) Physical Review B: Condensed Matter, 62, 1660

[25] Z. Ben Ayadi, L. El Mir, K. Djessas, S. Alaya, Thin Solid Films 517 (2009) 6305-6309.

[26] Hu, J. And R.G. Gordon,. Journal Of Applied Physics, **71**(2). (1992). 880-890.

[27] Monjoy Sreemany, Suchitra Sen, , Materials Chemistary And Physics 83 (2004) 169-177.

[28] S. Benramache , Elaboration Et Caractérisation Des Couches Minces De Zno Dopées Cobalt Et Indium,,Thés De Doctotrat Université Mohamed Khider – Biskra ,2012.

[29] E. Verploegen, R. Mondal, C. Bettinger, S. Sok, M. Toney, Z. Bao, Advanced Functional Materials 20, (2010) 3519-3529

[30] A.Hafdallah, Étude Du Dopage Des Couches Minces De Zno Élaborées Par Spray Ultraso-Nique,, Magister Thesis, Mentouri University, Constantine, 2007.

[31] A.R. West,'Solid State Chemistry' John Willey & Sons, Singapore, (2003).

[32] K. L. Chopra,'Thin Film Phenomena', Mcgraw Hill, New York (1969)

[33] Rop.In2p3.Fr/Img/Pdf/Couchesminces.Pdf

[34]C.A.Bishop, Vacuum Deposition Onto Webs , Films And Foils . William Androw Publishing New York , 2007

[35] Http://Www.Icmm.Csic.Es/Fis/English/Evaporacion_Electrones.Html

[36] Benelmadjat Hannane, "Elaboration Et Caractérisation Des Composites Dopés Par Des Agrégats Nanométriques De Semi-Conducteurs", Thèse Magister, Constantine (2007).

[37] H. Bendjdidi, Master Thesis, Mohamed Khider University, Biskra, 2010

[38] Http://En.Wikipedia.Org/Wiki/File:Arcsource_Sablevtype.Jpg

[39] O.Boussoum , Etude De L'effet D'une Couche Mince De Tio2 Sur Les Paramètres D'une Cellule Solaire Au Silicium , Thèse Magister, Université Mouloud Mammeri De Tizi-Ouzou,2011.

[40]S. Rahmane , These De Doctorat, Université De Mohamed Kheider Biskra , (2008).

[41] B.E.Warren, X-Ray Diffraction , Kindle Edition

[42] Http://Serc.Carleton.Edu/Research_Education/Geochemsheets/Techniques/Xrd.Html

[43] A.Moustaghfir, Élaboration Et Caractérisation De Couches Minces D'oxyde De Zinc. Application A La Photoprotection Du Polycarbonate, Doctorate Thesis, Blaise Pascal University, 2004.

[44] F.Zhu, K.Zhang, E.Guenther, Ch.S. Jin , Optimized Indium Tin Oxide Contact For Organic Light Emitting Diode Applications, Institute Of Materials Research & Engineering, Singapor, 2000.

[45] K.Daoudi, Elaboration Et Caractérisation De Films Minces D'oxyde D'indium Dope A L'etain Ob-Tenus Par Voie Sol-Gel ,Potentialité Pour La Réalisation D'électrodes Sur Silicium Poreux, Doctorat Thesis, Claude Bernard University – Lyon 1, 2002.

[46] M. Guglielmi, G. Carturan, J. Non-Cryst. Solids 100 (1988) 16-30.

[47] M.Z.-C. Hu, E.A. Payzant, C.H. Byers, J. Colloid Interface Sci. 222 (2000) 20-36.

[48] A.C. Pierre, Introduction To Sol‑Gel Processing, Kluwer Academic Publishers, Boston/Dordrecht/London, 1998, Pp. 91‑167.

[49] L. Armelao, M. Fabrizio, S. Gialanella, F. Zordan, Thin Solid Films 394 (2001) 90‑96.

[50] E. Hosono, S. Fujihara, T. Kimura, H. Imai, J. Sol‑Gel Sci. Technol. 29 (2004) 71‑79.

[51] D. Sun, M. Wong, L. Sun, Y. Li, N. Miyatake, H.J. Sue, J. Sol‑Gel Sci. Technol. 43 (2007) 237‑243.

[52] Sigma Aldrich Data: Physical Properties Of Solvents, Http://Www. Sigmaaldrich .Com/Img/Assets/13620/Labbasics Pg144.Pdf.

[53] S. Fujihara, E. Hosono, T. Kimura, J. Sol‑Gel Sci. Technol. 31 (2004) 165‑168.

[54] H. Wang, C. Xie, D. Zeng, J. Cryst. Growth 277 (2005) 372‑377.

[55] M.S. Tokumoto, V. Briois, C.V. Santilli, S.H. Pulcinelli, J. Sol‑Gel Sci. Technol. 26   (2003) 547‑551.

[56] Y. Natsume, H. Sakata, Thin Solid Films 372 (2000) 30‑36.

[57] A.E.J. Gonzalez, J.A.S. Urueta, R.S. Parra, J. Cryst. Growth 192 (1998) 430‑438.

[58] A.M.P. Santos, E.J.P. Santos, Thin Solid Films 516 (2008) 6210‑6214

[59] L. Znaidi / Materials Science And Engineering B *174 (2010) 18–30*

[60] M .Ebelmen, *Ann. Chim. Phys*, 15, 319*,* (1845).

[61] C. B. Hurd, Chem. Rev., 22, 403 (1938).

[62] C.J. Brinker, Sherrer G.W., Sol-Gel Science, The Physic And Chemistry Sol-Gel   Processing, Academic Press, San Diego, (1989).

[63] H. Cattey, Thèse De Doctorat, Université De Franche-Comté, Besançon, (1997).

[64] Http://Www.Iwt-Bremen.De/Wt/Wb/Solgel/Verfahren_Fr.Php.

[65] S. Rabaste, Thèse De Doctorat, Université Claude Bernard ‑ Lyon 1 (2003).

[66] M. Bathat, Thèse De Doctorat, Lyon (1992).

[67] Http://Www.Indiamart.Com/Holmarcoptomechatronicspvtltd/Thin-Film-Equipments.Html

[68] Http://Nanoequipment.Wordpress.Com/2011/03/08/Spin-Coater/

[69] L. Nadar ,Surfaces Fonctionnalisees A Base De Nanoparticules Metalliques Pour L'optique Et La Photonique , Thèse De Doctorat, L'universite Jean Monnet De Saint-Etienne, France ,2011.

[70] C .Matei Ghimbeu, Préparation Et Caractérisation De Couches Minces D'oxydes Métalliques Semiconducteurs Pour La Détection De Gaz Polluants Atmosphériques , Doctorate Thesis, Paul Verlaine University, Metz,2007.

[71] Jcpds, Joint Committee For Powder Diffraction Standards, Power Diffraction File For Inorganic Materials, 79 (1979) 2205.

[72] N. Nagayasamy, S.Gandhimathination, V. Veerasamy, Open Journal Of Metal, 2013, 3, 8-11

[73] Davood Raoufi , Taha Raoufi, ,Applied Surface Science 255 (2009) 5812–5817

[74] X. S. Wang, Z.C. Wu, J.F. Webb, Z.G. Liu, Applied Physics A **77**, 561 (2003).

[75] D. Bao, H. Gu, A. Kuang, Thin Solid Films 312 (1998) 37.

[76] S. Amirhaghi, V. Craciun, D. Craciun, J. Elders, I.W. Boyd, Microelectron. Eng. 25 (1994) 321.

[77]S. S. Shariffudin , Transactions On Electrical And Electronic Materi-Als Vol. 13, No. 2, Pp. 102-105, April 25, 2012

[78] J.G. Quinones-Galvan ,, I.M. Sandoval-Jiménez B, H. Tototzintle-Huitle , Results In Physics 3 (2013) 248–253,

<div dir="rtl">

تأثير سرعة الدوران و المذيبات، على الخصائص البنيوية و الضوئية للأغشية الرقيقة لأكسيد الزنك   المحظرة بطريقة سول جل (طلاء بالدوران)
Sol Gel (Spin Caoting) .

ملخص

قمنا في هذا العمل بدراسة تأثير نوع المذيب و كذا سرعة الدوران عل الأغشية الرقيقة لأكسيد الزنك المحضرة بطريقة المحلول هلام Sol Gel و بالضبط طريقة الترسيب بالتدوير Spin Caoting.

الدافع لاستخدام هذه التقنية هي البساطة و سهولة التحضير .

تم اذابة 3.2925 غ من خلات الزنك ZAD في 20 مل من أحد المذيبين ، الايثانول Eth أو البروبانول Prop و بإضافة 1.8 مل من مونوايثانولامين MEA و هذا لتسهيل ذوبان خلات الزنك . فأصبح تركيز المحلولين 0.75 مول /لتر و نسبة ZAD/MEA هي 2.

بالنسبة للمحلول الأول ذو المذيب الإيثانول، كانت سرعة الدوران محصورة بين 2000د/د   و 4000 د/د و بقفزات 500 د/د ، أما المحلول الثاني فكانت السرعة محصورة بين 350 د/د و 950د/د بقفزات 150د/د ، مع تثبيت باقي الوسائط .

من أجل معرفة تأثير هذين العاملين على خصائص الأغشية الرقيقة ، قمنا بدراسة الخصائص البنيوية والبصرية لهذه الأغشية باستعمال انعراج الأشعة السينية (XRD)، و المطيافية الضوئية (UV-Vis).

الكلمات الدالة (المفتاحية): شرائح الرقيقة – ZnO - Sol Gel   - الطلاء بالدوران – مذيبات – سرعة الدوران –الخصائص البنيوية و البصرية- أشعة سينية.

</div>

Rotational Speed And Solvent Effect, On the Structural And Optical properties of ZnO Thin Films, Prepared By Sol-Gel (Spin Coating) Method

ABSTRACT:

In this work we have studied the impact of the type of solvents and the rotational speed on the properties of the ZnO thin films prepared by Sol Gel (Spin Caoting) method.

The Motivation for the use of this method is the simplicity and the ease of preparation.

The solutions were obtained by dissolving 3.2925 g of zinc acetate (ZAD) in 20 ml of ethanol (Eth) or propanol (Propa) and adding 1.8 ml of this monoethanolamine. The MEA facilitate the solubility of the zinc acetate .The concentration of the solution became 0.75 mole / l , and the ratio of ZAD to MEA is 2.

For the first solution (ethanol solvent) , the speeds were limited between 2000 rpm and 4000 rpm ,with increment of 500 rpm , fore second solution, the speeds were between 350 rpm and 950 rpm with increment of 150 rpm , with fixing the rest of parameters .

In order to determine the impact of these two factors on the properties of these films , we have studied the structural and optical properties of these thin films by using x-ray diffraction (XRD), and optical spectroscopy.

Keyword (s):

Tin Films, ZnO, Sol Gel, Spin Coating, Solvents, Rotational Speed, Structural and Optical Properties, XRD

L'EFFET DU SOLVANT ET DE LA VITESSE DE ROTATION, SUR LE PROPRIETES SRUCTURALE ET OPTIOE DES COUCHES MINCES DE ZNO , PREPARE PAR LA METHODE SOL –GEL (SPIN CAOTING).

Résumé

Dans ce travail, nous avons étudié l'effet de la nature du solvant et la vitesse de rotation sur les propriétés des couches minces de ZnO préparés par la méthode Sol Gel (Spin caoting).

La motivation pour l'utilisation de cette méthode est la simplicité et la facilité de préparation.

les solutions ont été obtenues en dissolvant 3,2925 g de l'acétate de zinc (ZAD) dans 20 ml d'éthanol (Eth) ou le Propanol (Propa) , en ajoutant 1,8 ml de Monoethanolamine (MEA), le MEA facilite la solubilité de l' acétate de zinc. la concentration des solutions est devenue de 0,75 mol / L et le rapport de ZAD / MEA est égal à 2 .

Pour la première solution (solvant d'éthanol), les vitesses de rotation ont été limitées entre 2000 tpm et 4000 tpm avec un incrément de 500 tpm,   pour la deuxième solution les vitesses étaient entre 350 tours par minute et 950 tours par minute avec un incrément 150 tpm , avec l'installation du reste paramètres .

Afin de déterminer l'impact de ces deux facteurs , nous avons étudiées les propriétés structurales et optiques de ces couches minces par diffraction des rayons X (XRD) et par la spectroscopie optique.

Mots-clés :

Couches Minces - ZnO - Sol Gel - Spin Caoting - Solvants - Vitesse De Rotation - Propriétés Structurales Et Optiques - X-Ray